Max-Planck-Institut
für Meteorologie

MAX PLANCK
GESELLSCHAFT

International Max Planck Research School
on Earth System Modelling

Benchmark Calculations of the Climate Sensitivity of Radiative-Convective Equilibrium

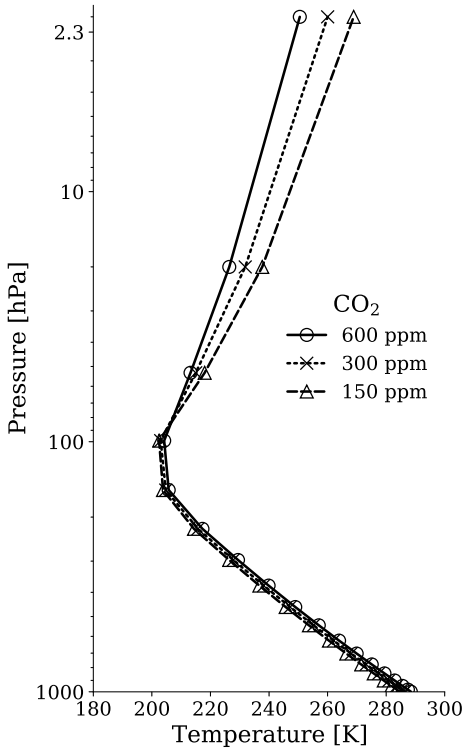

Lukas Kluft

Hamburg 2020

Berichte zur Erdsystemforschung
Reports on Earth System Science

239
2020

Hinweis

Die Berichte zur Erdsystemforschung werden vom Max-Planck-Institut für Meteorologie in Hamburg in unregelmäßiger Abfolge herausgegeben.

Sie enthalten wissenschaftliche und technische Beiträge, inklusive Dissertationen.

Die Beiträge geben nicht notwendigerweise die Auffassung des Instituts wieder.

Die "Berichte zur Erdsystemforschung" führen die vorherigen Reihen "Reports" und "Examensarbeiten" weiter.

Notice

The Reports on Earth System Science are published by the Max Planck Institute for Meteorology in Hamburg. They appear in irregular intervals.

They contain scientific and technical contributions, including Ph. D. theses.

The Reports do not necessarily reflect the opinion of the Institute.

The "Reports on Earth System Science" continue the former "Reports" and "Examensarbeiten" of the Max Planck Institute.

Anschrift / Address

Max-Planck-Institut für Meteorologie
Bundesstrasse 53
20146 Hamburg
Deutschland

Tel./Phone: +49 (0)40 4 11 73 - 0
Fax: +49 (0)40 4 11 73 - 298

name.surname@mpimet.mpg.de
www.mpimet.mpg.de

Layout

Bettina Diallo and Norbert P. Noreiks
Communication

Copyright

Benchmark Calculations of the Climate Sensitivity of Radiative-Convective Equilibrium

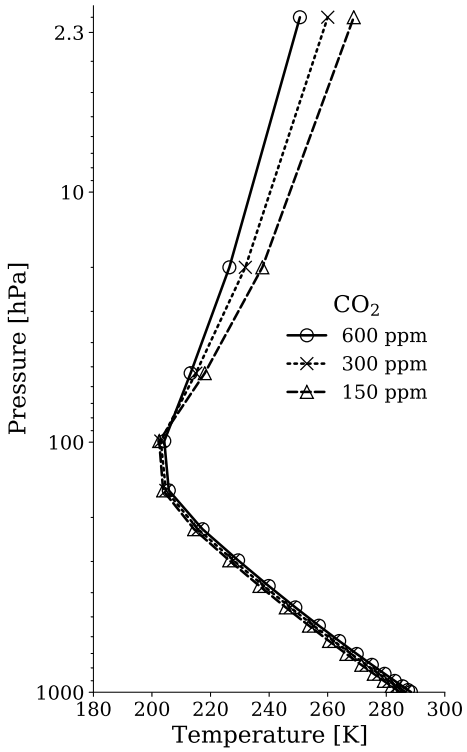

Lukas Kluft

Hamburg 2020

Lukas Kluft
aus Recklinghausen, Deutschland

Max-Planck-Institut für Meteorologie
The International Max Planck Research School on Earth System Modelling
(IMPRS-ESM)
Bundesstrasse 53
20146 Hamburg

Universität Hamburg
Erdsystemwissenschaften
Meteorologisches Institut
Bundesstr. 55
20146 Hamburg

Tag der Disputation: 25. November 2020

Folgende Gutachter empfehlen die Annahme der Dissertation:
Prof. Dr. Stefan A. Bühler
Prof. Dr. Bjorn Stevens

Vorsitzender des Promotionsausschusses:
Prof. Dr. Dirk Gajewski

Dekan der MIN-Fakultät:
Prof. Dr. Heinrich Graener

Berichte zur Erdsystemforschung / Max-Planck-Institut für Meteorologie 239
Reports on Earth System Science / Max Planck Institute for Meteorology 2020

ISSN 1614-1199

Abstract

The overarching theme of my research was to revisit a well-known model framework, radiative-convective equilibrium, and perform qualitative and quantitative benchmark simulations. Radiative-convective equilibrium (RCE) models are based on the assumption that the atmospheric state is only determined by the balance of incoming and outgoing radiation as well as buoyancy of air masses. This conceptual model has been proven valid for the tropical atmosphere by various observational studies. In addition, it is the foundation of the first numerical climate models and lead to the pioneering work of Manabe and Wetherald (1967) who investigated the thermal structure of the atmosphere under different boundary conditions—including a doubling of the CO_2 concentration.

The centerpiece of my research is the one-dimensional RCE model, `konrad`, that I developed together with Sally Dacie. The most striking difference to former modeling studies is the use of a state-of-the-art fast radiation scheme, the Rapid Radiative Transfer Model for global circulation models (RRTMG). RRTMG is widely used in comprehensive Earth system models, which, in addition to the reassessment of early modeling results, allows the comparison of changes in the radiative energy balance to more recent studies.

In my first study, I performed RCE simulations with perturbed CO_2 concentrations under different assumptions about the atmosphere and compared the surface warming to the results of Manabe and Wetherald (1967). I find that both models are in astonishing agreement given the marked differences in their treatment of radiation. Furthermore, I investigated the time-evolution of the temperature at the top of convection, which, in the real atmosphere, is associated with the altitude of high clouds. I find a warming of 0.5 K per K surface warming which supports a widely used assumption that the change of cloud-top temperatures is rooted in clear-sky physics.

The second study focuses on the temperature-dependence of the climate sensitivity. In general, the climate sensitivity is expected to increase with surface warming due to a moistening of the atmosphere, which is supported by a multitude of modeling studies. Some of these studies found a decrease in climate sensitivity as soon as surface temperatures rise above values of 310 K. We scrutinize this hypothesis by replacing RRTMG with a line-by-line radiative transfer model, the Atmospheric Radiative

Transfer Simulator (ARTS). These high-accuracy radiative transfer simulations show that the observed decrease of climate sensitivity at high surface temperatures in other studies is caused by the application of fast radiation schemes outside their range of validity. The clear-sky RCE does not show a temperature-dependence of the climate sensitivity at high surface temperatures.

In a final study, I quantified the effects of clouds on radiative forcing and the climate feedback. The presence of clouds reduces the effective radiative forcing by about 20 %, which would reduce surface warming. However, clouds also introduce a positive climate feedback, because of their tendency to keep an almost constant cloud-top temperature. Because both effects compensate each other the surface warming only slightly decreases due to the presence of clouds. The simulated evolution of cloud-top temperatures is tied to subtleties in the model formulation, which might explain differences in cloud feedbacks in more complex climate models.

The model `konrad` is developed under an open-source license and publicly available on GitHub. It may serve as a useful tool in both education and research and has already been used by Master students and other PhD candidates.

Zusammenfassung

Das zentrale Thema meiner Forschung war es, ein altbekanntes Konzeptmodell, das Strahlungs-Konvektions-Gleichgewicht (engl. *radiative-convective equilibrium*, RCE), neu aufzugreifen und sowohl qualitative als auch quantitative Vergleichsrechnungen durchzuführen. RCE-Modelle basieren auf der Annahme, dass der mittlere Zustand der Atmosphäre nur durch das Gleichgewicht der ein- und ausgehenden Strahlung sowie den Auftrieb von Luftmassen bestimmt wird. Dieses konzeptionelle Modell wurde durch verschiedene Beobachtungsstudien als für die tropische Atmosphäre gültig erwiesen. Darüber hinaus ist es die Grundlage für die ersten numerischen Klimamodelle und führte zur Pionierarbeit von Manabe und Wetherald (1967), welche die thermische Schichtung der Atmosphäre unter verschiedenen Randbedingungen untersuchten—einschließlich einer Verdoppelung des CO_2-Konzentration.

Das Herzstück meiner Forschung ist das eindimensionale RCE-Modell `konrad`, das ich zusammen mit Sally Dacie entwickelt habe. Der markanteste Unterschied zu früheren Modellierungsstudien ist die Verwendung eines modernen schnellen Strahlungsschemas, des *Rapid Radiative Transfer Model for Global Climate Models* (RRTMG). RRTMG wird in zahlreichen Erdsystemmodellen verwendet, was uns zusätzlich zur Wiederholung klassischer Modellierungsstuden den Vergleich mit neueren Studien ermöglicht.

In meiner ersten Studie führte ich RCE-Simulationen mit verschiedenen CO_2-Konzentrationen und unterschiedlichen Annahmen über die Atmosphäre durch und verglich die Oberflächenerwärmung mit den Ergebnissen von Manabe und Wetherald (1967). Ich fand heraus, dass die beiden Modelle in Anbetracht der deutlichen Unterschiede in der Implementation des Strahlungstransports erstaunlich gut übereinstimmen. Darüber hinaus untersuchte ich die zeitliche Entwicklung der Temperatur am Oberrand der aufsteigenden Luftmassen, an welchem sich in der echten Atmosphäre die Oberkanten hoher Wolken ausbilden. Unser Modell `konrad` simuliert eine Erwärmung von 0,5 K pro K Oberflächenerwärmung, was eine weit verbreitete Annahme stützt, dass die Änderung der Wolkentemperaturen von thermodynamischen Prozessen in der wolkenfreien Atmopshäre angetrieben wird.

Die zweite Studie konzentriert sich auf die Temperaturabhängigkeit der Klimasensitivität. Im Allgemeinen wird erwartet, dass die Klimasensitivität bei höheren Temperaturen und der daraus resultierenden Zunahme des Wasserdampfgehaltes

in der Atmosphäre zunimmt, was durch eine Vielzahl von Modellstudien gestützt wird. Einige dieser Studien finden eine Abnahme der Klimasensitivität, sobald die Oberflächentemperaturen über Werte von 310 K steigen. Wir überprüften diese Hypothese, indem wir RRTMG durch ein Referenz-Strahlungstransportmodell, den *Atmospheric Radiative Transfer Simulator* (ARTS), ersetzen. Diese hochgenauen Strahlungstransportsimulationen zeigen, dass die in anderen Studien beobachtete Abnahme der Klimasensitivität bei hohen Oberflächentemperaturen durch die Anwendung schneller Strahlungsschemata außerhalb ihres Gültigkeitsbereichs verursacht wurde. Das wolkenlose Strahlungs-Konvektions-Gleichgewicht zeigt bei hohen Oberflächentemperaturen keine Temperaturabhängigkeit der Klimasensitivität.

In einer abschließenden Studie habe ich die Auswirkungen von Wolken auf den Strahlungsantrieb und auf die Klimarückkopplungen quantifiziert. Das Vorhandensein von Wolken verringert den effektiven Strahlungsantrieb um etwa 20 %, was die Oberflächenerwärmung verringern würde. Wolken führen jedoch auch zu einer positiven Klimarückkopplung, da sie eine nahezu konstante Temperatur an ihrer Oberkante aufrechtzuerhalten. Da sich beide Effekte gegenseitig kompensieren, nimmt die Oberflächenerwärmung aufgrund von Wolken nur geringfügig ab. Die simulierte Entwicklung der Temperature and der Wolkenoberkante ist an Feinheiten in der Modellformulierung gebunden, was Unterschiede in den Wolkenrückkopplungen in komplexeren Klimamodellen erklären könnte.

Das Modell `konrad` wird unter einer Open-Source-Lizenz entwickelt und ist auf GitHub öffentlich verfügbar. Es kann als nützliches Instrument sowohl in der Bildung als auch in der Forschung genutzt werden und wurde bereits von Masterstudenten und anderen Doktoranden verwendet.

Acknowledgments

During my PhD, I have received a lot of help and support from many people.

First, I would like to thank my supervisors Stefan Bühler and Bjorn Stevens for the opportunity to conduct my research. Thank you, for many fruitful discussions that helped to sharpen the focus of my project. In this context, I would also like to thank my panel chair, Hartmut Graßl, for coordinating the various lines of thought during our panel meetings.

I am very grateful to Sally Dacie, for many enriching conversations about the development of `konrad`, our joint publications, and the struggles of PhD life in general.

I would also like to thank my colleagues at the working group *Radiation and Remote Sensing* at Universität Hamburg. Many thanks to Manfred Brath, who had a tremendous impact on my scientific development—and also shadow-supervised my PhD project. I have been privileged to work with Oliver Lemke, who helped to improve my "research code" significantly. Without your valuable input, `konrad` as is would not have been possible. Our many morning tech talks broadened my view on a variety of tech-related fields.

I am also very grateful to have met Theresa Mieslinger. Thank you, for uncounted Kaffeepausen, Feierabendbiere as well as scientific and moral support. She even made me run a half-marathon.

I would like to thank Manfred, Sally, Marc, Theresa I, and Theresa II for proof-reading my thesis. Your comments improved the manuscript a lot, and your assistance made the finishing weeks of my PhD much calmer than I would have thought possible.

Finally, I want to thank my family and friends for their various visits, chats, and general support that helped me take the breaks I needed in stressful times.

Contents

Motivation

Climate change is arguably one of the most urgent political problems. Scientists harness various lines of evidence to extend our knowledge of the climate system including paleoclimatological records, observational records by weather stations and satellites, and numerical models for predicting the Earth's future climate. Besides their ability to project future climate scenarios, numerical models offer the possibility to explore systems that resemble our current scientific understanding of the climate system. Numerical simulations offer the advantage that boundary conditions or single processes within the system can be modified to evaluate their significance.

The first numerical climate models date back to the 1960s, when Manabe and Wetherald described their radiative-convective equilibrium model. This conceptual framework of the tropical atmosphere presumes a balance between radiative cooling and the warming of ascending air parcels. Despite the simplicity of their model, Manabe and Wetherald (1967) profound insights into the Earth's atmosphere and its evolution in a changing climate. Thereby, they established the RCE framework as a valid approximative model of the atmosphere. They quantified the effect of a fixed relative humidity in a warming atmosphere, resulting in the first estimate of the water vapor feedback. In addition, they predicted that an increase of the CO_2 concentration is accompanied by a rapid stratospheric cooling; a process that is still considered as one of the main fingerprints of anthropogenic climate change. In the following years, a variety of climate models has been developed and served as a basis for a report by Charney et al. (1979), which can be seen as a predecessor of the IPCC reports. Since then, climate models have been constantly improved. In recent years, the milestone of cloud-resolving global models has been crossed (Satoh et al., 2019). Cloud-resolving models are hoped to give further insight into cloud feedbacks in the Earth system, which to this day are a main source of uncertainty.

But even in the era of cloud-resolving Earth system models that are run on Peta-scale high-performance computers, there is room left for conceptual models. The plethora of processes that are included in comprehensive Earth system models complicate the analysis of their results. At this point, conceptual models can be used to develop and test hypotheses about individual parts of the climate system, or to quote Somerville and Remer (1984) as saying:

> The purpose of a model such as ours is not to produce a comprehensive

> simulation but to gain insight into the behavior of more complex models and, perhaps, into the behavior of the climate system itself.

Following this spirit, I revisit the numerical RCE model by Manabe and Wetherald, which offers a well-defined problem formulation. Despite their simplicity, RCE models include the main atmospheric feedback processes that govern the clear-sky climate sensitivity. While doing so, they simulate the thermodynamical state of the atmosphere, which provides the basis for more elaborate processes such as the atmospheric circulation or cloud formation. For example, RCE models are able to simulate the change of cloud-top temperatures, thereby quantifying the strength of a main cloud-feedback mechanism. The knowledge gained from such conceptual modeling studies helps to interpret the extensive data generated by comprehensive climate models.

In the last decades, a variety of RCE models has been developed and used to enhance our understanding of the tropical atmosphere. However, these models are often not publicly available or provide only limited flexibility in their configuration. For that reason, the overarching theme of my PhD thesis was the development of a one-dimensional climate model with an easy-to-use interface to allow scientists and students to perform idealized numerical climate simulations. In cooperation with Sally Dacie, I developed the one-dimensional RCE model `konrad`, which provides a modular interface so that different model components can be freely combined. For example, the radiative heating rates can be simulated using either a state-of-the-art rapid radiation scheme or a high-accuracy line-by-line radiative transfer model.

During my PhD, I used `konrad` to test various hypotheses about the tropical atmosphere. This scientific journey starts with a revisit of the pioneering work by Manabe and Wetherald, continues with the first-ever usage of line-by-line radiative transfer during a climate simulation to study the temperature-dependence of climate feedbacks, and culminates with an assessment of the altitude-feedback of deep-convecting tropical clouds. This research yields important insights into the behavior of more complex models, for example the incorrect usage of radiative transfer schemes, which lead to false interpretations of the temperature-dependence of climate feedbacks (Section 2.2), or the strong link between the high-cloud feedback and the evolution of ozone concentrations in the tropical tropopause layer, which presently is not very well constrained in global circulation models (Section 2.3).

Chapter 1

Background

1.1 Radiative-convective equilibrium

A model is a simpler representation of a more complex system. Its purpose is the verification of hypotheses about a system in general or processes in the system. Depending on the hypothesis, models of different complexity are needed to provide useful information to answer a scientific question. Often, hierarchies of models with different complexity are used to investigate a problem (Jeevanjee et al., 2017; Maher et al., 2019). In climate sciences, these model hierarchies start on a conceptual level at which the fundamental physical concepts of a problem can be illuminated. And they end at comprehensive Earth System Models, which are used to test the liability of the concept in a complex environment close to the real atmosphere.

The simplest approach to model the Earth's surface temperature is through zero-dimensional energy balance models (Budyko, 1969). In equilibrium, the incoming solar radiation is balanced by the outgoing longwave radiation of the climate system, which is controlled by its temperature and emissivity. Energy balance models approximate the radiative effect of the atmosphere by a single absorption coefficient.

In a further step, one can include a vertical dimension to account for an atmospheric state that varies with altitude. This step enables estimating changes in the mean climate because basic atmospheric feedbacks can be represented. Using radiative transfer models, it is possible to calculate the radiative flux F between the individual model levels. If one assumes that the atmosphere is in hydrostatic equilibrium—which means no vertical motion—the vertical gradient of the net radiative flux can be converted into a radiative heating rate:

$$Q_\mathrm{r} = \frac{\partial T}{\partial t} = \frac{g}{c_p}\frac{\partial F}{\partial p} \tag{1.1}$$

with atmospheric temperature T, time t, Earth's standard gravity g, heat capacity c_p, and atmospheric pressure p.

The heating rate Q_r can be iteratively applied to the atmosphere to find an equilibrium state in which the radiative fluxes are in balance. This framework is known

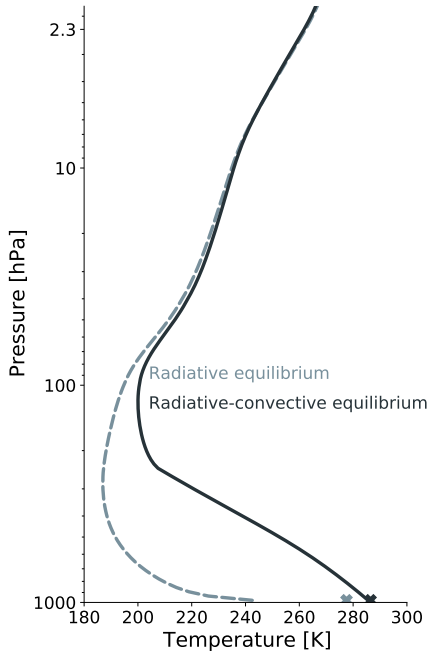

Figure 1.1: Temperature profiles in radiative equilibrium and radiative-convective equilibrium, calculated with the `konrad` model described below.

as radiative equilibrium and it is characterized by a strong vertical temperature lapse rate close to the surface (see Figure 1.1). In the real atmosphere, this temperature structure is unstable and triggers convection, the upward motion of warm air. This upward motion of air masses persists until the convective warming Q_c balances the radiative cooling

$$Q_r = Q_c \tag{1.2}$$

and a radiative-convective equilibrium is reached.

Figure 1.1 shows the temperature profiles in radiative equilibrium (RE) and in radiative-convective equilibrium (RCE). The strongest difference can be seen close to the surface where the RE develops a strong temperature gradient. This gradient is reduced by the convective warming in the RCE. The differences between both models are present throughout the whole troposphere up to 100 hPa. That is because the radiative cooling Q_r in this altitude region maintains convection (cp. Equation 1.2). Above 100 hPa, both models are in radiative equilibrium.

Observations show that the present-day tropics are close to an RCE. In contrast to high- and mid-latitudes, the Coriolis force is close to zero in the tropics, which limits the impact of dynamic processes on the mean atmospheric state. In addition, horizontal temperature gradients are adjusted quickly by gravity waves that emerge in regions of deep convection and radiate the temperature signal over wide distances; a phenomenon known as the Weak Temperature Gradient (Sobel and Bretherton, 2000; Charney, 1963). Due to the absence of large scale dynamics as well as weak horizontal gradients, radiation and convection are the dominant drivers in determining the

tropical mean atmosphere.

Since the pioneering work by Manabe and Wetherald, RCE models are the conceptual backbone of climate sciences. Despite their simple formulation, RCE models include the Planck, water vapor, and lapse-rate feedback, which are the most dominant radiative feedbacks in the climate system (Soden et al., 2008).

In recent years, Wing et al. (2017b) initiated the Radiative Convective Equilibrium Model Intercomparison Project (RCEMIP) to compare the representation of RCE across state-of-the-art climate models, including Large Eddy simulations and cloud-resolving models. These three-dimensional RCE models allow processes like the self-aggregation of clouds to be studied (Wing et al., 2017a). Within RCEMIP, the RCE is used as a well-defined boundary condition to investigate a limited set of processes without the complications from full global simulations.

Next to the RCEMIP simulations, classical 1D-RCE models are still used because of their ability to represent reasonable atmospheric states at low computational cost. In addition, different components can be easily added or replaced to test many-sided ideas about atmospheric processes, e.g., interactive atmospheric chemistry, the vertical humidity distribution, or different convection schemes. An incomplete list of more recent RCE studies includes Koll and Cronin (2018) who used atmospheres in RCE at different surface temperatures to simulate the outgoing longwave radiation with an offline line-by-line radiative transfer model. Thuburn and Craig (2002) used a 1D-RCE model to test the impact of interactive atmospheric chemistry on the tropical tropopause layer. Meraner et al. (2013) simulated the radiative feedback for a wide range of surface temperatures to investigate the state-dependence of the climate feedback in comparison to a global circulation model. These studies served as an inspiration for my research and shaped the development of our own 1D-RCE model `konrad`.

1.2 Development of `konrad`

The basis of my PhD research was the joint development of the radiative-convective equilibrium model, `konrad`, together with Sally Dacie. `konrad` is written in Python and provides a high-level interface that allows the user to easily set up various experiments. The source code is available on Github[1] under the MIT license. The latest stable version is provided through the Python Package Index[2].

The radiative transfer is handled by the Rapid Radiative Transfer Model for GCMs (RRTMG, Mlawer et al., 1997; Pincus et al., 2015), which is widely used in state-of-the-art climate models. RRTMG is accessed through the Climate Modelling and Diagnostics Toolkit (`climt`, Monteiro et al., 2018), which is a Python package that provides interfaces to various climate codes that are usually written in FORTRAN.

[1] https://github.com/atmtools/konrad
[2] https://pypi.org/project/konrad

The `konrad` model is built around a central `RCE` class, which handles the workflow of the model, i.e. the order in which the individual model components are called and coupled. These model components, which are implemented through Python classes, represent the different model physics. An overview of all model components in `konrad` is given in Figure 1.2. This object-oriented implementation makes `konrad` easily extensible. The abstract meta class `Component` defines a number of housekeeping methods that are for example used to organize the dimensions of variables, or the handling of attributes to control the behavior of a component. It is possible to add own implementations of any model component, which can be used for prototyping during model development, or if users want to perform experiments far from the ones that were thought of during the development. Model components can be freely combined, which allows the user to set up `konrad` in various configurations.

The usage of model components is best illustrated with an example. The radiative-convective equilibrium requires an assumption about the temperature lapse-rate in the troposphere. Historically, this is either a fixed lapse-rate of $6.5\,\mathrm{K\,km^{-1}}$ or the moist adiabat. In `konrad`, both variants are implemented by their own model component (see Figure 1.2). `FixedLapseRate` defines a fixed lapse-rate whose magnitude can be set when initializing the component `FixedLapseRate(lapse_rate=6.5)`. The `MoistLapseRate` class represents the moist adiabat. By default, the moist adiabat is updated after every time step to take a lapse-rate feedback due to a weakening of the moist adiabat in a warming climate into account. If this is not wanted, the moist adiabat can be fixed to its value from the first time step by passing the `fixed=True` keyword.

The different model components are passed to the `RCE` class during initialization. Listing 1.1 illustrates a minimal working example of a Python script to run `konrad`. The minimum requirement for a `konrad` simulation is an `Atmosphere` component and its corresponding pressure grid. In addition, positional and keyword arguments can be used to pass other model components or control parameters, i.e. the time step, the maximum runtime, or the verbosity can be set. The model output can be written to a netCDF 4 file at a user-defined output frequency.

In summary, `konrad` is a lightweight climate model that allows students and scientists to perform conceptual climate simulations at little computational cost. Despite its simplicity, `konrad` can be used to study a variety of scientific questions by utilizing its flexible interface.

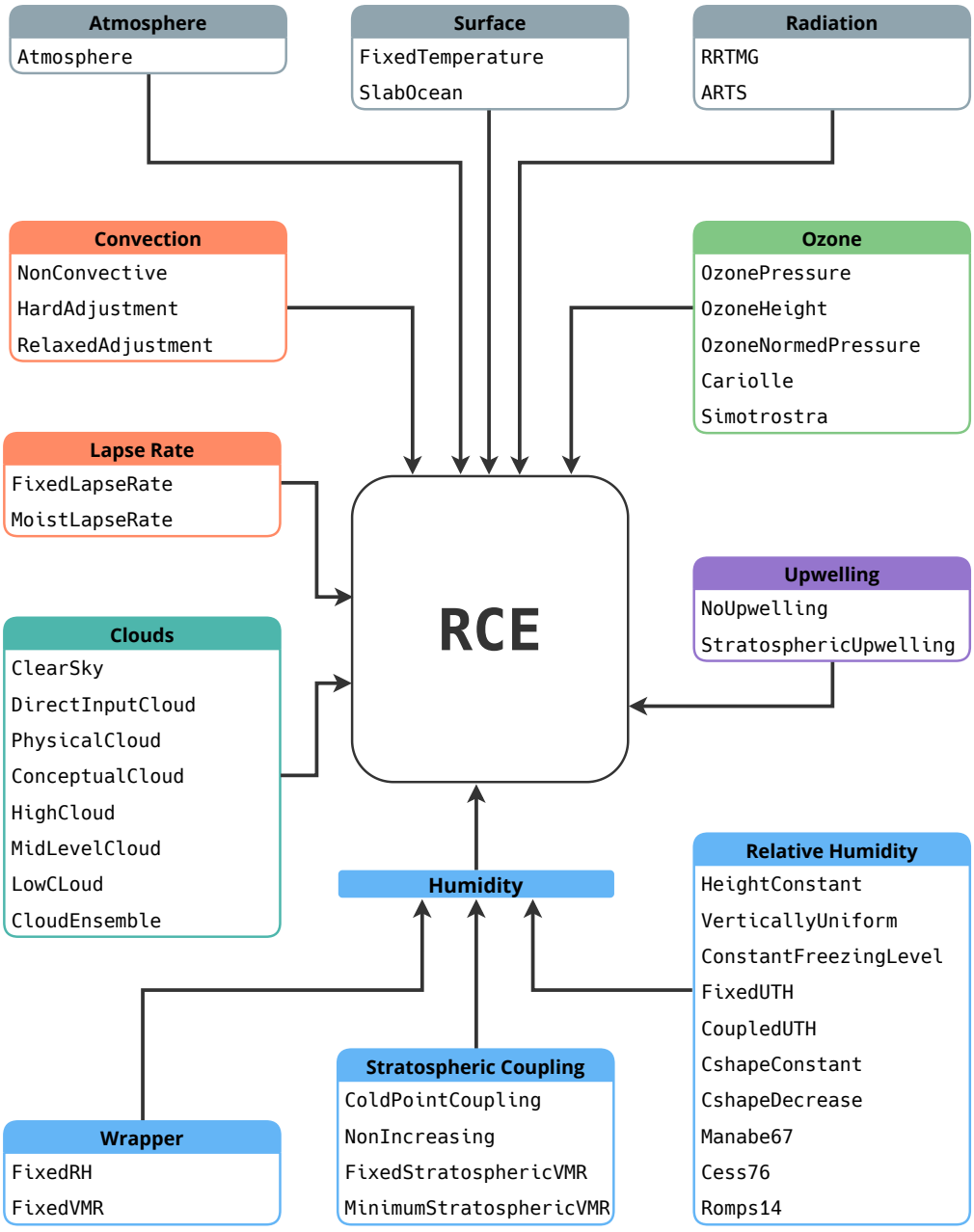

Figure 1.2: Overview of the different model components in `konrad`. The model components are passed to the `RCE` class during initialization to configure the model physics.

Listing 1.1: Example Python script to run `konrad`.

```
import konrad


konrad.enable_logging()

# Create an atmosphere component on an arbitrary pressure grid.
phlev = konrad.utils.get_quadratic_pgrid(1000e2, 1, num=256)
atmosphere = konrad.atmosphere.Atmosphere(phlev)

# Setup for the radiative-convective equilibrium simulation.
rce = konrad.RCE(
    atmosphere,
    humidity=konrad.humidity.FixedRH(
        rh_func=konrad.humidity.HeightConstant()
    ),  # Add a height-constant RH profile.
    lapserate=konrad.lapserate.MoistLapseRate(),
    timestep="6h",  # Set time step in model time.
    max_duration="500d",  # Set maximum runtime in model time.
)
rce.run()  # Start the simulation.
```

1.3 Climate sensitivity and radiative feedbacks

One of the key goals of climate sciences is to quantify the climate sensitivity, which is the response of the climate system to an external perturbation to its radiative balance. This measure can be used to predict the impact of changes in the boundary conditions, e.g., changes in the solar constant or increasing greenhouse gas concentrations. The climate sensitivity links the global mean surface temperature to changes of the net radiation and therefore enables the comparison of comprehensive Earth system models with conceptual models like `konrad`. Here, I will outline the general concept of climate sensitivity, radiative forcing, and radiative feedback—a more detailed derivation and discussion is given in Ghil and Lucarini (2020, Sec. IV).

Let us consider a system in which the net radiation F at the top of the atmosphere is a function of the mean surface temperature T by $F = F(T)$. Furthermore, we assume that there is a steady-state $T = T_0$ such that $F(T_0) = 0$. If we apply a radiative forcing ΔF to the system, e.g. by an increase in the CO_2 concentration, there has to be a corresponding change in surface temperature ΔT to maintain the radiative equilibrium:

$$F(T_0 + \Delta T) + \Delta F = 0 \quad . \tag{1.3}$$

For small ΔT and smooth $F = F(T)$ we can linearize the system around T_0:

$$\Delta F = -\lambda \cdot \Delta T \tag{1.4}$$

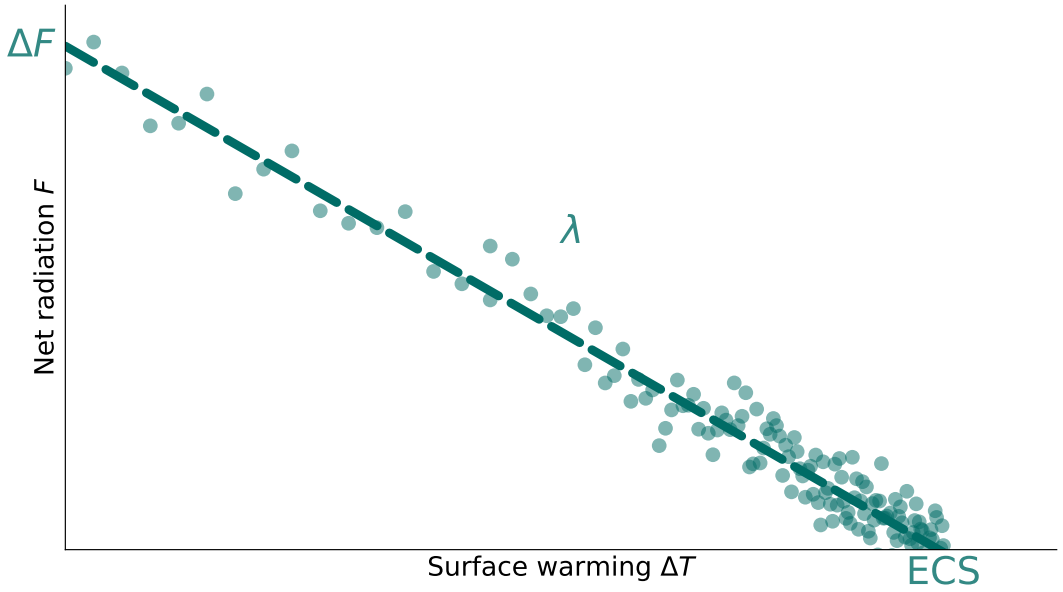

Figure 1.3: Conceptual sketch of the so called "Gregory plot". The net radiation F is plotted as a function of surface warming ΔT. The slope of the regression line is the climate feedback parameter λ (see Equation 1.4). When approaching the ECS, the individual dots (which represent single time steps) are more clustered because the temperature change slows down as the surface temperature converges to its equilibrium value.

with radiative feedback parameter λ and radiative forcing ΔF. The eventual temperature change that is required to reach the new equilibrium state for a particular forcing, namely that of a doubling of the CO_2 concentration, is called the equilibrium climate sensitivity (ECS). It is related to the radiative forcing $\Delta F_{2\times CO_2}$ and the radiative feedback λ by

$$\Delta T_{2\times CO_2} = \text{ECS} = \frac{\Delta F_{2\times CO_2}}{\lambda} \quad . \tag{1.5}$$

As a consequence, both an increase in the external forcing ΔF and a decrease in the feedback λ can increase the equilibrium temperature of the climate system.

Gregory et al. (2004) proposed a way to estimate the radiative feedback as the linear regression of the radiative imbalance against the surface temperature change. An advantage of this method is that the climate system does not need to reach the new equilibrium state. Full Earth system models often do not equilibrate during their runtime because of the massive heat capacity of the oceans and the expense of running the model for such a long time. Figure 1.3 shows a conceptual sketch of the so called "Gregory plot". It is a visual representation of Equation 1.4 and displays all stated quantities: The radiative forcing ΔF is given as the y-intercept of the regression line, the radiative feedback λ is the slope of the regression line, and the ECS is marked by the x-intercept.

The radiative feedback λ is the change in net radiation with surface warming and can be influenced by various processes in the climate system. One of the most fundamental feedbacks is the Planck feedback, which describes the change in outgoing longwave radiation due to temperature changes solely: A higher surface temperature increases the longwave emission, which reduces the initial radiative forcing until a new equilibrium at higher surface temperatures is reached. If no other feedback is present, a doubling of the CO_2 concentration causes a surface warming of only about 1 K (Manabe and Wetherald, 1967). In the real atmosphere, however, various additional feedbacks modify the strength of the total climate feedback. For example, the amount of water vapor is expected to increase with global warming (Soden et al., 2005). As a consequence, the atmosphere becomes optically thicker and less radiation is emitted into space (Koll and Cronin, 2018), which adds a positive feedback to the climate system. In contrast, changes in the vertical temperature lapse rate allow the atmosphere to emit more radiation with surface warming, which adds a negative lapse-rate feedback. The total feedback λ can decomposed into a sum of individual feedbacks, which follows from the additive nature of partial derivatives:

$$\lambda = \lambda_{\mathrm{PL}} + \lambda_{\mathrm{WV}} + \lambda_{\mathrm{LR}} + \dots \tag{1.6}$$

with Planck feedback λ_{PL}, water vapor feedback λ_{WV}, lapse-rate feedback λ_{LR}, and possible further feedbacks. The feedback decomposition is used to compare the strength of individual feedback processes quantitatively. In conceptual models like `konrad`, this can be done by independent model runs that either include a process x or not; the corresponding feedback λ_x is given as the difference between the feedback parameters of both simulations. This approach is not feasible in full climate models, in which a plethora of feedback mechanisms work simultaneously and depend on one another.

For full climate models, Soden et al. (2008) introduced a method to decompose the climate feedback into its individual components by dividing it into two terms:

$$\lambda_x = \frac{\partial F}{\partial x}\frac{\partial x}{\partial T_{\mathrm{s}}} \quad . \tag{1.7}$$

The first term is the so called "radiative kernel". It describes the differential response of the net radiation to changes in a quantity x and can be calculated using a radiative transfer model. The second term is the change in x with surface warming ΔT_{s} and is derived from the perturbed climate simulation. The method allows the strength of different feedback processes to be compared between climate models. In particular, it is possible to compare models that implement a different number of feedback mechanisms. For example, if only one of two models includes the feedback of coupled sea-ice in the high latitudes, their total climate feedback will most likely differ. Nevertheless, using a feedback decomposition, their water vapor feedbacks can still be compared.

Hence, the framework of feedback decomposition makes it possible to compare the strength of climate feedbacks present in `konrad` with more complex Earth system models.

Chapter 2

Key results

Its simple model formulation and flexible implementation allow `konrad` to be used for a wide range of numerical experiments. In the following sections, I will introduce three studies that I have conducted using `konrad`. The first publication (Section 2.1) describes `konrad` in more detail and quantifies its climate sensitivity in comparison to classical studies. The second study (Section 2.2) illuminates the temperature-dependence of clear-sky feedbacks in extreme climates by using a line-by-line radiative transfer model. In the third study (Subsection 2.3), I quantify the cloud-altitude feedback of an idealized cloud scene in `konrad`. In addition, I will summarize two studies that I have contributed to as co-author and outline future projects (Section 2.4).

2.1 Re-examining classical RCE models

In the first study (Appendix A), I re-examine the work by Manabe and Wetherald (1967, MW67 hereafter). Even though the model formulations are very similar, some details, especially in the handling of atmospheric radiative transfer, have been significantly improved over the last decades. The goal was to check if an RCE with a state-of-the-art radiative transfer simulates the same climate sensitivity as the historical MW67 model.

I find that the equilibrium climate sensitivity (ECS) is in surprising agreement between `konrad` and MW67. When using the simplest model configuration, i.e. fixed absolute humidity and a constant temperature lapse rate of $6.5\,\mathrm{K\,km^{-1}}$, the resulting ECS is virtually the same—1.34 K for konrad and 1.36 K for MW67. Even when taking water vapor and lapse-rate feedback into account, the ECS estimates differ by less than 10 %.

I performed RCE simulations with consecutive doublings of the CO_2 concentrations ranging from 0.5 to 8 times its present-day value. I find that the increase in the effective radiative forcing (which includes rapid adjustments in the stratosphere) deviates from the logarithmic dependence on the CO_2 concentration which is found

for the instantaneous forcing (Huang and Bani Shahabadi, 2014). This deviation was already found by Gregory et al. (2015) in global circulation models. It is presumably caused by the stratospheric adjustment, which shows a more linear dependence on the CO_2 concentration and hence leads to a stronger increase of the effective forcing.

Furthermore, the set of simulations allows us to investigate the state-dependence of the ECS. Meraner et al. (2013) found a robust increase of the climate sensitivity at higher surface temperatures that is mainly driven by an increase of the water vapor feedback. In contrast, I find an increase in ECS of only about 15 %, which I attribute almost entirely to a strengthening of the radiative forcing. However, our results span a smaller range of surface temperatures of 8 K and are run with smaller values of relative humidity.

In addition to our assessment of the climate sensitivity, I investigated more recent conceptual ideas on the development of convective top temperatures. In our study, the clear-sky convective top temperature increases by about 0.5 K per K surface warming, which is consistent with the "proportionally higher anvil temperature" (PHAT) hypothesis. Zelinka and Hartmann (2010) originally introduced the PHAT hypothesis to describe the evolution of cloud top temperatures in a warming climate. Its driving mechanisms, however, are based in clear-sky thermodynamics, which explains its presence in our clear-sky simulations. I find that the validity of the PHAT hypothesis depends on details of the chosen relative humidity profile: If the chosen humidity profile is not consistent with the temperature profile, virtually any relation of upper-tropospheric temperatures can be modeled in a warming climate. This is a relevant constraint when constructing conceptual models with prescribed temperature or humidity distributions.

2.2 Temperature-dependence of clear-sky climate sensitivity

In recent years, several studies discussed the state-dependence of the climate feedback parameter, which is its change with global mean surface temperature. A temperature-dependent feedback parameter has severe impact on the constraints by paleoclimatological records as well as inter-model comparisons (Knutti et al., 2017). The common explanation for clear-sky temperature-dependence is an increase of the water vapor feedback: in a warming climate, the absolute humidity is expected to increase due to enhanced evaporation. The additional water vapor increases the optical thickness of the Earth's atmosphere and closes the so called atmospheric emission window. As a consequence, a larger portion of the electromagnetic spectrum is governed by water vapor absorption, which is interpreted as an increase of the water vapor feedback.

Meraner et al. (2013) tested this hypothesis for a wide range of surface tempera-

tures between 280 and 323 K and found a robust increase of the climate sensitivity for temperatures up to 305 K. Above, the climate sensitivity decreases. This has been confirmed by Romps (2020) using a limited-area cloud-resolving model. An earlier study by Rennó (1997) was the first to describe different possible equilibria in 1D-RCE simulations. In Kluft et al. (2019), I already investigated the temperature-dependence with `konrad`. I found that the temperature-dependence of the climate feedback is negligible, and that an apparent increase in ECS is driven by a strengthening of the radiative forcing. However, the results in Kluft et al. (2019) are subject to some restrictions: First, I have run `konrad` with a low relative humidity of only 40 % to tune the surface temperature to tropical values. Recent findings in the Master thesis by Stella Bourdin show that the base relative humidity profile has a significant impact on the strength of the water vapor feedback. It is possible that our simulations are too dry in general to show an increase of the water vapor feedback. Second, the simulations cover a surface temperature range of only 8 K. This range is smaller than in the other studies that investigated the state-dependence (Meraner et al., 2013; Koll and Cronin, 2018).

In the second study (Appendix B), `konrad` is run for a wide range of surface temperatures between 285 K and 315 K. The surface temperature is adjusted using a surface enthalpy sink, which allows us to tune the model to virtually any surface temperature without affecting the radiative transfer directly. A common problem when studying state-dependencies is that fast radiative transfer schemes become error-prone at higher temperatures. Their computational efficiency is based on skillful selection of frequency bands that correspond to emission by specific gases (Mlawer et al., 1997; Pincus et al., 2015). For these bands, lookup tables are precalculated, which allows the schemes to compute broadband radiative fluxes efficiently. However, the accuracy of these schemes decreases, if the atmospheric state deviates too much from the reference simulations used to compile the lookup tables. Therefore, I replaced the longwave radiation scheme with a line-by-line radiative transfer model. Shortwave fluxes are still computed with RRTMG, because the change in outgoing longwave radiation (OLR) is the more decisive component for the clear-sky climate feedback. Computing the longwave radiation with such high accuracy is unprecedented and only affordable due to the computational efficiency of a 1D-RCE model. This allowed us, for the first time, to perform line-by-line radiative transfer simulations within extreme climate simulations. I used the Atmospheric Radiative Transfer Simulator (ARTS; Buehler et al., 2018; Eriksson et al., 2011) to simulate the OLR for 32,768 individual frequencies between 10 and 3,250 cm^{-1}.

Using different values for the surface enthalpy sink, `konrad` was run to different equilibrium temperatures at present-day boundary conditions. Afterwards, the CO_2 concentration was doubled to investigate the radiative forcing and feedback. I find a robust increase of the climate feedback for moderate surface temperatures

between 285–300 K. However, in contrast to previous studies (Meraner et al., 2013; Romps, 2020), I cannot confirm the decrease of the climate feedback at high surface temperatures above 305 K. I am able to show that the previously found decrease is caused by inaccuracies in the fast radiation schemes. Even though the pre-calculated lookup tables in RRTMG cover surface temperatures up to 320 K, their construction leads to errors above 308 K: Following the moist adiabat at such high surface temperatures leads to an out-of-bounds temperature for the lookup table in the upper troposphere. When using line-by-line radiative transfer, the tropical clear-sky climate is stable even at high surface temperatures.

The constancy of the radiative feedback at surface temperatures above 305 K is caused by a closing of the atmospheric window between 800 and 1000 cm^{-1}. This is in agreement with a qualitative model by Ingram (2010). Ingram (2010) predicts that atmospheres, in which water vapor is the only relevant greenhouse gas, will keep a constant emission temperature—which would eventually cause a zero feedback. I can confirm this hypothesis in good approximation in spectral regions that are dominated by water-vapor absorption. Because some parts of the spectrum are dominated by other gases, like CO_2, the total radiative feedback stays negative, which prevents a runaway climate state, even at high surface temperatures.

These results suggest that the tropical climate is stable even at high surface temperatures. Moreover, the temperature-dependence of the climate sensitivity vanishes above surface temperatures of about 308 K.

2.3 Cloud-altitude feedbacks

The RCE studies presented so far are limited to clear-sky conditions. Although this assumption is useful to understand fundamental mechanisms related to water vapor and lapse-rate feedbacks, it is an oversimplification of the climate system. In a final step, I introduce clouds to close this gap and construct a more realistic conceptual model of the tropical atmosphere. Earlier studies already introduced clouds in simplified ways (Manabe and Wetherald, 1967; Ramanathan and Coakley, 1978; Hartmann, 2015). These studies focused on the cloud radiative effect (CRE), which I define as the difference in all-sky radiative fluxes F_{all} compared to the clear-sky

$$\mathrm{CRE} = F_{\mathrm{all}} - F_{\mathrm{clear}} \quad . \tag{2.1}$$

The CRE is caused by increased reflection in the shortwave, and decreased emission in the longwave part of the electromagnetic spectrum due to clouds. For simplicity, in earlier studies clouds were represented as one-layer blocks that were fixed in pressure coordinates. Later, it became apparent that fixing the cloud-top temperature is a more reasonable approach (Zelinka and Hartmann, 2010). This has a severe consequence for the climate system, because it prevents clouds from increasing their longwave emission in a warming climate, which adds a positive cloud radiative

feedback to the system. Because this feedback is controlled by the evolution of cloud top altitudes, it is often referred to as cloud-altitude feedback. Other feedbacks, e.g. from changes in cloud area fraction or cloud thickness, are neglected in this study. In the third study (Appendix C), I investigate two main questions.

1. Is it possible to simulate clouds that result in a CRE as observed from space in a 1D-RCE model?

2. What is the cloud radiative feedback of these clouds?

The representation of clouds in radiative transfer requires a set of cloud optical properties. In the real atmosphere, these optical properties depend on the physical properties of the cloud, e.g. the amount and phase of cloud particles. For our RCE study, one needs to choose a set of cloud physical properties to simulate clouds with a reasonable CRE close to observations. For that reason, I ran a large Monte Carlo ensemble with almost 100,000 members. Each member was run with a random combination of cloud optical properties. The resulting CRE for each ensemble member was compared to the CERES EBAF satellite data (Doelling, 2019, Edition 4.1). Based on their root-mean-squared error, the best 1,024 ensemble members were selected for further simulations. The ensemble members in the subsample deviate less than $4\,\mathrm{Wm}^{-2}$ from the CRE in the CERES satellite climatology.

The selected subsample was forced with a doubling of the CO_2 concentration to investigate cloud feedbacks. Fixing high clouds at a constant pressure level (FAP) adds a large negative radiative feedback of about $-0.7\,\mathrm{Wm}^{-2}\mathrm{K}^{-1}$, which is in the same order of magnitude as the total clear-sky feedback. The feedback is caused by an increase in outgoing longwave radiation in the upper troposphere. Hence, the cloud feedback can be seen as an amplification of the lapse-rate feedback, which enhances the upper-tropospheric warming compared to the surface. If the cloud tops are fixed at a constant temperature (FAT), their emission temperature cannot change. Because of the contrast to the otherwise negative temperature feedbacks in the clear-sky (Planck and lapse-rate), this adds a slightly positive cloud feedback of about $0.1\,\mathrm{Wm}^{-2}\mathrm{K}^{-1}$. Finally, I am investigating the so called PHAT hypothesis: In theory, changes in the static stability will cause the cloud top to rise less than it would take to maintain a constant temperature. As a consequence, the equilibrium cloud top temperature will be "proportionally higher". The PHAT mechanism is implemented by setting the cloud top height to the level of maximum clear-sky subsidence divergence. This level is associated with strong mass outflow from convective into subsidence regions and therefore sets a physical limit to deep-cloud formation.

I find that coupling high clouds to the maximum clear-sky divergence results in a decrease of cloud top temperature of about 0.5 K per K surface warming, in stark contrast to the PHAT hypothesis, which predicts a 0.5 K increase. Therefore, in our simulations, PHAT clouds add an additional positive cloud feedback that is

even larger than FAT. The decreasing trend in cloud-top temperature is caused by the upward shift of the ozone layer in our model configuration: As the troposphere deepens, the ozone layer is shifted upwards, which cools the upper troposphere. This radiative cooling affects the level of maximum clear-sky divergence and therefore the high-cloud top.

From existing literature it is not clear how the ozone layer will evolve in a warming climate. A strengthening of the Brewer-Dobson circulation (Eichelberger and Hartmann, 2005) would increase the transport of ozone-poor air into the lower stratosphere. Therefore, an upward shift of the ozone profile might be a plausible assumption in our conceptual model. However, the impact of changing ozone concentrations is highly debated. While Nowack et al. (2015) find a cooling of about 1 K for a quadrupling of the CO_2 concentration, Marsh et al. (2016) estimate the effect to be negligible. If the ozone layer in `konrad` is kept at a fixed height, the cloud-top temperature rises by about 0.5 K per K (consistent with PHAT), which leads to a slightly negative cloud feedback.

In conclusion, the PHAT cloud feedback can be interpreted as an amplification of the clear-sky temperature change in the upper troposphere. This temperature is highly affected by the treatment of ozone in `konrad`—keeping it fixed or normalizing it with the troposphere depth. Both treatments of the ozone distribution are non-physical, but can be interpreted as a reasonable range against which studies with more complex atmospheric chemistry can be compared. Furthermore, the results suggest that models cannot be expected to consistently represent cloud-altitude feedbacks as long as they show different trends in lower stratospheric ozone.

2.4 Additional studies

Besides my own research, `konrad` has been used in other studies that I coauthored. In this section, I will briefly outline existing, ongoing, and future projects that use `konrad`.

Dacie et al. (2019) used `konrad` to investigate the tropical tropopause layer (TTL). The TTL is located around the cold-point tropopause and is shaped by a variety of processes, i.e. radiation, convection, and atmospheric chemistry. What makes the TTL so interesting is that the timescales of the processes that shape it can be in the same order of magnitude. Dacie et al. (2019) implemented a new convection scheme enabling a smooth relaxation between the radiatively driven stratosphere and the convectively mixed troposphere. Among others, we analyzed how the ozone profile controls the temperature in the TTL and how it influences surface warming. We find that the effect of ozone alone is small, but that it can be amplified by feedbacks with the water vapor concentration (clouds were not included in this study).

The results in Dacie et al. (2019) are focused on the impact of the mean ozone

profile. Based on this, a new project will focus on the importance of interactive ozone in the tropical atmosphere. The simulations will compare different treatments of the vertical ozone distribution, from different climatologies, over simple normalization approaches as used in Section 2.2 and 2.3, and the usage of atmospheric chemistry like the Cariolle scheme (Cariolle and Teyssèdre, 2007).

In a Master's thesis that I co-supervised, Stella Bourdin quantified the impact of the chosen relative humidity profile on the climate sensitivity. This study was motivated by our findings in Kluft et al. (2019). Previously it has been assumed that the water vapor feedback is constrained by the change in the absolute humidity due to preserved relative humidity. Here, we find a significant impact of the chosen base relative humidity and the climate sensitivity. Furthermore, the relevance of relative-humidity perturbations in different altitudes was analyzed. We confirm that the upper troposphere plays a decisive role in controlling the climate sensitivity in agreement with previous studies (Soden et al., 2008; Vial et al., 2013). In addition, an increase in the relative humidity close to the surface shows a cooling effect on the climate.

Finally, there is an initiative to implement an aerosol component in `konrad`. The goal of these studies is to quantify the radiative aerosol forcing during and after volcanic eruptions. Here, `konrad` can be used to construct lightweight ensembles with different eruption strengths.

In conclusion, `konrad` has been used in a wide range of conceptual studies. These collaborations helped to gain insight into related fields of research that I would have otherwise missed. I am looking forward to see how `konrad` will be used in future.

Chapter 3

Summary and conclusion

During my PhD, I developed, together with Sally Dacie, the one-dimensional radiative-convective equilibrium model `konrad`. The model is inspired by the pioneering work of Manabe and Wetherald (1967). In contrast to their work, `konrad` is build around a more complex state-of-the-art radiation scheme, which is also used in various climate models.

In my first study (Appendix A), I re-performed some of the original Manabe and Wetherald (1967) simulations. I showed that even with modern treatment of radiative transfer our results are in astonishing agreement with their results. Furthermore, I tested a hypothesis about the development of upper-tropospheric temperatures. The so called "proportionally higher anvil temperature" (PHAT) hypothesis suggests that cloud tops will slightly warm under global warming and add a positive climate feedback. I found that this upper-tropospheric warming is also a robust signal of the convective-top temperatures in clear-sky RCE as long as the vertical distributions of temperature and water vapor are handled in a consistent way. This represents a significant constraint for other conceptual modeling studies.

In my second study (Appendix B), I investigated the temperature-dependence of clear-sky climate feedbacks. In general, the temperature-dependence of the total climate feedback is expected to be positive due to an increase of atmospheric water vapor. Therefore, a warmer initial climate should result in a stronger warming. However, at high surface temperatures above 305 K even the qualitative dependence is under debate. I tested whether the accuracy of radiative transfer in these extreme atmospheric conditions has an impact on the temperature-dependence. For that reason, I replaced the longwave component of our radiation scheme with a line-by-line radiative transfer model. Line-by-line models are usually used as reference during the development of fast radiation schemes. Because simulations with `konrad` are lightweight in general, it is possible to spend computational effort on these high-accuracy radiative transfer simulations. I find that the temperature-dependence of the clear-sky feedback vanishes at surface temperatures above 305 K. When using the default radiation scheme, the temperature-dependence is similar to other modeling

studies. I am able to pinpoint the differing behavior at high temperatures to an out-of-bounds use of lookup tables in the fast radiation code RRTMG. This revision of the upper limit of the radiation scheme puts a severe constraint on modeling studies. While it is very likely that other conceptual studies suffer from these limitations, one has to check the impact on more comprehensive models; the inter-column variability and presence of other processes like clouds may partly compensate the presumed errors in the radiative transfer.

In my third study (Appendix C), I investigated the impact of clouds in `konrad`. Here, I was especially interested in an explicit simulation of the PHAT mechanism. I first implemented a method to calculate noise-free all-sky fluxes for inhomogeneous cloud scenes. Then, I tuned the cloud optical properties using a large Monte Carlo ensemble with 100,000 members to match the cloud radiative effect found in satellite observations. I find that the presence of clouds reduces the radiative forcing — due to a doubling of CO_2 — by about 20 %, which is mostly balanced by a decrease of the climate feedback. However, I find that the sign of the cloud feedback is tied to the handling of the vertical ozone distribution in `konrad`. If the ozone profile is coupled to the development of the temperature profile, the upper troposphere cools with surface warming. This effect leads to a negative cloud feedback, in contrast to the PHAT hypothesis. Although this ozone coupling is not physical, it is not unreasonable either, and it sets conceptual boundaries for comprehensive climate models whose treatment of atmospheric chemistry is vastly different.

Over the time of my PhD studies, I have learned that conceptual models have a tremendous value by helping to understand more complex models. And this value is likely to increase because climate models include more and more processes and are run at cloud-resolving scales, producing an unprecedented amount of data. We, as scientific community, need model hierarchies to understand them. In order for these hierarchies to be a valuable tool, we need to focus on a fundamental art of science: hypothesis formulation. The simplicity of a conceptual model is only useful, if there is a clear hypothesis to test. Only then, the necessary components are known and a suitable model can be chosen. In this case, it does not matter that more complex processes are neglected, because in the end:

> All models are wrong, but some are useful. (George Box, 1976, adapted)

Bibliography

Budyko, M. I. (1969). "The effect of solar radiation variations on the climate of the Earth". In: *Tellus* 21.5, pp. 611–619. DOI: 10.3402/tellusa.v21i5.10109. URL: https://doi.org/10.3402/tellusa.v21i5.10109.

Buehler, S. A. et al. (2018). "ARTS, the atmospheric radiative transfer simulator — version 2.2, the planetary toolbox edition". In: *Geoscientific Model Development* 11.4, pp. 1537–1556. DOI: 10.5194/gmd-11-1537-2018.

Cariolle, D. and H. Teyssèdre (Jan. 2007). "A revised linear ozone photochemistry parameterization for use in transport and general circulation models: multi-annual simulations". In: *Atmospheric Chemistry and Physics Discussions* 7.1, pp. 1655–1697. URL: https://hal.archives-ouvertes.fr/hal-00328036.

Charney, J. G. (1963). "A note on large-scale motions in the tropics". In: *Journal of the Atmospheric Sciences* 20.6, pp. 607–609.

Charney, J. G. et al. (1979). *Carbon dioxide and climate: a scientific assessment*. Tech. rep.

Dacie, Sally et al. (Sept. 2019). "A 1D RCE Study of Factors Affecting the Tropical Tropopause Layer and Surface Climate". In: *Journal of Climate* 32.20, pp. 6769–6782. ISSN: 0894-8755. DOI: 10.1175/JCLI-D-18-0778.1. URL: https://doi.org/10.1175/JCLI-D-18-0778.1.

Doelling, David (2019). *CERES Energy Balanced and Filled (EBAF) TOA and Surface Monthly means data in netCDF Edition 4.1*. DOI: 10.5067/TERRA-AQUA/CERES/EBAF_L3B.004.1. URL: https://asdc.larc.nasa.gov/project/CERES/CERES_EBAF_Edition4.1.

Eichelberger, Scott J. and D. L. Hartmann (2005). "Changes in the strength of the Brewer-Dobson circulation in a simple AGCM". In: *Geophysical Research Letters* 32.15. DOI: 10.1029/2005GL022924. eprint: https://agupubs.onlinelibrary.wiley.com/doi/pdf/10.1029/2005GL022924. URL: https://agupubs.onlinelibrary.wiley.com/doi/abs/10.1029/2005GL022924.

Eriksson, P. et al. (2011). "ARTS, the atmospheric radiative transfer simulator, Version 2". In: *Journal of Quantitative Spectroscopy and Radiative Transfer* 112.10, pp. 1551–1558. DOI: 10.1016/j.jqsrt.2011.03.001.

Ghil, M. and V. Lucarini (July 2020). "The physics of climate variability and climate change". In: *Reviews of Modern Physics* 92 (3), p. 035002. DOI: 10.

1103/RevModPhys.92.035002. URL: https://link.aps.org/doi/10.1103/RevModPhys.92.035002.

Gregory, J. M. et al. (2004). "A new method for diagnosing radiative forcing and climate sensitivity". In: *Geophysical Research Letters* 31.3, pp. 1–4. DOI: 10.1029/2003GL018747.

Gregory, J. M. et al. (2015). "The inconstancy of the transient climate response parameter under increasing CO_2". In: *Philosophical Transactions of the Royal Society A* 373.2054, p. 20140417. DOI: 10.1098/rsta.2014.0417.

Hartmann, D. L. (2015). *Global physical climatology*. Vol. 103. Newnes.

Huang, Yi and Maziar Bani Shahabadi (2014). "Why logarithmic? A note on the dependence of radiative forcing on gas concentration". In: *Journal of Geophysical Research: Atmospheres* 119.24, pp. 13, 683–13, 689. DOI: 10.1002/2014JD022466. eprint: https://agupubs.onlinelibrary.wiley.com/doi/pdf/10.1002/2014JD022466. URL: https://agupubs.onlinelibrary.wiley.com/doi/abs/10.1002/2014JD022466.

Ingram, W. J. (2010). "A very simple model for the water vapour feedback on climate change". In: *Quarterly Journal of the Royal Meteorological Society* 136.646, pp. 30–40. DOI: 10.1002/qj.546.

Jeevanjee, Nadir et al. (2017). "A perspective on climate model hierarchies". In: *Journal of Advances in Modeling Earth Systems* 9.4, pp. 1760–1771. DOI: 10.1002/2017MS001038. eprint: https://agupubs.onlinelibrary.wiley.com/doi/pdf/10.1002/2017MS001038. URL: https://agupubs.onlinelibrary.wiley.com/doi/abs/10.1002/2017MS001038.

Kluft, L. et al. (2019). "Re-examining the first climate models: Climate sensitivity of a modern radiative-convective equilibrium model". In: *Journal of Climate* 32.23, pp. 8111–8125. DOI: 10.1175/JCLI-D-18-0774.1.

Knutti, Reto et al. (2017). "Beyond equilibrium climate sensitivity". In: *Nature Geoscience* 10.10, pp. 727–736.

Koll, D. D. B. and T. W. Cronin (2018). "Earth's outgoing longwave radiation linear due to H2O greenhouse effect". In: *Proceedings of the National Academy of Sciences* 115.41, pp. 10293–10298. ISSN: 0027-8424. DOI: 10.1073/pnas.1809868115.

Maher, Penelope et al. (2019). "Model Hierarchies for Understanding Atmospheric Circulation". In: *Reviews of Geophysics* 57.2, pp. 250–280. DOI: 10.1029/2018RG000607. eprint: https://agupubs.onlinelibrary.wiley.com/doi/pdf/10.1029/2018RG000607. URL: https://agupubs.onlinelibrary.wiley.com/doi/abs/10.1029/2018RG000607.

Manabe, S. and R. T. Wetherald (1967). "Thermal equilibrium of the atmosphere with a given distribution of relative humidity". In: *Journal of the Atmospheric*

Sciences 24.3, pp. 241–259. DOI: 10.1175/1520-0469(1967)024<0241:TEOTAW>2.0.CO;2.

Marsh, Daniel R. et al. (2016). "Stratospheric ozone chemistry feedbacks are not critical for the determination of climate sensitivity in CESM1(WACCM)". In: *Geophysical Research Letters* 43.8, pp. 3928–3934. DOI: 10.1002/2016GL068344. eprint: https://agupubs.onlinelibrary.wiley.com/doi/pdf/10.1002/2016GL068344. URL: https://agupubs.onlinelibrary.wiley.com/doi/abs/10.1002/2016GL068344.

Meraner, K. et al. (2013). "Robust increase in equilibrium climate sensitivity under global warming". In: *Geophysical Research Letters* 40.22, pp. 5944–5948. DOI: 10.1002/2013GL058118.

Mlawer, E. J. et al. (1997). "Radiative transfer for inhomogeneous atmospheres: RRTM, a validated correlated-k model for the longwave". In: *Journal of Geophysical Research* 102, pp. 16663–16682.

Monteiro, J. M. et al. (2018). "sympl (v. 0.4.0) and climt (v. 0.15.3) – towards a flexible framework for building model hierarchies in Python". In: *Geoscientific Model Development* 11.9, pp. 3781–3794. DOI: 10.5194/gmd-11-3781-2018.

Nowack, Peer J et al. (2015). "A large ozone-circulation feedback and its implications for global warming assessments". In: *Nature Climate Change* 5.1, pp. 41–45.

Pincus, R. et al. (2015). "Radiative flux and forcing parameterization error in aerosol-free clear skies". In: *Geophysical Research Letters* 42.13, pp. 5485–5492. DOI: 10.1002/2015GL064291.

Ramanathan, V. and J. A. Coakley (1978). "Climate modeling through radiative-convective models". In: *Reviews of Geophysics and Space Physics* 16.4, pp. 465–489.

Rennó, Nilton O. (1997). "Multiple equilibria in radiative-convective atmospheres". In: *Tellus A: Dynamic Meteorology and Oceanography* 49.4, pp. 423–438. DOI: 10.1034/j.1600-0870.1997.t01-3-00002.x. eprint: https://onlinelibrary.wiley.com/doi/pdf/10.1034/j.1600-0870.1997.t01-3-00002.x. URL: https://onlinelibrary.wiley.com/doi/abs/10.1034/j.1600-0870.1997.t01-3-00002.x.

Romps, D. M. (2020). "Climate Sensitivity and the Direct Effect of Carbon Dioxide in a Limited-Area Cloud-Resolving Model". In: *Journal of Climate* 33.9, pp. 3413–3429. DOI: 10.1175/JCLI-D-19-0682.1. eprint: https://doi.org/10.1175/JCLI-D-19-0682.1. URL: https://doi.org/10.1175/JCLI-D-19-0682.1.

Satoh, Masaki et al. (2019). "Global cloud-resolving models". In: *Current Climate Change Reports* 5.3, pp. 172–184.

Sobel, A. H. and C. S. Bretherton (2000). "Modeling Tropical Precipitation in a Single Column". In: *Journal of Climate* 13.24, pp. 4378–4392. DOI: 10.1175/1520-0442(2000)013<4378:MTPIAS>2.0.CO;2.

Soden, B. J. et al. (Nov. 2005). "The Radiative Signature of Upper Tropospheric Moistening". In: *Science* 310.5749, pp. 841–844. DOI: 10.1126/science.1115602.

Soden, B. J. et al. (2008). "Quantifying Climate Feedbacks Using Radiative Kernels". In: *Journal of Climate* 21.14, pp. 3504–3520. DOI: 10.1175/2007JCLI2110.1.

Somerville, Richard C. J. and Lorraine A. Remer (1984). "Cloud optical thickness feedbacks in the CO_2 climate problem". In: *Journal of Geophysical Research: Atmospheres* 89.D6, pp. 9668–9672. DOI: 10.1029/JD089iD06p09668. eprint: https://agupubs.onlinelibrary.wiley.com/doi/pdf/10.1029/JD089iD06p09668. URL: https://agupubs.onlinelibrary.wiley.com/doi/abs/10.1029/JD089iD06p09668.

Thuburn, J. and G. C. Craig (2002). "On the temperature structure of the tropical substratosphere". In: *Journal of Geophysical Research: Atmospheres* 107.D2, ACL 10-1–ACL 10-10. DOI: 10.1029/2001JD000448.

Vial, J. et al. (2013). "On the interpretation of inter-model spread in CMIP5 climate sensitivity estimates". In: *Climate Dynamics* 41.11, pp. 3339–3362. DOI: 10.1007/s00382-013-1725-9.

Wing, A. A. et al. (2017a). "Convective Self-Aggregation in Numerical Simulations: A Review". In: *Surveys in Geophysics* 38.6, pp. 1173–1197. DOI: 10.1007/s10712-017-9408-4.

Wing, A. A. et al. (2017b). "Radiative-Convective Equilibrium Model Intercomparison Project". In: *Geoscientific Model Development Discussions* 2017, pp. 1–34. DOI: 10.5194/gmd-2017-213.

Zelinka, M. D. and D. L. Hartmann (2010). "Why is longwave cloud feedback positive?" In: *Journal of Geophysical Research: Atmospheres* 115.D16, p. D16117. DOI: 10.1029/2010JD013817,.

Appendix A

Re-examining the first climate models: Climate sensitivity of a modern radiative-convective equilibrium model

Lukas Kluft, Sally Dacie, Stefan A. Buehler, Hauke Schmidt and Bjorn Stevens

Published online on 4 November 2019 in *Journal of Climate*
https://doi.org/10.1175/JCLI-D-18-0774.1

Contributions: L.K. and S.D. developed the RCE model; L.K. performed the research and analysed the data; L.K. wrote the draft manuscript; all authors contributed to the discussion of the results and the manuscript at all stages.

Abstract

We revisit clear-sky one-dimensional radiative-convective equilibrium (1D-RCE) and determine its equilibrium climate sensitivity to a CO_2 doubling (ECS) and associated uncertainty. Our 1D-RCE model, konrad, uses the Rapid Radiative Transfer Model for GCMs (RRTMG) to calculate radiative fluxes in the same way as in comprehensive climate models. These are verified by a line-by-line radiative transfer model, with which we also investigate their spectral distribution. Changing the model configuration of konrad enables a clear separation between the water vapor and the lapse rate feedbacks, as well as the interaction between the two. We find that the radiative feedback and ECS are sensitive to the chosen relative humidity profile, resulting in an ECS range of 2.09–2.40 K. Using larger CO_2 forcings we find that the

radiative feedback changes up to 10 % for surface temperatures of 291–299 K. Although the ECS is similar to previous studies, it arises from the compensation of a larger clear sky forcing ($4.7\,\mathrm{Wm^{-2}}$) and more strongly negative feedbacks ($-2.3\,\mathrm{Wm^{-2}K^{-1}}$). The lapse rate feedback and the feedback from the interaction of lapse rate and humidity compensate each other, but the degree of compensation depends on the relative humidity profile. Additionally, the temperature profile is investigated in a warming climate. The temperature change at the convective top is half as large as at the surface, consistent with the proportionally higher anvil temperature hypothesis, as long as the humidity is consistently coupled to the temperature profile.

A.1 Introduction

Equilibrium climate sensitivity (ECS), the change in surface temperature in response to a doubling of atmospheric CO_2, is arguably one of the most important quantities when discussing climate change. Since the pioneering work by Manabe and Wetherald (1967), a hierarchy of models has been developed to simulate Earth's reaction to an external forcing. But even for the most simple models in this hierarchy, such as radiative-convective equilibrium under fixed relative humidity, its value is not known with precision (Schlesinger, 1986), which makes constraining ECS for more realistic scenarios a challenge that continues to this day (Stevens et al., 2016).

The simple framework of one-dimensional radiative-convective equilibrium (RCE) is fundamental to the understanding of climate change. Such a framework forms the theoretical backdrop against which more complex models have been developed and compared, and greatly influenced the climate debate since its very beginning (Charney et al., 1979).

In this paper we report on efforts to formulate a precise RCE problem, estimate its ECS, and explore its sensitivity to its numerical formulation and the choice of the assumed relative humidity profile. We assume clear-skies, fixed relative humidity, fixed ozone and a saturated isentropic lapse rate. Not taking clouds into account is a deliberate choice, as their inclusion introduces a considerable number of additional degrees of freedom, which are best tackled separately. The precise formulation of the problem allows other models to be compared to our calculations, thereby establishing a benchmark.

Because it is not immediately clear which relative humidity profile is most representative of the atmosphere‘s response to warming, or even the extent to which RCE is sensitive to the homogeneity assumption implied by the selection of a single relative humidity profile, we explore the sensitivity of our calculations to different profiles of relative humidity. We do so by constructing an ensemble of different humidity distributions, which allows us to explore how the response to greenhouse forcing depends on the assumed profile.

The clear-sky formulation allows us to address the question as to whether there is a state-dependence in the simplest possible representation of the climate system, as has been argued in a number of studies. Meraner et al. (2013), for instance, argue that an enhanced water vapor feedback leads to a state-dependence of the ECS, whereas Colman and McAvaney (2009) find a balancing of water vapor and lapse rate feedback in a warmer climate in a global climate model (GCM).

In most experiments we use a radiation scheme, that trades accuracy for computational efficiency. By using line-by-line radiative transfer simulations we evaluate the fidelity of these base calculations and pinpoint how different radiative feedbacks are distributed spectrally.

Besides its impact on ECS, water vapor also impacts the temperature profile and its evolution in a warming climate. Hartmann and Larson (2002) described its role as a "thermostat" for the temperature of the tops of the deepest clouds in the fixed anvil temperature (FAT) hypothesis. A more general approach that takes changes in static stability into account results in a proportionally higher anvil temperature (Zelinka and Hartmann, 2010, PHAT). Both FAT and PHAT are based on the interplay of clear-sky radiation and water vapor. In our study, the RCE model is run with different vertical relative humidty distributions and forced with a wide range of CO_2 concentrations to quantify its agreement with the FAT, or PHAT, hypothesis.

A.2 Problem formulation

The model is configured in a way to simulate the tropical atmosphere, which is to first order in radiative-convective equilibrium (Popke et al., 2013). Like the original Manabe and Wetherald (1967) model, the new 1D-RCE model is based on a radiation scheme which calculates radiative heating for each atmospheric layer (see Section A.2.1). We apply this heating to determine a provisional temperature profile including a coupled surface temperature. Afterwards this predicted profile is modified through a convective adjustment (see Section A.2.3). If no convective adjustment is made, the model calculates a pure radiative equilibrium, which results in a convectively unstable thermal structure at lower levels of the atmosphere. Finally, the absolute humidity is recalculated based on the new temperature profile and the assumed relative humidity (see Section A.2.2). Alternatively, the model implements the assumption of fixed absolute humidity, if this step is omitted. The steps are repeated iteratively until an equilibrium state is reached. The full model flow is illustrated in Figure A.1. The model, konrad, is developed under the MIT License and available on `github.com/atmtools/konrad`. The simulations in this study have been performed using Version 0.6.6 (Kluft and Dacie, 2019).

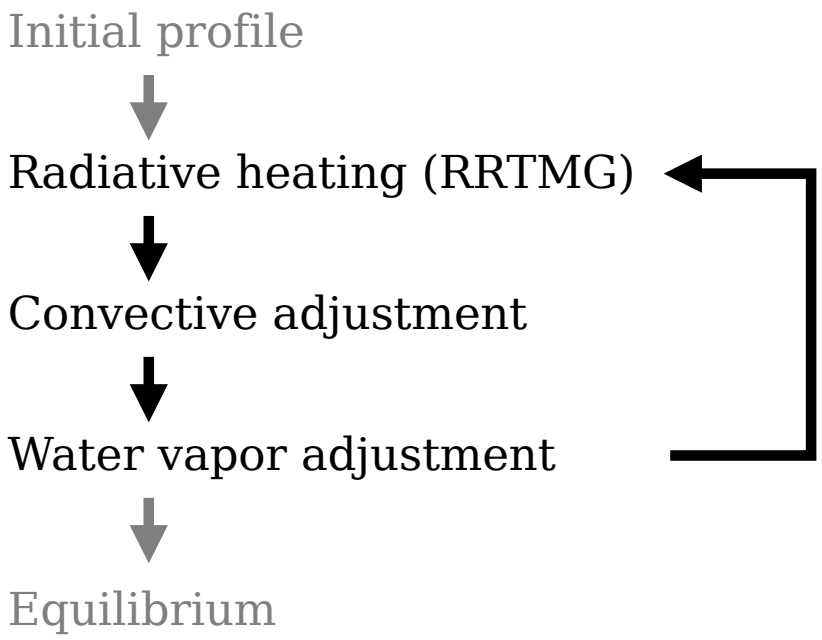

Figure A.1: Illustration of the general model flow. The tasks printed in black are performed iteratively until an equilibrium is found.

A.2.1 Radiation (RRTMG)

For computing radiation, we use the Rapid Radiative Transfer Model for GCMs (RRTMG, Mlawer et al., 1997). RRTMG is used in various GCMs and has been compared to reference radiative transfer models (Pincus et al., 2015). As part of this study, we also compare RRTMG to a benchmark line-by-line code to both test our implementation of RRTMG and assess the sensitivity to the representation of radiative transfer. We use RRTMG through the CliMT Python interface (Monteiro et al., 2018).

Simulations are performed under clear-sky conditions without a diurnal cycle. Thus the choice of the solar geometry attempts to account for these simplifications so as to yield a control simulation that is not too different from conditions representative of the present-day Earth. Just decreasing the solar constant is not sufficient as the optical path through the atmosphere would then be underestimated. Following Cronin (2014) we choose a solar irradiance of $510\,\mathrm{Wm}^{-2}$ and a zenith angle of 47.88°. This results in an incoming shortwave flux of $342\,\mathrm{Wm}^{-2}$ at the top of the atmosphere while also keeping the amount of atmospheric absorption in the right proportion. The latter is important for computing radiative heating rates. The configured incoming radiation is lower than observed values in the tropics to compensate for energy transport to the extratropics, which is missing in konrad (Popke et al., 2013). A description of the resultant temperature profile for a present-day atmospheric composition is given in Section A.3.

RRTMG uses the correlated-k method to allow efficient calculation of fluxes integrated over the full electromagnetic spectrum (Mlawer et al., 1997). The scheme is tuned by using output data from line-by-line models to identify significant parts of the spectrum. The atmospheric states covered by this optimisation are based on present-day climate as well as modified conditions like a doubling of CO_2 concentration. Errors (other than those associated with an incorrect implementation) can occur when the climate differs significantly from the underlying reference (e.g. strongly increased CO_2 or temperatures that exceed precalculated lookup tables). We compared the longwave heating rates for different equilibrium states to the line-by-line radiative transfer model ARTS (Buehler et al., 2018; Eriksson et al., 2011). The differences found are smaller than $0.1\,\mathrm{K\,day^{-1}}$ in the troposphere and smaller than $0.6\,\mathrm{K\,day^{-1}}$ above the tropopause, in agreement with a comparison by Pincus et al. (2015). In addition, a comparison between the radiative feedbacks calculated using RRTMG and ARTS is given in Section A.4.5.

A.2.2 Atmospheric state

The atmosphere is discretized in mass space, and thus we adopt fixed pressure, p, coordinates. The pressure grid is constructed using linearly increasing step sizes in $\ln(p)$ and is approximately given by

$$\ln(p/p_\mathrm{t}) = -\frac{\ln(p_\mathrm{s}/p_\mathrm{t})}{2}\left(\frac{i^2}{N^2} + \frac{i}{N}\right) + \ln(p_\mathrm{s}/p_\mathrm{t}) \tag{A.1}$$

with surface pressure p_s (1000 hPa), pressure at model top p_t (1 Pa), and level index i in the range of [0–N]. This ensures adequate resolution of the upper stratosphere while keeping the majority of the grid points in the troposphere. The latter is important to resolve changes of the convective top and the cold point tropopause height more accurately.

We performed simulations with the number of vertical levels ranging from 100 to 1000. The equilibrium surface temperatures for the lowest and highest vertical resolution differ by about 0.3 K. The difference vanishes with increasing number of levels and only affects absolute temperatures; the climate sensitivity is almost independent of the vertical resolution. In the following, simulations are performed with 500 vertical levels to better resolve the tropopause region. Our model atmosphere includes prescribed vertical profiles of relative humidity and ozone as a function of p. In addition, several gases with constant volume mixing ratios are included (see Table A.1). The trace gas concentrations are chosen to be consistent with the ones used for the Radiative-Convective Equilibrium Model Intercomparison Project (Wing et al., 2017, RCEMIP).

The ozone volume mixing ratio is a function of pressure p and is also chosen to

Table A.1: Volume mixing ratios (VMR) of different gases following the RCEMIP configuration (Wing et al., 2017).

Gas	VMR	
O_2	21	%
CO_2	348	ppmv
CH_4	1650	ppbv
N_2O	306	ppbv
CO	0	—

follow the RCEMIP prescription:

$$\mathrm{O_3}(p) = g_1 \cdot \left(\frac{p}{1\,\mathrm{hPa}}\right)^{g_2} \cdot \exp\left(-\frac{p}{g_3}\right) \tag{A.2}$$

where $g_1 = 3.6478\,\mathrm{ppmv}$, $g_2 = 0.83209$ and $g_3 = 11.3515\,\mathrm{hPa}$. The ozone profile is set in the beginning of the simulation and kept constant throughout the whole simulation. In a companion study, we investigate how changes in this profile affect the equilibrium state (Dacie et al., 2019).

As baseline for the troposphere, we prescribe the vertical relative humidity distribution as a function of p in the same way as Manabe and Wetherald (1967, their Eq. 3):

$$\mathrm{RH}(p) = \mathrm{RH_s} \cdot \frac{p/p_\mathrm{s} - 0.02}{1 - 0.02} \tag{A.3}$$

with relative humidity at the surface $\mathrm{RH_s}$ (77 %) and surface pressure p_s (1000 hPa).

This profile differs from the observed mean state of humidity mostly through the lack of a secondary peak in the upper troposphere. Our motivation for choosing this profile was the comparison to the historical study as well as the simplicity of its specification. In Sections A.4.4 and A.5.2, we explore the consequences of this assumption by investigating how our results change for a vertically uniform relative humidity as well as a profile with a second upper tropospheric humidity peak.

Relative humidity is defined with respect to saturation over water for temperatures above 0 °C and with respect to saturation over ice for temperatures below −23 °C. For intermediate temperatures the equilibrium pressure is computed as a combination of the values over water and ice according to the IFS documentation (ECMWF, 2018, their Eq. 12.13). The equilibrium pressures are calculated using empirical formulations by Murphy and Koop (2005).

The absolute humidity in the stratosphere is kept constant at the volume mixing ratio found at the cold point tropopause which moistens the stratosphere if the tropopause warms with surface warming.

A.2.3 Convective adjustment

Following Manabe and Wetherald (1967), we perform an energy conserving convective adjustment in the troposphere, which acts to cool the surface and warm the atmosphere. Our implementation of the convective adjustment differs from that described in Manabe and Wetherald (1967) and (Liou, 2002), and is described in detail in the Appendix. Briefly, we adjust our temperature profile to the saturated isentropic lapse rate, thus taking into account potential energy changes and contribution from the enthalpy of vaporization associated with convection in a saturated column. Although the relative humidity profile is not saturated, use of the saturated isentropic lapse rate is justified by the assumption that atmospheric convection only occurs in saturated regions which cover a very small fraction of the tropics, but set the temperature profile for the whole tropics in accordance with the weak temperature gradient balance (Sobel and Bretherton, 2000; Charney, 1963).

The way the convective adjustment redistributes energy results in a distinct convective top. Below this convective top the atmosphere is in a state of radiative-convective equilibrium, and above in a state of radiative equilibrium. In a companion study we explore the consequences of relaxing this hard adjustment (Dacie et al., 2019).

The saturated isentropic lapse rate depends on the atmospheric temperature and pressure and is calculated following Bohren and Albrecht (1998, their Eq. 6.111):

$$\frac{\mathrm{d}T}{\mathrm{d}z} = -\frac{g}{c_p}\frac{1 + l_\mathrm{v} w_\mathrm{s}/R_\mathrm{d}T}{1 + l_\mathrm{v}^2 w_\mathrm{s}/c_p R_\mathrm{v} T^2} \tag{A.4}$$

with gravitational acceleration g, isobaric specific heat capacity c_p, enthalpy of vaporization l_v, saturation mixing ratio w_s, gas constants for the surrounding (dry) air R_d and water vapor R_v, and temperature T (see Table A.2 for values). As a simplification l_v is assumed to be constant, thus not vary with temperature.

The assumed lapse rate does not account for fusion enthalpies, and thus neglects contributions from the ice phase. The saturated isentropic lapse rate allows a temperature feedback to be taken into account: In a warming climate, the saturated isentropic lapse rate gets less steep, because ascending saturated air parcels are moister and therefore release more latent heat. Hence, the upper troposphere will warm more than the surface (Manabe and Stouffer, 1980, their Sec. 5). The strength of this lapse rate feedback is quantified alongside other decomposed feedbacks in Section A.4.3.

A.2.4 Surface

We assume a slab surface with an albedo of 0.2 and a heat capacity of 215 $\mathrm{MJ\,m^{-2}\,K^{-1}}$. It can be interpreted as being a well-mixed ocean with a depth of 50 m. The heat capacity damps the surface warming rate and prevents strong vertical temperature

changes which could otherwise occur in single timesteps. The chosen total heat capacity of the surface is a significant tuning parameter for the timescales of the model. For our studies, however, only the equilibrium states are relevant, which we have verified as being independent of the chosen heat capacity. Chosen surface constants are given in Table A.2.

Table A.2: Surface properties and physical constants used within konrad.

Variable	Value	Unit
Enthalpy of vaporization l_v	2,501	$\mathrm{kJ\,kg^{-1}}$
Gravitational acceleration g	9.81	$\mathrm{m\,s^{-2}}$
Gas constant (dry air) R_d	287.06	$\mathrm{J\,kg^{-1}\,K^{-1}}$
Gas constant (water vapor) R_v	461.52	$\mathrm{J\,kg^{-1}\,K^{-1}}$
Specific heat capacity c_p	1,003.5	$\mathrm{J\,K^{-1}}$
Surface albedo	0.2	
Surface depth	50	m
Surface density	1,025	$\mathrm{kg\,m^{-3}}$
Surface heat capacity	4,185.5	$\mathrm{J\,kg^{-1}K^{-1}}$

A.3 Control climate

Figure A.2 shows the equilibrium temperature profiles for different CO_2 concentrations as well as a temperature climatology for comparison. The climatology is based on tropical ocean profiles (30°S–30°N) from the ERA5 reanalysis from January 2008 to May 2018.

Konrad captures the temperature structure of the tropical atmosphere as represented by the ERA5 reanalysis. The failure of konrad to form a sharper temperature inversion at the tropopause is indicative of the absence of several processes, like overshooting convection and the Brewer-Dobson circulation, both of which act to cool the atmosphere in those heights through adiabatic cooling (Dacie et al., 2019). In addition, radiative effects of clouds may also play a role.

Overall the RCE framework allows us to simulate a tropical temperature profile that is in qualitative agreement with observations. The resulting temperature profile and surface temperature are used as reference for our sensitivity studies.

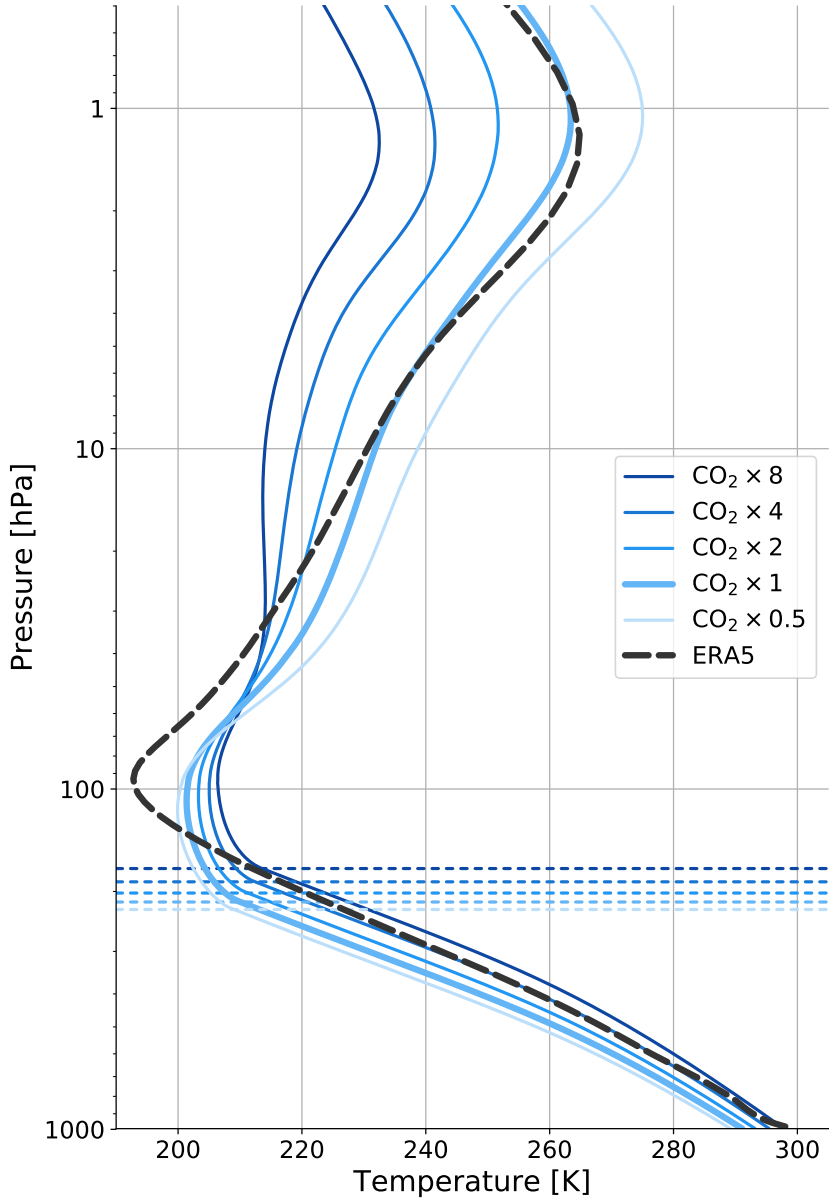

Figure A.2: Equilibrium temperature profiles for different CO_2 concentrations (in colors). For each profile the convective top is marked in dashed lines. The ERA5 tropical temperature climatology is shown in dashed black. The figure is clipped at 0.5 hPa to better visualize the troposphere.

A.4 Radiative feedback

A.4.1 Comparison to historical setup

In a first experiment, we reproduce the simulations by Manabe and Wetherald (1967) with our RCE model. Konrad is run under different assumptions about the humidity and lapse rate to quantify their effects, especially on feedbacks. The different model configurations are forced with a doubling of CO_2. An overview of the corresponding

Table A.3: Equilibrium climate sensitivity [K] for different RCE models and model configurations. The models are konrad, Manabe and Wetherald (1967, MW67), Manabe and Wetherald (1975, MW75), and Hunt and Wells (1979, H79).

Model configuration	konrad	MW67	MW75	H79
Fixed abs. humidity, constant lapse rate ($6.5\,\mathrm{K\,km^{-1}}$)	1.34	1.36	—	—
Fixed rel. humidity, constant lapse rate ($6.5\,\mathrm{K\,km^{-1}}$)	2.65	2.92	—	2.2
Fixed rel. humidity, saturated isentropic lapse rate	2.09	—	1.95	1.81

ECS estimates for konrad as well as historical studies for comparison is given in Table A.3.

The most basic configuration is an RCE with fixed absolute humidity distribution and a constant lapse rate of $6.5\,\mathrm{K\,km^{-1}}$. This configuration has an ECS of 1.34 K, which is in very close agreement with Manabe and Wetherald (1967).

Next, calculations are performed in which the relative humidity is kept constant following the profile specified in Equation A.3. This introduces a positive water vapor feedback that increases the ECS by 1.31 K (+98%) to a value of 2.65 K. This is slightly larger than Manabe and Wetherald (1967), however Manabe and Wetherald (1975) mention a decrease in sensitivity after incorporating a superior radiation model, consistent with the interpretation that the larger value that they obtain arises from differences in the treatment of the radiative transfer.

Finally, the constant lapse rate is replaced by a saturated isentropic lapse rate. This introduces a negative lapse rate feedback which reduces the surface warming by 0.56 K (−21%). The estimate for an RCE with combined water-vapor–lapse-rate feedback is 2.09 K, which is in very good agreement with previous clear-sky estimates.

We conclude that the historical ECS estimates are in good agreement, but slightly higher than our modern implementation of a 1D-RCE model. Remaining differences are likely attributed to discrepancies in the exact composition of the atmosphere or details in the radiative transfer calculations.

A.4.2 Climate radiative feedback

We study the sensitivity of konrad to an abrupt change in the CO_2 concentration by a factor of 0.5, 2, 4 or 8. The instantaneous radiative forcing for a doubling of the CO_2 concentration is $2.92\,\mathrm{W\,m^{-2}}$ for the reference case, which incidentally is in perfect agreement with the mean of the CMIP5 models found by Collins et al. (2006). However, for different model configurations used throughout this study we

find instantaneous forcings between 2.75–3.15 $\mathrm{W\,m^{-2}}$, which we mainly attribute to differences in the temperature profiles (Huang et al., 2016).

In contrast, the effective radiative forcing, which includes stratospheric adjustment, is 4.73 $\mathrm{Wm^{-2}}$ which is larger than the number of 3.7 $\mathrm{Wm^{-2}}$ often cited in literature. Possible reasons for this deviation from global mean estimates are the different temperature structure (Huang et al., 2016), an overestimation of the stratospheric cooling due to a missing ozone-temperature feedback (Shepherd and Jonsson, 2008), and a missing cloud masking effect.

The surface temperature changes for all simulations are given in Table A.4. In addition, the climate feedback parameter

$$\lambda = -\frac{\Delta F_{\mathrm{TOA}}}{\Delta T_{\mathrm{s}}} \tag{A.5}$$

is given. It quantifies how a surface temperature change ΔT_{s} feeds back to the radiative imbalance ΔF_{TOA}.

The climate feedback parameter λ is determined using a method introduced by Gregory et al. (2004): we regress the radiative imbalance at the top of the atmosphere against the surface temperature change for every timestep. The climate feedback parameter is defined as the fitted slope. We exclude the phase of stratospheric adjustment by only using time steps after the net radiative flux reaches its peak. The Gregory method is justified by the almost perfect linear relationship between the radiative imbalance and surface temperature change (see Figure A.3). A comparison of the regression line with the actual data points shows differences that are smaller than 0.05 $\mathrm{Wm^{-2}}$.

Figure A.3 shows the effective radiative forcing F_{eff} (y-intercept of the linear regression), the surface temperature change ΔT_{s} (x-intercept) and climate feedback parameter (slope of the dashed lines) for each simulation. For every doubling in the CO_2 concentration there is an almost constant increase in the simulated surface warming. As a consequence, the total climate feedback parameter is almost constant at 2.33 $\mathrm{Wm^{-2}K^{-1}}$. Differences in the temperature change for different CO_2 doublings are mostly attributable to changes in the forcing (a similar increase in forcing with increasing CO_2 is also reported by Gregory et al. (2015)). Although the radiative transfer becomes increasingly unreliable as one moves away from reference concentrations, konrad runs stably for CO_2 concentrations ranging from 0.25 to 128 times the present-day and the feedbacks do not diverge substantially from those inferred by extrapolating from the conditions shown here.

A.4.3 Decomposed feedbacks

Furthermore, we want to quantify the magnitude of the different radiative feedbacks in konrad. A common approach is the radiative kernel method described by Soden et al. (2008). The method allows response patterns of the Earth system to be

transferred into radiative feedbacks using offline radiative transfer simulations. By contrast, our model formulation and the linearity of the climate feedback allow us to decompose the radiative feedback using different model configurations that leave out specific processes:

- The Planck feedback λ_{PL} is defined by the regression of radiative imbalance against surface temperature for an experiment in which the tropospheric lapse rate and the absolute humidity are fixed constant.

- In the water vapor configuration the relative humidity profile is fixed. The water vapor feedback λ_{WV} is defined as the increase of λ between the Planck and water vapor configuration. Note that, in contrast to existing literature (Soden et al., 2008), this definition of the water vapor feedback does not consider changes in the temperature lapse rate.

- In the lapse rate configuration the temperature profile is convectively adjusted to a saturated isentropic lapse rate that is calculated from the atmospheric state (Equation A.4) but with fixed absolute humidity. The lapse rate feedback λ_{LR} is defined as the increase of λ between the Planck and lapse rate configuration.

- In the reference configuration the atmosphere is adjusted to a coupled saturated isentropic lapse rate and the relative humidity profile is fixed. Here, the water vapor and lapse rate feedbacks act combined, with introduces a non-linear feedback caused by the lapse-rate-driven increase of upper tropospheric humidity. We define the magnitude of this additional water-vapor–lapse-rate feedback $\lambda_{\mathrm{WV}\wedge\mathrm{LR}}$ in a way, that the individual feedbacks add up to the total radiative feedback:

$$\lambda = \lambda_{\mathrm{PL}} + \lambda_{\mathrm{WV}} + \lambda_{\mathrm{LR}} + \lambda_{\mathrm{WV}\wedge\mathrm{LR}} \tag{A.6}$$

  In the definition of Soden et al. (2008) the water vapor feedback includes both λ_{WV} and $\lambda_{\mathrm{WV}\wedge\mathrm{LR}}$.

The decomposed magnitudes of the Planck, water vapor, lapse rate, and water-vapor–lapse-rate feedback are shown in Table A.4.

The non-constancy (increase) of the forcing with successive CO_2 doubling is accompanied by a decrease in the strength of the Planck feedback. In addition, there is a slight strengthening of the water vapor feedback due to increased absorption in the atmospheric window (Koll and Cronin, 2018). The lapse rate feedback in the order of $1.9\,\mathrm{Wm^{-2}K^{-1}}$ also increases for stronger forcings. When evaluating changes in the feedback parameter one has to keep in mind, that different model configurations, including or neglecting different adjustment processes, have different climate sensitivities. As a result, even an eightfold increase in CO_2 does not lead to a large temperature change for the Planck and lapse rate configurations, which are both run with fixed absolute humidity. Considering all adjustment processes

in our standard configuration, the changes of the water vapor and the lapse rate feedback have compensating signs, so that their sum is almost constant (Colman and McAvaney, 2009; Cronin and Wing, 2017; Soden et al., 2008; Vial et al., 2013).

The additional water-vapor–lapse-rate feedback is $1.47\,\mathrm{Wm^{-2}K^{-1}}$ close to the value of the water vapor feedback. The combined $\lambda_{\mathrm{WV}\wedge\mathrm{LR}}$ decreases stronger with the radiative forcing than both λ_{WV} and λ_{LR}. The decrease is in the same order of magnitude as the decrease of the Planck feedback resulting in an almost constant total feedback (compensating signs). Through our feedback decomposition, we find the upper tropospheric component of the water vapor feedback ($\lambda_{\mathrm{WV}\wedge\mathrm{LR}}$) to be essential for the compensation. For our simulations, the climate feedback parameter changes by 2.1 % across simulations spanning four doublings of the atmospheric CO_2 concentration (Table A.4). Over this range the state (temperature) changes by 6.5 K about a working temperature near 295 K. Over the same temperature range, Meraner et al. (2013) estimate a change in sensitivity of 30 % (for their constant 80 % relative humidity profile), which they attribute to changing feedbacks. Konrad's climate sensitivity changes by 26 % for these four doublings, similar to what is reported by Meraner et al. (2013), but almost all of konrad's change can be attributed to the forcing increasing with progressive doublings rather than from changes in feedback. The near constancy of konrad's net feedback arises from a balancing of individual feedbacks, that each change more than their net (see Table A.4). Experiments using different solar forcing, much larger changes in CO_2 (both not shown) or different humidity profiles (see Section A.4.4) — which allow us to push the model to much larger temperatures — eventually experience larger changes in sensitivity. This appears to be indicative of larger changes in feedbacks (rather than just forcings) and is being investigated in a further study.

In general, both the radiative forcing and feedbacks are larger than GCM estimates from radiative kernels. The water vapor and lapse rate feedbacks are almost twice as large in magnitude compared to global mean estimates by Soden et al. (2008, for GCMs) and Cronin and Wing (2017, for 3D-RCE). The discrepancy may, to some extent, arise from differences in the spatial sampling. Cronin and Wing (2017) find much larger water vapor feedbacks, in closer agreement with our results, for high surface temperatures in their small-domain 3D-RCE configuration (personal communication). Another reason may be related to missing cloud masking in our clear-sky configuration. In comprehensive Earth system models the feedback in the middle and lower troposphere might be covered by cloud layers. This interpretation is consistent with the much larger water vapor kernels in the clear as compared to all-sky calculations (Soden et al., 2008, their Fig. 2).

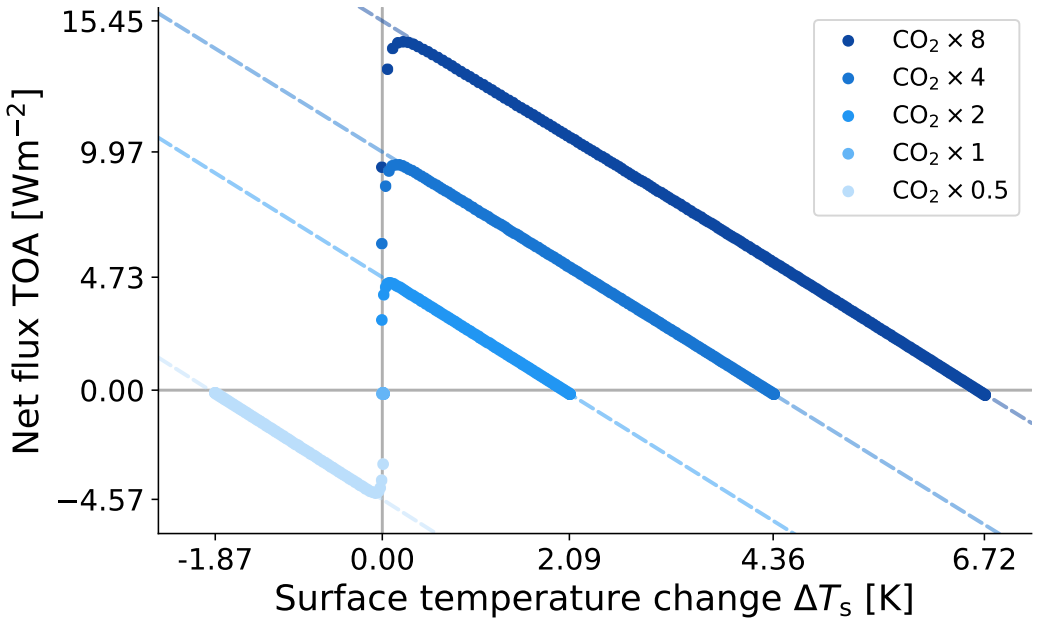

Figure A.3: Top of the atmosphere radiative imbalance against surface temperature change ΔT_s (so called Gregory plot) for different CO_2 concentrations (in colors). A linear regression is shown in dashed lines for each simulation. For different CO_2 concentrations, the x-labels highlight the ΔT_s and the y-labels the effective radiative forcing.

A.4.4 Sensitivity to assumed water vapor distribution

The assumption of a relative humidity profile that is exponentially decaying with height is not realistic for the tropical atmosphere. Observations have shown that especially the upper troposphere is much more humid (Zelinka and Hartmann, 2011) and Minschwaner and Dessler (2004) have found the upper tropospheric humidity to be important for the climate sensitivity. In the absence of overlying clouds, the middle tropospheric humidity also plays an important role in governing the radiative feedback (Soden et al., 2008; Vial et al., 2013). Therefore, we test how our results are affected by the choice of the vertical relative humidity distribution. Although there are more realistic models of the tropical relative humidity distribution (Romps, 2014), we deliberately decide to choose models that are simple in their specification.

In the tropical atmosphere, cloud detrainment causes an upper tropospheric humidity (UTH) peak at the convective top. We modify Equation A.3 by including a UTH peak that is mathematically described using a normal distribution in $\ln(p)$ space:

$$\mathrm{RH}_{\mathrm{UTH}}(p) = r_{\mathrm{uth}} \exp\left(-\pi \ln^2\left(p/p_{\mathrm{uth}}\right)\right) \tag{A.7}$$

with pressure level p_{uth} and magnitude r_{uth} (75 %) of the peak. The actual relative humidity distribution is given by the maximum of the Manabe model (Eq. A.3) and

Table A.4: Surface temperature change ΔT_s [K] and climate feedback λ [$\mathrm{Wm^{-2}K^{-1}}$] for different CO_2 forcings. In addition, the decomposed Planck λ_{PL}, water vapor λ_{WV}, lapse rate λ_{LR}, and combined water-vapor–lapse-rate $\lambda_{WV\wedge LR}$ feedbacks are given.

CO_2	ΔT_s	λ_{PL}	λ_{WV}	λ_{LR}	$\lambda_{WV\wedge LR}$	λ
×0.5	-1.87	-3.76	1.66	-1.86	1.56	-2.37
×2	2.09	-3.63	1.70	-1.88	1.47	-2.34
×4	4.36	-3.55	1.71	-1.90	1.43	-2.32
×8	6.72	-3.48	1.72	-1.92	1.35	-2.32

the UTH peak (Eq. A.7) for each pressure level:

$$\mathrm{RH}(p) = \max\{\mathrm{RH},\ \mathrm{RH}_{\mathrm{UTH}}\} \tag{A.8}$$

The UTH peak is idealized in order to fulfill two requirements: First, a shift of the UTH peak does not change the relative humidity in the lower troposphere, which also has a significant impact on the climate sensitivity and could obscure possible UTH effects. Secondly, a shift of the UTH peak does not change its magnitude. Both requirements are necessary to perform comprehensible sensitivity studies. The UTH peak is coupled to the temperature profile by setting its location p_{uth} equal to the pressure at the convective top as one might expect to happen if convective detrainment levels correlate with the height of the convective top (Zelinka and Hartmann, 2010).

Another approach is to assume a vertically uniform relative humidity distribution, which is often used when constructing atmospheric profiles for radiative feedback simulations (Meraner et al., 2013; Koll and Cronin, 2018; Thuburn and Craig, 2002). We have chosen a vertically uniform relative humidity of 40 % to account for sub-saturated subsidence regions which cover a vast part of the tropics. The chosen distribution also allows us to perform stable simulations over a wide range of radiative forcings. Higher humidities above roughly 60 % produce a runaway feedback in konrad. This is in accordance with Pierrehumbert (1995) who finds the tropical atmosphere to be close to a runaway green house if the fraction of subsidence regions, which act as "radiator fins", decreases. In reality, if the tropics alone were close to a runaway greenhouse state and they did warm more than the rest of the planet, transport to mid/high latitudes would also increase.

Figure A.4 shows the modified relative humidity profiles with UTH peaks at 125, 170 and 225 hPa (green) alongside the Manabe (blue) and the vertically uniform (yellow) distribution. The relative humidity distribution is used to calculate the water vapor amount in the troposphere. In the stratosphere the absolute humidity is fixed to the volume mixing ratio at the cold point tropopause.

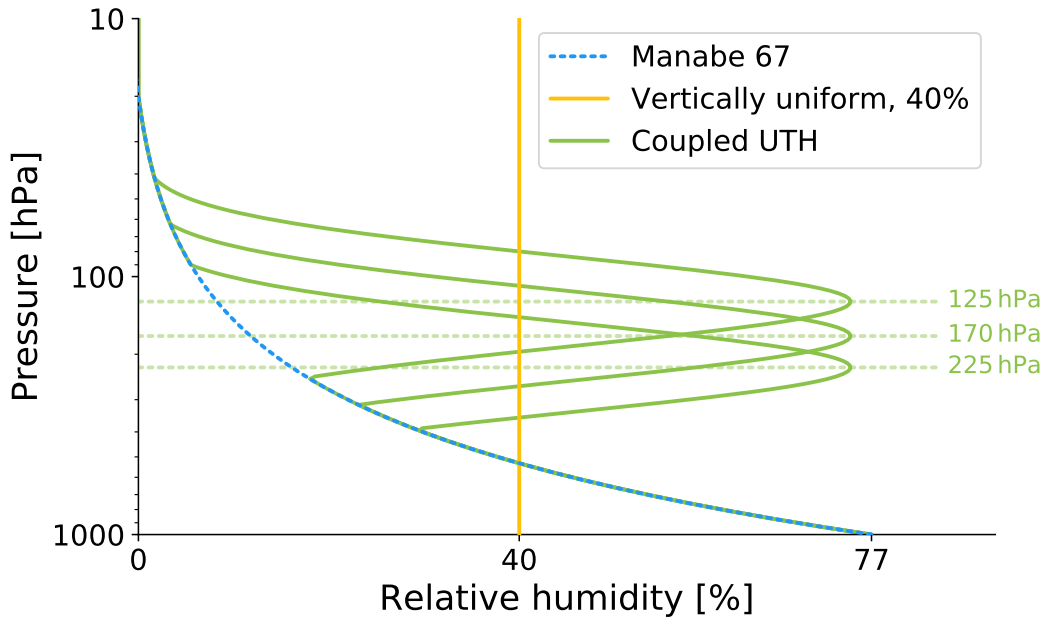

Figure A.4: Idealized vertical distributions of relative humidity: Manabe and Wetherald (1967) model (blue), a vertically uniform relative humidity of 40 % (yellow), and a coupled UTH peak (green, different heights are shown to illustrate how the peak behaves when shifted). The stratospheric water vapor, however, is set constant to the absolute humidity at the cold point tropopause.

Experiments were first performed with different surface humidities for each profile (not shown) and indicate that for a given form of the humidity distribution the feedback varies roughly linearly with the integrated water vapor. This approximate linearity justifies the representation of the tropical atmosphere using a mean humidity profile in a single column model.

Differences in ECS as a function of the given humidity profile are up to 20 %. Some of these differences can be explained by the aforementioned, and near linear, dependence on the integrated water vapor implied by each profile, but the shape of the profile also is important. To explore these effects we decompose the radiative feedbacks (Figure A.5). The Planck feedback is in the order of $-3.5\,\mathrm{Wm^{-2}K^{-1}}$ for all humidity distributions. Small differences arise from the fact that the initial states for each relative humidity distribution differ. The weakening of the Planck feedback for stronger forcings (darker colors) due to increased CO_2 absorption is a robust feature for all configurations.

The water vapor feedback is in the order of $1.7\,\mathrm{Wm^{-2}K^{-1}}$ for all configurations, with the coupled UTH peak giving the strongest feedback of $1.8\,\mathrm{Wm^{-2}K^{-1}}$. The vertically uniform distribution has a slightly lower feedback compared to the other distributions. This is caused by decreased water vapor absorption in the atmospheric window due to the rather low relative humidity of 40 %. All configurations show a

slight increase of the water vapor feedback for stronger radiative forcings, which can be explained by a closing of the atmospheric window between 800–1200 cm^{-1} (Koll and Cronin, 2018).

The additional water-vapor–lapse-rate feedback results from an increase in upper tropospheric humidity associated with the change in temperature lapse rate. The increase in humidity leads to an upward shift of the emission level to a colder temperature, leading to a positive feedback, which we find to be in the range of 1.47–1.71 $\mathrm{Wm}^{-2}\mathrm{K}^{-1}$. For the Manabe and coupled UTH distribution, the relative humidity decreases with height, which limits the upward shift of the emission level. As a result, the water-vapor–lapse-rate feedback decreases under warming. This leads, in combination with an increased Planck feedback, to an almost constant total feedback. For the vertically uniform distribution, however, the water-vapor–lapse-rate feedback is almost constant irrespective of the applied warming. As the Planck feedback is no longer balanced, the total radiative feedback λ tends to show a state-dependence. The increase of the climate feedback between a doubling and an octupling of the CO_2 concentration is 7.4 % for a surface temperature change of about 8 K. Meraner et al. (2013) find an increase in ECS of roughly 30 % for the same temperature range.

In summary, the strength of the individual radiative feedbacks depends on the absolute humidity the atmosphere contains and how that humidity is distributed. A vertically uniform humidity distribution prevents a strengthening of the additional water-vapor–lapse-rate feedback under increased radiative forcing. This leads, in combination with a decreasing Planck feedback, to a slightly larger state-dependence of the total climate feedback than for the reference configuration.

A.4.5 Comparison to a line-by-line radiative transfer model

We perform line-by-line radiative transfer simulations to verify the radiative feedbacks calculated with RRTMG and to gain insight in their spectral distribution. ARTS is used to calculate the outgoing longwave radiation (OLR) spectrum $E_{\mathrm{OLR}}(\nu)$ on a frequency grid that covers 30,000 equidistant grid points between 1–3000 cm^{-1}. Gas absorption was taken into account by using the HITRAN database (Gordon et al., 2017) and the MT_CKD model for the continuum absorption of water vapor, CO_2, and molecular nitrogen (Mlawer et al., 2012, Version 2.52).

We simulate the OLR after the stratospheric adjustment as well as in equilibrium to calculate the spectral radiative feedback λ_ν, which can be integrated to determine the radiative feedback:

$$\lambda = \int \lambda_\nu \, \mathrm{d}\nu = \int \frac{\mathrm{d}E_{\mathrm{OLR}}(\nu)}{\mathrm{d}T_{\mathrm{s}}} \, \mathrm{d}\nu \tag{A.9}$$

Here, the spectral radiative feedback is calculated by dividing the difference of the simulated OLR spectra by the surface temperature change. As ARTS is only capable of simulating the longwave radiative feedback the shortwave component

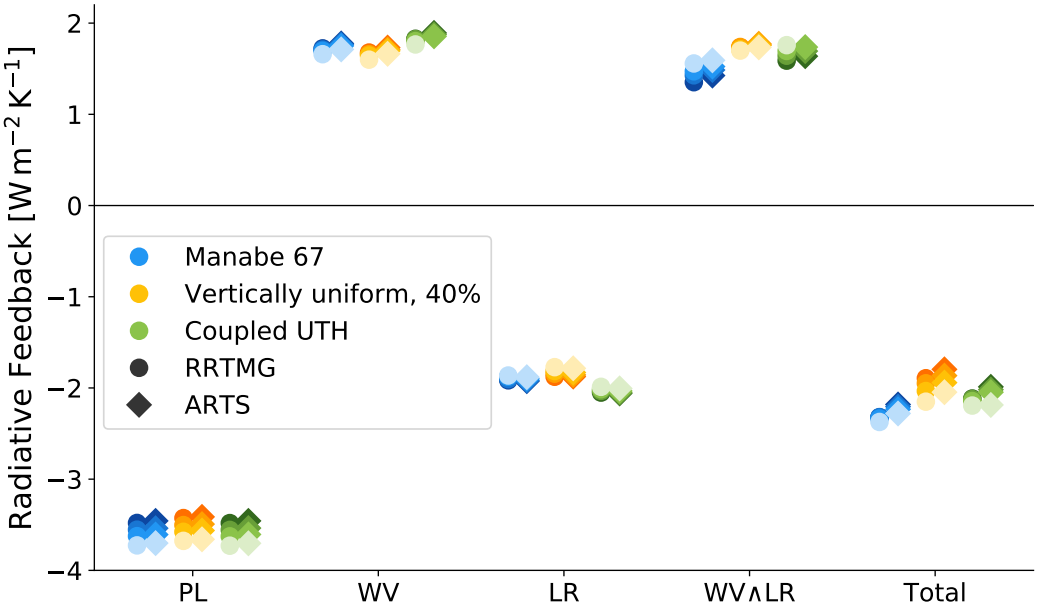

Figure A.5: Decomposed radiative feedbacks for different relative humidity distributions: the reference Manabe and Wetherald (1967) model (blue), a vertically uniform relative humidity of 40 % (yellow), and a coupled UTH peak (green). Feedbacks are calculated using the radiation scheme RRTMG (circles), which is used to run the RCE, and an offline line-by-line model ARTS (diamonds) for comparison. Simulations have been performed with forcings of 0.5, 2, 4 and 8 times CO_2 (darker colors indicate higher CO_2 levels).

is used from RRTMG. The results are shown as diamonds alongside the RRTMG feedbacks (circles) in Figure A.5. The Planck and lapse rate feedbacks are almost the same for ARTS and RRTMG (differences $\leq 1\,\%$). We find, that RRTMG slightly underestimates the water vapor feedback by about 3 % and overestimates the total radiative feedback by about 5 %. The differences seem to be systematic and slightly increase from 4 % to 6 % for a doubling and an octupling of CO_2 respectively. The comparison to the line-by-line model is robust for all vertical humidity distributions regarded in our study.

In addition, the line-by-line simulations can be used to interpret the spectral fingerprint of different radiative feedbacks. Figure A.6 shows the OLR spectrum E_{OLR} for konrad in reference configuration as a qualitative baseline. In addition, the 10 cm^{-1} running mean is shown to smooth the fractal character of the spectrum. The spectrum can be qualitatively divided into three spectral regions, that are of interest for the radiative feedbacks: first an atmospheric window region between 800–1200 cm^{-1}, in which the overall absorption is weak and limited to water vapor absorption in the lower troposphere. Second, the optically thick CO_2 band between 500–800 cm^{-1}, and third, a less absorbent region below 500 cm^{-1} dominated by upper

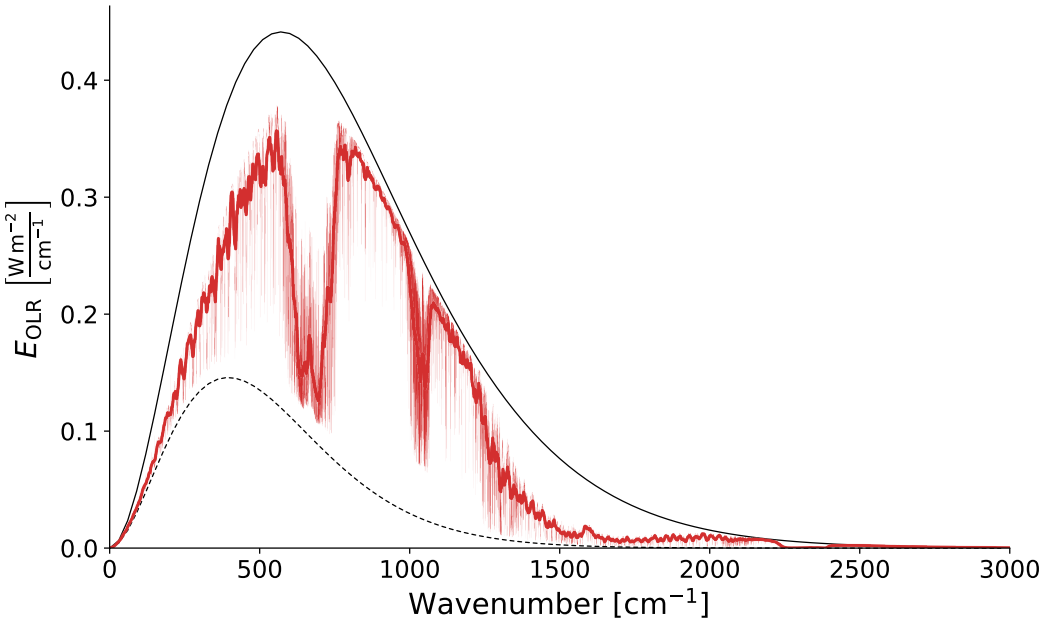

Figure A.6: Outgoing longwave radiation E_{OLR} (thin red line) and the $10\,\mathrm{cm^{-1}}$ running mean (thick red line) as a function of wavenumber. In addition, the black-body radiation B_ν at surface temperature (solid black line) and at cold point temperature (dashed black line) are shown.

tropospheric water vapor absorption.

Figure A.7 shows the spectral radiative feedbacks for different humidity distributions. The results are smoothed using a $10\,\mathrm{cm^{-1}}$ running mean. In the top left panel (PL), results for konrad in Planck configuration are shown. The spectral radiative feedback is almost the same for all humidity distributions, with small differences mainly caused by differences in the initial states. As reference, the radiative feedback of a black-body at surface temperature is shown. The black-body curve envelops the atmospheric Planck feedback, which is significantly decreased by CO_2 and water vapor absorption.

In the top right panel (WV), the spectral water vapor feedback is shown, which is positive throughout the whole spectrum. In the CO_2 band between 500–800 $\mathrm{cm^{-1}}$ the water vapor feedback is close to zero (Ingram, 2010). Differences in the vertical humidity distribution can be directly observed in the spectral space: The vertically uniform distribution is drier in the lower troposphere than the other distributions, which leads to a smaller radiative feedback in the atmospheric window region between 800–1200 $\mathrm{cm^{-1}}$ (Koll and Cronin, 2018). In contrast, the radiative feedback below $500\,\mathrm{cm^{-1}}$ is increased due to higher values of upper tropospheric humidity.

The center left panel (LR) shows the spectral lapse rate feedback. The lapse rate feedback is governed by the temperature profile, therefore the curves are similar for all humidity distributions. The strongest lapse rate feedback is located around

$500\,\mathrm{cm}^{-1}$, where the emission level of the OLR is in the upper troposphere, which warms more than the surface. There is another spectral region near $1300\,\mathrm{cm}^{-1}$ where the emission level is similar, but it constitutes much less radiative feedback due to a smaller temperature dependance of the Planck function there.

The additional combined water-vapor–lapse-rate feedback (WV∧LR) is shown in the center right panel. Like the water vapor feedback, it is positive throughout the whole spectrum, but it is mainly dominant for wavenumbers below $500\,\mathrm{cm}^{-1}$, which corresponds to the upper troposphere. The vertically uniform relative humidity results in the strongest water-vapor–lapse-rate feedback, as a deepening of the troposphere is accompanied by a persistent moistening of the upper troposphere. This leads to the most striking difference in the total spectral radiative feedback, which is the sum of all other feedbacks (bottom left panel): For wavenumbers below $500\,\mathrm{cm}^{-1}$ the radiative feedback for the vertically uniform distribution is decreased by a factor of two compared to the other humidity distributions.

It is worth noting that the division of the traditional water vapor feedback into two terms, WV and WV∧LR, leads to a deeper understanding of the tendency for intermodel differences between water vapor and lapse rate feedbacks to cancel, as noted by many GCM studies: It is really the intermodel difference in LR and WV∧LR feedbacks that tends to cancel, since both are driven by changes in the tropospheric lapse rate.

Furthermore, it is worth noting that the feedback in the far-infrared spectral region below $600\,\mathrm{cm}^{-1}$ dominates the individual LR, WV and WV∧LR feedbacks. Due to compensating effects the total feedback is up to an order of magnitude smaller than the individual feedbacks (Ingram, 2010; Koll and Cronin, 2018). Nonetheless, the total feedback in this region is particularly sensitive to differences in the vertical humidity structure, as it affects the relative strength of the individual feedbacks.

A.5 PHAT mechanism

A.5.1 Historical studies and modern theory

In a next step the vertical temperature structure in and around the tropopause and its evolution under increased CO_2 concentrations is investigated. Early computations of ECS using RCE first started to include clouds on fixed pressure levels (FAP) as this was the easiest approach computationally. It later became apparent that it might be more plausible to consider to fix the high clouds at temperature, rather than pressure levels (Augustsson and Ramanathan, 1977), an idea whose theoretical justification was formulated in terms of the Fixed Anvil Temperature hypothesis (FAT) by Hartmann and Larson (2002). The chosen approach has a significant impact on ECS, leading to estimates ranging from 1.21–2.31 K (Cess, 1976; Ramanathan and Coakley, 1978). Zelinka and Hartmann (2010) have shown that, if anvil clouds

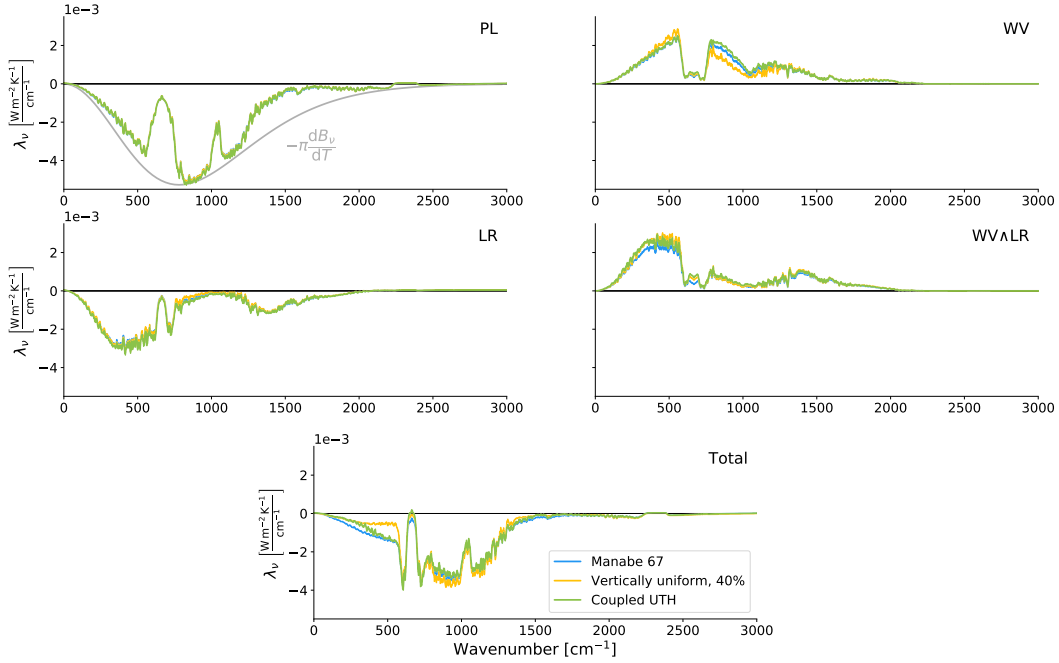

Figure A.7: Decomposed spectral climate feedback as a function of wavenumber. The Planck (PL), water vapor (WV), lapse rate (LR), combined water-vapor–lapse-rate WV∧LR, and total feedbacks have been calculated for different relative humidity distributions. In panel PL, the temperature derivative of the Planck curve at surface temperature is shown as reference.

are associated with the maximum radiatively driven divergence, changes in static stability result in proportionally higher anvil temperatures with increasing surface temperature (PHAT). Latest observations and numerical simulations have shown PHAT to be a more realistic description of changes to cloud top temperatures (Cronin and Wing, 2017; Kuang and Hartmann, 2007; Zelinka and Hartmann, 2010; Zelinka and Hartmann, 2011). As both FAT and PHAT are based on clear-sky radiation, one of them should be verifiable in an RCE framework. We use the temperature at the convective top as proxy for the cloud top temperature and how it might change with surface warming (Figure A.8).

A.5.2 Sensitivity to assumed water vapor distribution

The convective top temperature in our reference configuration (blue circles) increases 1.17 K for a doubling of the CO_2 concentration, which is roughly half the observed surface temperature change of 2.09 K and a fifth of what FAP predicts. The modified humidity distributions with a coupled UTH have a slightly weaker rate of increase of convective top temperature with surface warming. Still they are well described by the PHAT hypothesis. Simulations with larger CO_2 perturbations show that this ratio is robust for a wide range of surface temperature changes, consistent with GCM

findings by Zelinka and Hartmann (2010).

In a follow-up experiment, the UTH peak is prescribed at different pressure levels between 125–225 hPa (every 25 hPa). For these configurations, the present-day equilibrium surface temperatures range from 294.5–296.6 K, which is about 1–3 K warmer than the reference. Every model configuration is forced with consecutive CO_2 doublings between 0.5 and 8 times the present-day concentration. The presence of a fixed UTH peak has a significant impact on the evolution of convective top temperatures (Figure A.8): Increasing the humidity below the level of the convective top (light green triangles) increases the rate of change of convective top temperature with surface warming. A UTH peak that is fixed at the initial convective top pressure is close to the PHAT line, but has a slightly weaker rate of increase of convective top temperature with surface warming.

Most striking are the results for the two peaks located above the convective top (dark triangles). The additional humidity above the convective top increases the radiative cooling leading to a FAT-like behaviour. The highest UTH peak at 125 hPa even leads to negative changes in convective top temperatures, although this simulation is not realistic, as the UTH peak is rather high, which results in a too moist lower stratosphere.

We conclude that the PHAT hypothesis describes the change in convective top temperatures well for the vertical humidity distributions considered in our study. When using a more complex vertical humidity distribution its structure has to be coupled to the temperature profile in order to not artificially distort the PHAT mechanism.

A.5.3 Climate sensitivity

The effect of the UTH peaks on ECS can be inferred from the x-distance between values in Figure A.8. Coupling the UTH peak to the convective top results in ECS estimates in between the Manabe and a vertically uniform relative humidity distribution. A fixed UTH peak at different prescribed heights results in a spread of ECS estimates from 2.28–2.77 K, or feedbacks of -2.24 to $-1.79\,\mathrm{Wm^{-2}K^{-1}}$ respectively. This should be considered when trying to setup "realistic" 1D-RCE simulations using observed relative humidity distributions: Imposing a UTH peak that is not properly coupled to the temperature structure will impact the ECS estimate.

A.6 Summary and conclusions

We defined and performed benchmark calculations for a simple clear-sky RCE problem. The ECS for konrad in reference configuration with fixed relative humidity, fixed ozone and saturated isentropic lapse rate is 2.09 K, slightly higher than the 1.95 K found by Manabe and Wetherald (1975).

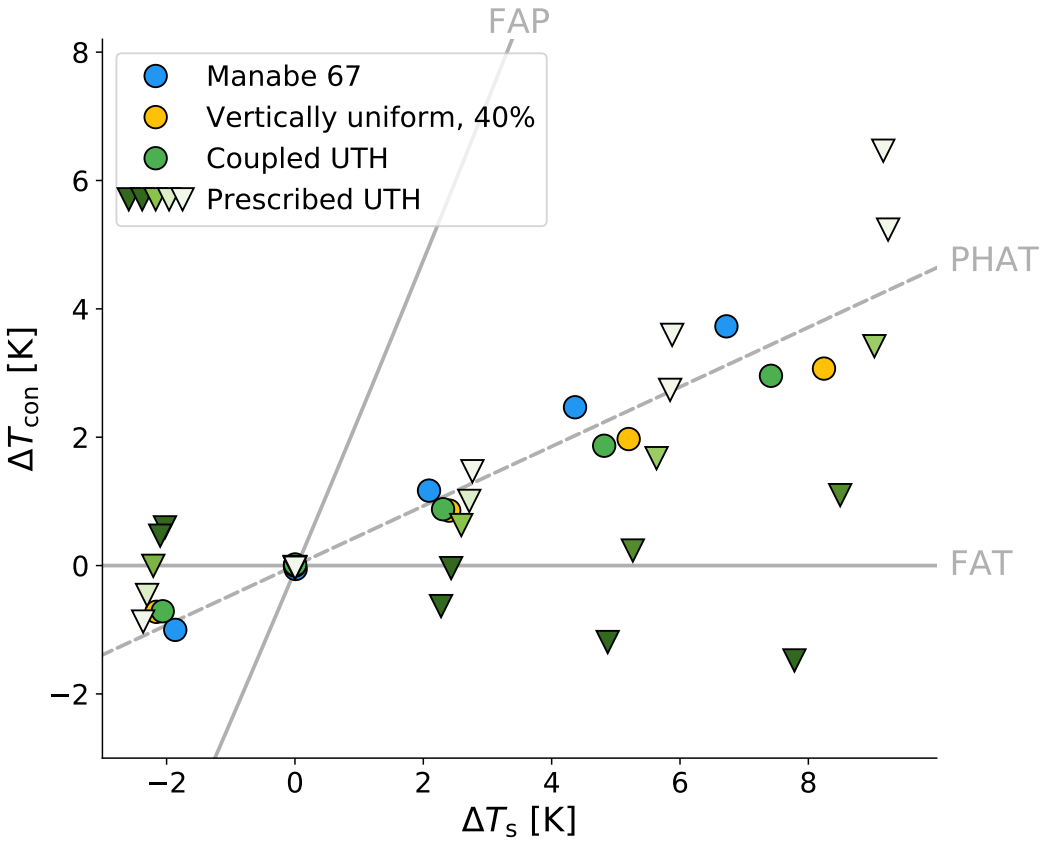

Figure A.8: Change in convective top temperature ΔT_{con} against change in surface temperature ΔT_{s} for different CO_2 concentrations and vertical humidity distributions: Manabe 67 (blue circles), a vertically uniform humidity distribution (yellow circle), UTH peak coupled to the convective top (green cirlce), UTH peak at fixed prescribed heights between 125–225 hPa (triangles; darker colors represent lower pressure [higher altitude]). The reference PHAT curve is following Zelinka and Hartmann (2010, their Fig. 9).

Furthermore, we quantified the decomposed climate radiative feedbacks. The water vapor and lapse rate feedback are almost twice as large in magnitude as global mean estimates, but compensate each other. Possible reasons for their increase are differences in the model region and a missing cloud masking effect in our clear-sky model. We find that a substantial component of the combined water-vapor and lapse-rate feedbacks comes from the interaction of the two, which explains their degree of compensation in more complex models.

A comparison of different vertical relative humidity distributions results in ECS ranges from 2.09–2.40 K with corresponding radiative feedbacks of −2.34 to $-2.03\,\mathrm{Wm^{-2}K^{-1}}$. Changes in the radiative feedbacks with successive doublings are less than 10 % for a range of surface temperatures between 291–299 K. The strength of the state-dependence itself depends on the shape of the assumed humidity profile:

A vertically uniform relative humidity distribution results in an almost constant combined water-vapor–lapse-rate feedback for different forcings. As the Planck feedback decreases with stronger CO_2 forcings, the total feedback shows tendencies of a state-dependency.

The results are robust for a range of CO_2 forcing from 0.5–8 times the present-day concentration, i.e. four doublings. A comparison of our results using the radiation scheme RRTMG with the line-by-line model ARTS shows differences in the total climate feedback of about 5 %. The errors are of systematic nature and do not substantially increase for stronger forcings.

The change in convective top temperatures is half as much as the surface temperature change and is consistent with the PHAT hypothesis. The tendency of konrad to verify PHAT rests on the assumption that the relative humidity profile is coupled to the temperature profile, and departures from PHAT become apparent if they become decoupled.

All results are limited to clear-sky radiation. Future work will explore the implications of extra degrees of freedom as introduced by clouds.

Acknowledgments. Contains modified Copernicus Climate Change Service Information (ERA5) [2018].
We thank Manfred Brath for many frutiful discussions and for providing the set-up for the ARTS simulations.
Stefan Buehler was supported through the Cluster of Excellence CliSAP (EXC177), Universität Hamburg, funded by the German Science Foundation (DFG).
Kerry Emanuel developed an RCE model with the name CONRAD in the 1990s. We thank him for happily allowing us to use the name `konrad` for our new model.
We thank Robert Pincus for fruitful discussion.
The model source is developed under the MIT License and available on `github.com/atmtools/konrad`.

Appendix

A convective adjustment is performed if the atmosphere is unstable to convection in the troposphere. The adjustment fixes the temperatures according to a specified lapse rate, given in $\mathrm{K\,km^{-1}}$, which is converted to $\mathrm{K\,Pa^{-1}}$ under the assumption of hydrostatic equilibrium.

The change in enthalpy of an atmospheric layer due to a temperature change $(\Delta T)_{\mathrm{atm}}$ is proportional to $\rho c_p (\Delta T)_{\mathrm{atm}}\,\mathrm{d}z$, where ρ is the density, c_p is the heat capacity at constant pressure (also assumed to be constant with height) and $\mathrm{d}z$ is the thickness of the layer. This can be rewritten (assuming hydrostatic equilibrium) in pressure coordinates as $\frac{c_p}{g}(\Delta T)_{\mathrm{atm}}\mathrm{d}p$, where g is the gravitational acceleration, assumed to be constant with height. The corresponding energy change of the surface

is $\Delta z \rho_s c_s (\Delta T)_s$, where Δz is the thickness of the surface layer, ρ_s the density and c_s the heat capacity. The surface layer is assumed to be at one temperature (it does not vary with depth). Then, the energy conservation equation required for the convective adjustment is

$$\int_0^{p_s} \frac{c_p}{g} (\Delta T)_{atm} dp + \Delta z \rho_s c_s (\Delta T)_s = 0 \tag{A.10}$$

The integral runs over the whole atmosphere, but there is no convective adjustment above a certain pressure level, p_c, called the convective top. The convective temperature change in the atmosphere $(\Delta T)_{atm}$ is a function of pressure and is given by

$$\Delta T_{atm}(p) = T_{con}(p) - T_{rad}(p) \tag{A.11}$$

where T_{rad} is the temperature profile after radiative heating rates have been applied and T_{con} is the convectively adjusted temperature profile

$$T_{con}(p) = \begin{cases} T_{con,s} - \int_p^{p_s} \gamma_p \, dp & \text{if} \quad p > p_c \\ T_{rad}(p) & \text{if} \quad p \leq p_c \end{cases} \tag{A.12}$$

Here, γ_p is the change in temperature of the convective profile with pressure ($\gamma_p > 0$), p_s is the surface pressure and $T_{con,s}$ is the convectively adjusted surface temperature. We assume that convection acts to cool the surface and warm the troposphere and thus do not allow convection to cool the atmosphere. The pressure level p_c is defined as the highest atmospheric level (lowest pressure level) which satisfies $T_{con}(p_c) \geq T_{rad}(p_c)$ and no convective adjustment is applied above this level.

The equations above, or similar equations with a different treatment of the surface, hold for the convective adjustment of many previous RCE models, including Manabe and Wetherald (1967) and MacKay and Khalil (1991). However, our computational implementation differs. We start with by guessing a surface temperature, $T_{con,s}$ and calculate the corresponding convectively adjusted temperature profile according to equation A.12. Then we test how close this profile is to satisfying energy conservation (equation A.10). We update our surface temperature and repeat the procedure iteratively, until we find a surface temperature and corresponding profile which satisfy equation A.10.

Bibliography

Augustsson, T. and V. Ramanathan (1977). "A Radiative-Convective Model Study of the CO2 Climate Problem". In: *Journal of the Atmospheric Sciences* 34.3, pp. 448–451. DOI: 10.1175/1520-0469(1977)034<0448:ARCMSO>2.0.CO;2.

Bohren, C. F. and B. A. Albrecht (1998). *Atmospheric thermodynamics*. Oxford University Press, Inc.

Buehler, S. A. et al. (2018). "ARTS, the atmospheric radiative transfer simulator — version 2.2, the planetary toolbox edition". In: *Geoscientific Model Development* 11.4, pp. 1537–1556. DOI: 10.5194/gmd-11-1537-2018.

Cess, R. D. (1976). "Climate Change: An Appraisal of Atmospheric Feedback Mechanisms Employing Zonal Climatology". In: *Journal of the Atmospheric Sciences* 33.10, pp. 1831–1843. DOI: 10.1175/1520-0469(1976)033<1831:CCAAOA>2.0.CO;2.

Charney, J. G. (1963). "A note on large-scale motions in the tropics". In: *Journal of the Atmospheric Sciences* 20.6, pp. 607–609.

Charney, J. G. et al. (1979). *Carbon dioxide and climate: a scientific assessment*. Tech. rep.

Collins, W. D. et al. (2006). "Radiative forcing by well-mixed greenhouse gases: Estimates from climate models in the Intergovernmental Panel on Climate Change (IPCC) Fourth Assessment Report (AR4)". In: *Journal of Geophysical Research* 111, D14317. DOI: 10.1029/2005JD006713.

Colman, R. and B. McAvaney (2009). "Climate feedbacks under a very broad range of forcing". In: *Geophysical Research Letters* 36.1. DOI: 10.1029/2008GL036268.

Cronin, T. W. (2014). "On the Choice of Average Solar Zenith Angle". In: *Journal of the Atmospheric Sciences* 71.8, pp. 2994–3003. DOI: 10.1175/JAS-D-13-0392.1.

Cronin, T. W. and A. A. Wing (2017). "Clouds, Circulation, and Climate Sensitivity in a Radiative-Convective Equilibrium Channel Model". In: *Journal of Advances in Modeling Earth Systems* 9.8, pp. 2883–2905. DOI: 10.1002/2017MS001111.

Dacie, Sally et al. (Sept. 2019). "A 1D RCE Study of Factors Affecting the Tropical Tropopause Layer and Surface Climate". In: *Journal of Climate* 32.20, pp. 6769–6782. ISSN: 0894-8755. DOI: 10.1175/JCLI-D-18-0778.1. URL: https://doi.org/10.1175/JCLI-D-18-0778.1.

ECMWF (2018). “IFS Documentation CY45R1”. In: ECMWF. Chap. Part IV: Physical processes. URL: https://www.ecmwf.int/node/18714.

Eriksson, P. et al. (2011). “ARTS, the atmospheric radiative transfer simulator, Version 2”. In: *Journal of Quantitative Spectroscopy and Radiative Transfer* 112.10, pp. 1551–1558. DOI: 10.1016/j.jqsrt.2011.03.001.

Gordon, I. E. et al. (2017). “The HITRAN2016 molecular spectroscopic database”. In: *Journal of Quantitative Spectroscopy and Radiative Transfer* 203, pp. 3–69. DOI: 10.1016/j.jqsrt.2017.06.038.

Gregory, J. M. et al. (2004). “A new method for diagnosing radiative forcing and climate sensitivity”. In: *Geophysical Research Letters* 31.3, pp. 1–4. DOI: 10.1029/2003GL018747.

Gregory, J. M. et al. (2015). “The inconstancy of the transient climate response parameter under increasing CO_2”. In: *Philosophical Transactions of the Royal Society A* 373.2054, p. 20140417. DOI: 10.1098/rsta.2014.0417.

Hartmann, D. L. and K. Larson (2002). “An important constraint on tropical cloud - climate feedback”. In: *Geophysical Research Letters* 29.20, pp. 12-1–12-4. DOI: 10.1029/2002GL015835.

Huang, Y. et al. (2016). “Inhomogeneous radiative forcing of homogeneous greenhouse gases”. In: *Journal of Geophysical Research: Atmospheres* 121.6, pp. 2780–2789. DOI: 10.1002/2015JD024569.

Hunt, B. G. and N. C. Wells (1979). “An assessment of the possible future climatic impact of carbon dioxide increases based on a coupled one-dimensional atmospheric-oceanic model”. In: *Journal of Geophysical Research: Oceans* 84.C2, pp. 787–791. DOI: 10.1029/JC084iC02p00787.

Ingram, W. J. (2010). “A very simple model for the water vapour feedback on climate change”. In: *Quarterly Journal of the Royal Meteorological Society* 136.646, pp. 30–40. DOI: 10.1002/qj.546.

Kluft, Lukas and Sally Dacie (Mar. 2019). *atmtools/konrad: A radiative-convective equilibrium model for Python.* DOI: 10.5281/zenodo.2597967. URL: https://doi.org/10.5281/zenodo.2597967.

Koll, D. D. B. and T. W. Cronin (2018). “Earth’s outgoing longwave radiation linear due to H2O greenhouse effect”. In: *Proceedings of the National Academy of Sciences* 115.41, pp. 10293–10298. ISSN: 0027-8424. DOI: 10.1073/pnas.1809868115.

Kuang, Z. and D. L. Hartmann (2007). “Testing the Fixed Anvil Temperature Hypothesis in a Cloud-Resolving Model”. In: *Journal of Climate* 20.10, pp. 2051–2057. DOI: 10.1175/JCLI4124.1.

Liou, K. N. (2002). *An Introduction to Atmospheric Radiation.* Academic Press.

MacKay, R.M. and M.A.K. Khalil (1991). "Theory and development of a one dimensional time dependent radiative convective climate model". In: *Chemosphere* 22.3, pp. 383–417. ISSN: 0045-6535. DOI: 10.1016/0045-6535(91)90326-9.

Manabe, S. and R. J. Stouffer (1980). "Sensitivity of a global climate model to an increase of CO2 concentration in the atmosphere". In: *Journal of Geophysical Research: Oceans* 85.C10, pp. 55290–5554. DOI: 10.1029/JC085iC10p05529.

Manabe, S. and R. T. Wetherald (1967). "Thermal equilibrium of the atmosphere with a given distribution of relative humidity". In: *Journal of the Atmospheric Sciences* 24.3, pp. 241–259. DOI: 10.1175/1520-0469(1967)024<0241:TEOTAW>2.0.CO;2.

— (1975). "The Effects of Doubling the CO2 Concentration on the climate of a General Circulation Model". In: *Journal of the Atmospheric Sciences* 32.1, pp. 3–15. DOI: 10.1175/1520-0469(1975)032<0003:teodtc>2.0.co;2.

Meraner, K. et al. (2013). "Robust increase in equilibrium climate sensitivity under global warming". In: *Geophysical Research Letters* 40.22, pp. 5944–5948. DOI: 10.1002/2013GL058118.

Minschwaner, K. and A. E. Dessler (2004). "Water Vapor Feedback in the Tropical Upper Troposphere: Model Results and Observations". In: *Journal of Climate* 17, pp. 1272–1282. DOI: 10.1175/1520-0442(2004)017<1272:WVFITT>2.0.CO;2.

Mlawer, E. J. et al. (1997). "Radiative transfer for inhomogeneous atmospheres: RRTM, a validated correlated-k model for the longwave". In: *Journal of Geophysical Research* 102, pp. 16663–16682.

Mlawer, E. J. et al. (2012). "Development and recent evaluation of the MT_CKD model of continuum absorption". In: *Philosophical Transactions of the Royal Society A* 370.1968, pp. 2520–2556. DOI: 10.1098/rsta.2011.0295.

Monteiro, J. M. et al. (2018). "sympl (v. 0.4.0) and climt (v. 0.15.3) – towards a flexible framework for building model hierarchies in Python". In: *Geoscientific Model Development* 11.9, pp. 3781–3794. DOI: 10.5194/gmd-11-3781-2018.

Murphy, D. M. and T. Koop (2005). "Review of the vapour pressures of ice and supercooled water for atmospheric applications". In: *Quarterly Journal of the Royal Meteorological Society* 131.608. DOI: 10.1256/qj.04.94.

Pierrehumbert, R. T. (1995). "Thermostats, Radiator Fins, and the Local Runaway Greenhouse". In: *Journal of the Atmospheric Sciences* 52.10, pp. 1784–1806. DOI: 10.1175/1520-0469(1995)052<1784:TRFATL>2.0.CO;2.

Pincus, R. et al. (2015). "Radiative flux and forcing parameterization error in aerosol-free clear skies". In: *Geophysical Research Letters* 42.13, pp. 5485–5492. DOI: 10.1002/2015GL064291.

Popke, D. et al. (2013). "Climate and climate change in a radiative-convective equilibrium version of ECHAM6". In: *Journal of Advances in Modeling Earth Systems* 5.1, pp. 1–14. DOI: 10.1029/2012MS000191.

Ramanathan, V. and J. A. Coakley (1978). "Climate modeling through radiative-convective models". In: *Reviews of Geophysics and Space Physics* 16.4, pp. 465–489.

Romps, D. M. (2014). "An Analytical Model for Tropical Relative Humidity". In: *Journal of Climate* 27.19, pp. 7432–7449. DOI: 10.1175/JCLI-D-14-00255.1. URL: https://doi.org/10.1175/JCLI-D-14-00255.1.

Schlesinger, M. E. (1986). "Equilibrium and transient climatic warming induced by increased atmospheric CO2". In: *Climate Dynamics* 1.1, pp. 35–51. ISSN: 1432-0894. DOI: 10.1007/BF01277045.

Shepherd, T. G. and A. I. Jonsson (2008). "On the attribution of stratospheric ozone and temperature changes to changes in ozone-depleting substances and well-mixed greenhouse gases". In: *Atmospheric Chemistry and Physics* 8.5, pp. 1435–1444. DOI: 10.5194/acp-8-1435-2008.

Sobel, A. H. and C. S. Bretherton (2000). "Modeling Tropical Precipitation in a Single Column". In: *Journal of Climate* 13.24, pp. 4378–4392. DOI: 10.1175/1520-0442(2000)013<4378:MTPIAS>2.0.CO;2.

Soden, B. J. et al. (2008). "Quantifying Climate Feedbacks Using Radiative Kernels". In: *Journal of Climate* 21.14, pp. 3504–3520. DOI: 10.1175/2007JCLI2110.1.

Stevens, B. et al. (2016). "Prospects for narrowing bounds on Earth's equilibrium climate sensitivity". In: *Earth's Future* 4.11, pp. 512–522. DOI: 10.1002/2016EF000376.

Thuburn, J. and G. C. Craig (2002). "On the temperature structure of the tropical substratosphere". In: *Journal of Geophysical Research: Atmospheres* 107.D2, ACL 10-1–ACL 10-10. DOI: 10.1029/2001JD000448.

Vial, J. et al. (2013). "On the interpretation of inter-model spread in CMIP5 climate sensitivity estimates". In: *Climate Dynamics* 41.11, pp. 3339–3362. DOI: 10.1007/s00382-013-1725-9.

Wing, A. A. et al. (2017). "Radiative-Convective Equilibrium Model Intercomparison Project". In: *Geoscientific Model Development Discussions* 2017, pp. 1–34. DOI: 10.5194/gmd-2017-213.

Zelinka, M. D. and D. L. Hartmann (2010). "Why is longwave cloud feedback positive?" In: *Journal of Geophysical Research: Atmospheres* 115.D16, p. D16117. DOI: 10.1029/2010JD013817,.

— (2011). "The observed sensitivity of high clouds to mean surface temperature anomalies in the tropics". In: *Journal of Geophysical Research* 116.D23, p. D23103. DOI: 10.1029/2011JD016459,.

Appendix B

Temperature-dependent clear-sky feedbacks in radiative-convective equilibrium

Lukas Kluft, Sally Dacie, Manfred Brath, Stefan A. Buehler, and Bjorn Stevens

Rejected with invitation for resubmission in *Geophysical Research Letters*
Preprint published online on 28 June 2020
https://doi.org/10.1002/essoar.10503468.1

Contributions: L.K. and S.D. developed the RCE model; L.K. performed the research and analysed the data; L.K. wrote the draft manuscript; all authors contributed to the discussion of the results and the manuscript at all stages.

Abstract

We quantify the temperature-dependence of clear-sky radiative feedbacks in a tropical radiative-convective equilibrium model. The longwave radiative fluxes are computed using a line-by-line radiative transfer model to ensure accuracy in very warm and moist climates. The one-dimensional model is tuned to surface temperatures between 285 and 313 K by modifying a surface enthalpy sink, which does not directly interfere with radiative fluxes in the atmosphere. The total climate feedback increases from -1.7 to $-0.8\,\mathrm{Wm^{-2}K^{-1}}$ for surface temperatures up to 305 K due to a strengthening of the water-vapor feedback. The temperature-dependence maximizes at surface temperatures around 297 K, which is close to the present-day tropical mean temperature. At surface temperatures above 305 K, the atmosphere becomes fully opaque and the radiative feedback is almost constant. This near-constancy is in agreement with a

theoretical model of the water-vapor feedback presented by Ingram (2010), but in disagreement with other modeling studies.

Plain Language Summary

Climate sensitivity, the change in surface temperature in response to a doubling of atmospheric CO_2, is one of the most important quantities when discussing climate change. Our current understanding is that this surface warming depends on the current state of the climate system.

We analyze how temperature affects the climate sensitivity by running a simple climate model at different surface temperatures. We find that the climate sensitivity is stronger at warmer temperatures, i.e. that a warmer climate system warms more, in agreement with other climate models. However, we find that this temperature-dependence vanishes at temperatures above 305 K (32°C). While previous modeling studies did not find this behavior because of their simplified representation of radiative processes in the atmosphere, our findings are consistent with a conceptual model of climate sensitivity.

B.1 Introduction

The state-dependence of the climate feedback, that is its change with surface temperature, is of great interest when studying climate change. It has to be taken into account when comparing global climate models among each other or with historical observations. Although recent work focuses on changes to cloud feedbacks due to changes in self-aggregation, cloud amount, or cloud height (Cronin and Wing, 2017; Hohenegger and Stevens, 2016; Becker and Stevens, 2014), there is also discussion about a temperature-dependence to the more fundamental clear-sky radiative feedbacks.

Meraner et al. (2013) find a robust increase of the climate feedback by analyzing an ensemble of artificial atmosphere profiles covering surface temperatures from 280 to 310 K. They attribute changes to a strengthening of the water-vapor feedback. This is in line with the work of Koll and Cronin (2018), who analyzed changes in the spectral outgoing longwave radiation. They found a closing of the atmospheric emission window due to increased continuum absorption caused by the abundance of water vapor at higher temperatures. Romps (2020) used a cloud-resolving model to run simulations for a vast range of surface temperatures to find the corresponding equilibrium CO_2 concentrations. They confirm the increase of the climate feedback with temperature up to 308 K; at higher surface temperatures they find a decrease of the climate feedback estimates.

In Kluft et al. (2019), we analyzed changes of clear-sky radiative feedbacks in a one-dimensional radiative-convective equilibrium (RCE) model by consecutive

doublings of the CO_2 concentration between 0.5 to 8 times a reference concentration. This study was the first to compare the response of RCE using offline line-by-line radiative transfer calculations. They agreed well with the fast radiation scheme RRTMG (Mlawer et al., 1997) in the temperature regimes examined, as well as allowing us to gain insight into the spectral dependence of the clear-sky feedbacks.

Because there is no evidence that RRTMG is valid over such a wide range of temperatures and good reason to think it might not be, we here replace the longwave component of the radiative transfer scheme with the line-by-line model ARTS. In contrast to Kluft et al. (2019) the line-by-line model is used online to calculate the heating rates used to force the RCE model.

We sample a wide range of surface temperatures by introducing a surface enthalpy sink. We argue that this method is best suited to analyze state-dependencies, as it does not affect the radiative balance in ways other than by changing the surface temperature, which is intended. This, and the use of line-by-line radiative transfer, allows us to push the model to higher temperatures — outside of the range where commonly used radiative transfer schemes have been validated, and where past studies hinted at a runaway greenhouse effect.

B.2 Tuning the model to different climate states

To analyze temperature-dependencies the observed climate model needs to be tuned to different equilibrated initial states. In principle, this can be achieved by changing any boundary condition of the system, like the solar constant or the surface albedo. For simpler models, like 1D-RCE, it is also possible to modify the relative humidity distribution. However, this raises the intrinsic problem that it is no longer obvious if changes in a quantity result from the modified state or the modified boundary condition itself. We will illustrate this by discussing modifications of the solar constant, the relative humidity, and the poleward enthalpy transport.

Adjusting the solar constant is a straight-forward approach to tune the surface temperature of an RCE model. This method has a long history for many types of climate models (Budyko, 1969). Using this technique it is possible to cover a wide range of surface temperatures. However, a reduction in insolation has an impact on the shortwave fluxes and the derived shortwave heating rates. The shortwave heating directly controls the stratospheric temperature profile, which is in a pure radiative equilibrium.

Another way to tune the surface temperature is to adjust the relative humidity: Decreasing the amount of water vapor at a given temperature allows more radiation to be emitted into space, which reduces the simulated surface temperature. We used this method in Kluft et al. (2019) to simulate tropical surface temperatures while keeping the sun-geometry and solar constant at global mean values. However, tuning

the relative humidity modulates the strength of the water-vapor feedback as it limits the absolute amount of atmospheric water vapor at a given temperature.

We here pursue a third option to simulate different surface temperature states in an RCE model, namely adding a surface enthalpy sink (Drotos et al., 2020; Hohenegger and Stevens, 2016; Becker and Stevens, 2014). From the global zonal mean radiation budget we know that there is very significant export of heat from the tropics to the extratropics by the atmosphere and ocean circulations (Niiler, 1992). Modeling studies suggest that it is strong enough to balance the increased insolation in the tropics compared to the extra-tropics, which results in a net energy uptake close to the global mean insolation (Popke et al., 2013). For simplicity, we assume that all the heat transport takes place in the ocean. The ocean enthalpy sink is implemented by accounting for an offset when deriving the surface heating from the energy budget:

$$\frac{\partial T_\mathrm{s}}{\partial t} = \frac{\Delta F_\mathrm{rad} + F_\mathrm{con} + F_\mathrm{s}}{C_\mathrm{s}} \tag{B.1}$$

with surface temperature T_s, net radiative fluxes at the surface ΔF_rad, convective flux F_con, surface heat capacity C_s, and ocean enthalpy sink F_s.

The temperature-dependence of the radiative feedback can be studied by using different values for F_s. Changing F_s changes the outgoing longwave radiation through the surface temperature only, but does not directly affect other radiative quantities. This is a decisive advantage compared to the tuning methods mentioned earlier. From the point of view of radiative fluxes, this method is very similar to fixing the surface temperature at given values and comparing the outgoing longwave radiation (Meraner et al., 2013). Both methods result in a non-zero net radiation at the top of the atmosphere. However by specifying F_s to achieve a desired surface temperature one explicitly models the surface equilibration, consistent with an assumed ocean heat capacity, thus preserving the time-scales of the adjustment process (Cronin and Emanuel, 2013).

B.3 Model configuration

The simulations in this study have been performed using the RCE model konrad (Kluft and Dacie, 2020, p. v0.8.0), which is developed under the MIT License and is freely available on `github.com/atmtools/konrad`.

We replace the longwave component of the radiation scheme with the line-by-line radiative transfer model ARTS (Buehler et al., 2018; Eriksson et al., 2011). ARTS is used to calculate the longwave radiative fluxes based on 32,768 equidistant frequency points between 10–3,250 cm^{-1}. Gas absorption is based on the HITRAN database (Gordon et al., 2017) and the MT_CKD model for the continuum absorption of water vapor, CO_2, and molecular nitrogen (Mlawer et al., 2012, Version 2.52).

B.3.1 Boundary conditions

The boundary conditions are following Kluft et al. (2019) in general: The reference CO_2 concentration is 348 ppmv and the surface albedo is set to 0.2 to account for some reflection by clouds, that are not included in our clear-sky model. We have decreased the ocean depth to 1 m to accelerate the simulations and compensate for the increased computational cost due to the line-by-line radiative transfer.

There are some modifications to more closely represent the tropical atmosphere. The solar constant is set to $551.58\,\mathrm{Wm}^{-2}$ at an zenith angle of 42.05° resulting in an insolation of $409.6\,\mathrm{Wm}^{-2}$ (Wing et al., 2017; Cronin, 2014). The relative humidity in the troposphere is set to 80 % up to the cold-point tropopause above which the volume mixing ratio is kept constant. This ensures a reasonable amount of humidity in the upper troposphere, which is key for the interaction of lapse-rate and water-vapor feedbacks (Minschwaner and Dessler, 2004; Kluft et al., 2019).

We introduce an enthalpy sink in the ocean mixed layer, which we imagine as a poleward ocean enthalpy transport, which allows our model to be tuned to virtually any surface temperature. A surface heat transport F_s of $-66\,\mathrm{Wm}^{-2}$ results in a net energy influx that is equal to the global mean of around $343\,\mathrm{Wm}^{-2}$ and a surface temperature of 298 K in agreement with a GCM study by Popke et al. (2013).

B.3.2 Treatment of ozone

Konrad does not include atmospheric chemistry, hence atmospheric trace gases are represented as vertical profiles of volume mixing ratios that do not change with time. This assumption is reasonable for most trace gases, especially if the atmospheric state does not deviate much from the present-day climate.

The latter assumption, however, is not valid when simulating atmospheres with much warmer surface temperatures than currently observed. The expansion of the troposphere in a warming climate in combination with an ozone profile that is fixed on pressure levels causes high ozone concentrations in the upper troposphere. In the real atmosphere, chemical depletion acts as a ozone sink in the troposphere.

If this is not taken into account, a fixed ozone profile acts as a “temperature ramp” for the tropopause and leads to an unreasonable increase of tropopause temperatures in a warming climate (Dacie et al., 2019). A fixed prescribed ozone profile leads to a runaway in our simulations, when temperatures exceed 300 K (not shown). This runaway is most likely caused by the unphysical high ozone concentrations in the upper troposphere.

Therefore, we couple the ozone profile to a reference level in the atmospheric temperature profile, which we have chosen to be the cold-point tropopause. When this reference level changes its altitude the ozone profile is shifted by the same amount in logarithmic pressure coordinates.

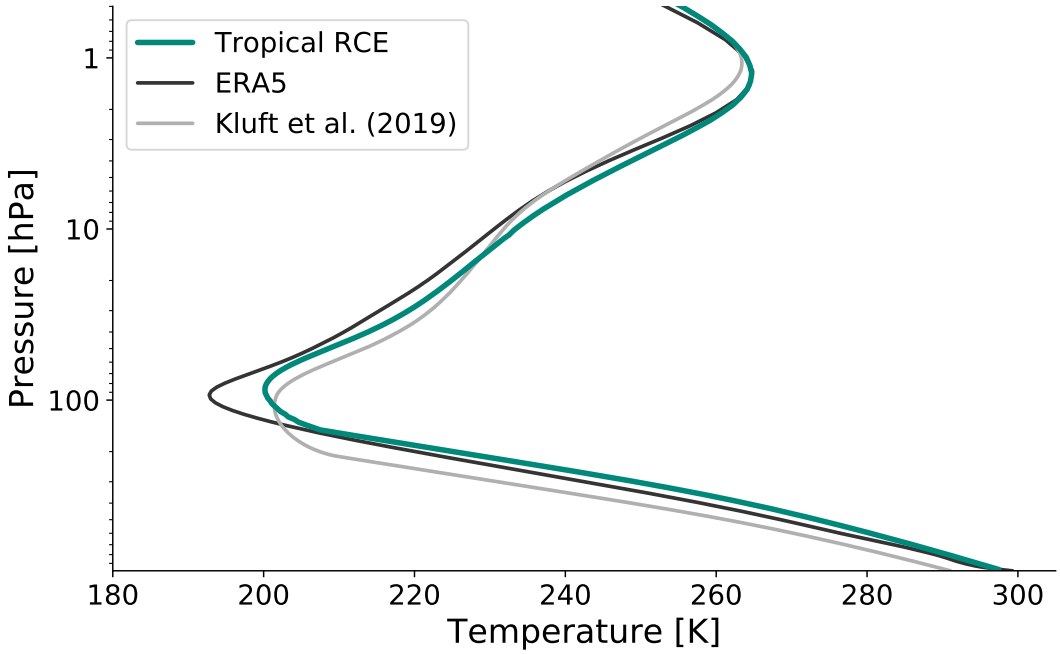

Figure B.1: Equilibrium temperature profile as a function of atmospheric pressure for an RCE with global insolation (Kluft et al., 2019, grey), our tropical configuration (teal), and a tropical reanalysis (black). The figure is clipped at 0.5 hPa to better visualize the troposphere.

B.3.3 Reference climate

Figure B.1 shows the temperature profiles for two RCE configurations as well as a climatology based on tropical ocean profiles (30°S–30°N) from ERA5 from January 2008 to May 2018. The new tropical configuration (teal) leads to an improved representation of the shape of the tropical tropopause in comparison to Kluft et al. (2019, grey). This can be attributed to both an increased insolation which warms the stratosphere around the ozone layer, as well as an increased longwave cooling around the cold point due to a higher water vapor content.

In summary, the modified model configuration better represents the tropical mean atmosphere (boundary conditions) and allows accurate studies of clear-sky radiative feedbacks for a wide range of surface temperatures (line-by-line radiation).

Our model does not include some of the features known to influence the state of the observed tropical atmosphere, for instance clouds, or variations of humidity, both of which have spatial variability linked to tropical circulation systems. Nonetheless we believe the insights derived from our study are informative about the actual atmosphere, and about more complex models used to study it.

B.4 Radiative feedbacks

B.4.1 Decomposed climate feedbacks

We want to quantify the (surface) temperature-dependence for different radiative clear-sky feedbacks. Following Gregory et al. (2004), let us take the radiative feedback parameter λ from the linear regression of the top-of-the-atmosphere radiative imbalance ΔF_{TOA} against the surface temperature change ΔT_{s}:

$$\lambda = -\frac{\Delta F_{\mathrm{TOA}}}{\Delta T_{\mathrm{s}}} \tag{B.2}$$

The linear regression is performed after the stratosphere has adjusted to the instantaneous forcing by only using values 30 days after the radiative imbalance reaches its maximum (Gregory plots for different surface temperatures are shown in the supporting information).

Following Kluft et al. (2019) the total radiative feedback is decomposed into its components, the Planck λ_{PL}, the water-vapor λ_{WV}, the lapse rate λ_{LR}, and an additional water-vapor–lapse-rate feedback $\lambda_{\mathrm{WV}\wedge\mathrm{LR}}$ by using separate model runs in which individual feedback mechanisms are selectively turned on or off.

The only exception from this calculation is the Planck feedback. The simplest model configuration, which is used to determine the Planck feedback, still has a coupled ozone profile. In combination with a discrete vertical grid, this can lead to small differences in how model runs react to a given radiative forcing. These differences propagate through the whole feedback decomposition, because the Planck feedback is subtracted from every other radiative feedback. Therefore, we are using an analytical model to determine the Planck feedback based on the boundary conditions of our model.

In general, the Planck feedback λ_{PL} is defined as the response of the outgoing longwave radiation J to changes in the surface temperature T_{s}. For a black-body, J is described by the Stefan-Boltzmann law

$$J = \sigma T^4 \tag{B.3}$$

with Stefan-Boltzmann constant σ and temperature T. For the Earth's atmosphere, the Planck feedback λ_{PL} can be approximated using the temperature derivative of the Stefan-Boltzmann law but using the effective temperature T_ϵ:

$$-\lambda_{\mathrm{PL}} = \frac{\partial J}{\partial T} \approx 4\sigma T_\epsilon^3 \tag{B.4}$$

The effective temperature of the climate system T_ϵ is defined as the temperature of a black-body that would emit the same amount of radiation. In equilibrium, T_ϵ is constrained by the net amount of shortwave radiation that enters the system, and can be computed by again using the Stefan-Boltzmann law:

$$T_\epsilon = \sqrt[4]{\frac{(1-\alpha)\cdot S_0 \cdot \cos(\theta) - F_{\mathrm{s}}}{\sigma}} \tag{B.5}$$

with surface albedo $\alpha = 0.2$, solar constant $S_0 = 551.58\,\mathrm{Wm}^{-2}$, solar zenith angle $\theta = 42.05°$, and ocean enthalpy sink F_s. By using Equation B.4 and B.5 we are able to compute the Planck feedback for the boundary conditions of each ensemble member.

Konrad is run with different values of the surface enthalpy sink ranging from -52 to $-82\,\mathrm{Wm}^{-2}$, which results in surface temperatures between 313 K and 285 K. After euqilibrating to the initial conditions, every model configuration is forced with a doubling of the CO_2 concentration. Figure B.2a shows the strength of the individual radiative feedbacks as a function of the initial surface temperature. In addition, a cubic spline is fitted for every individual feedback (solid lines) to estimate its temperature-dependence, i.e. $\partial\lambda/\partial T_\mathrm{s}$ (shown in Figure B.2b).

The magnitude of the water-vapor (blue) and lapse-rate (red) feedbacks are larger than in Kluft et al. (2019). This difference can be attributed to the modified model configuration and, on its own, is evidence of a state-dependent climate feedback.

The water-vapor feedback (blue) increases from 2.3 to $3.7\,\mathrm{Wm}^{-2}\mathrm{K}^{-1}$ with increasing surface temperature. Meraner et al. (2013) find a similar increase of the ECS in their RCE-like calculations, which they also attribute to changes in the water-vapor feedback. Koll and Cronin (2018) performed line-by-line radiative transfer calculations to show that this is mainly driven by rapidly increasing continuum absorption in the atmospheric window. We find the same increase of the water-vapor feedback for surface temperatures up to 305 K. At even higher surface temperatures, when the atmospheric window is fully opaque, the water-vapor feedback is almost constant.

The decreasing temperature lapse rate in a warmer climate (Manabe and Stouffer, 1980, Sec. 5) leads to a strengthening of the lapse-rate feedback (red) from -1.8 to -6.5 $\mathrm{Wm}^{-2}\mathrm{K}^{-1}$. The increase of lapse-rate feedback is more than twice as large as that of the water-vapor feedback, but balanced by its self-induced moistening of the upper troposphere, the WV$\wedge$LR feedback (Colman and McAvaney, 2009; Minschwaner and Dessler, 2004; Kluft et al., 2019). The balancing of both feedbacks is robust for all simulated surface temperatures (compare LR and WV$\wedge$LR in Figure B.2).

As a result, the total radiative feedback λ (grey) is dominated by the temperature-dependence of the water-vapor feedback and increases from -1.7 to $-0.8\,\mathrm{Wm}^{-2}\mathrm{K}^{-1}$ for surface temperatures between 285 K and 308 K. For the same temperature range, Meraner et al. (2013) find a higher increase of from -2 to $-0.67\,\mathrm{Wm}^{-2}\mathrm{K}^{-1}$ (estimated from their Figure 4). The strongest temperature-dependence is found for surface temperatures around 297 K (Figure B.2b), which is about the present-day tropical mean temperature. We attribute this to a rapid closing of the atmospheric window due to absorption by the water-vapor self-continuum (Koll and Cronin, 2018).

"Understanding the extreme spread in climate sensitivity within the Radiative-Convective Equilibrium Model Intercomparison Project" (n.d.) quantified the mean clear-sky feedback for 16 cloud-resolving models in RCE configuration. Their estimate

of $-0.8\,\mathrm{Wm^{-2}K^{-1}}$ is in perfect agreement with our estimate at comparable surface temperatures, which indicates a robustness of the tropical clear-sky feedbacks.

For surface temperatures above 305 K the total radiative feedback is almost constant. This behavior has been predicted by Ingram (2010) in a qualitative model of the atmospheric water-vapor feedback: When the atmosphere is cold and dry, emission from the surface escapes to space. This emission increases as surface temperature increases giving a negative (Planck) feedback. As the atmosphere warms, it becomes more moist and optically thick. Eventually, the atmospheric window closes and emission from the surface is irrelevant because it no longer reaches space. Then, as the atmosphere warms and moistens, the optical depth increases and the emission layer shifts upwards. The increase in optical depth is controlled by the equilibrium water vapor pressure, which is a function of temperature. Assuming that temperatures in the troposphere are set by a lapse rate that is also a function of temperature (approximately true for the moist adiabat), the optical depth is a function of temperature only. As a result, the emission layer shifts upwards approximately maintaining a fixed temperature. In this case, the amount of emission does not change and we have zero feedback irrespective of further atmospheric warming.

Though the qualitative model suggests a zero feedback, we find a non-zero total feedback in our simulations. Ingram (2010) assumes that water vapor is the only relevant greenhouse gas and that it becomes opaque in the entire spectrum. In our model other gases like CO_2 are included and emission from these gases as well as the surface (in parts of the spectrum that are not opaque) can also affect the total feedback. This allows the climate system to increase its emission at certain wavenumbers (Section B.5) and maintain a negative total feedback.

B.4.2 Discussion of state-dependence at high temperatures

In general, we find a robust increase of the total climate feedback for temperatures between 285 and 305 K which is in agreement with modeling studies by Meraner et al. (2013) and Romps (2020). However, differences emerge at high surface temperatures. Both studies find a stronger increase of the total radiative feedback which is followed by a decrease (more negative) at surface temperatures above 308 K.

To understand these differences we repeated the simulations using the radiation scheme RRTMG, which has been used by the two studies, to compute both longwave and shortwave heating rates. Figure B.3a shows the decomposed radiative feedbacks for konrad using RRTMG (dashed lines) versus those calculated using ARTS (solid lines). An estimate of the temperature-dependence when using RRTMG is shown in the supporting information.

When using RRTMG the total feedback changes about 79 % from -1.72 to $-0.36\,\mathrm{Wm^{-2}K^{-1}}$ for surface temperatures of 285 K and 308 K respectively. This

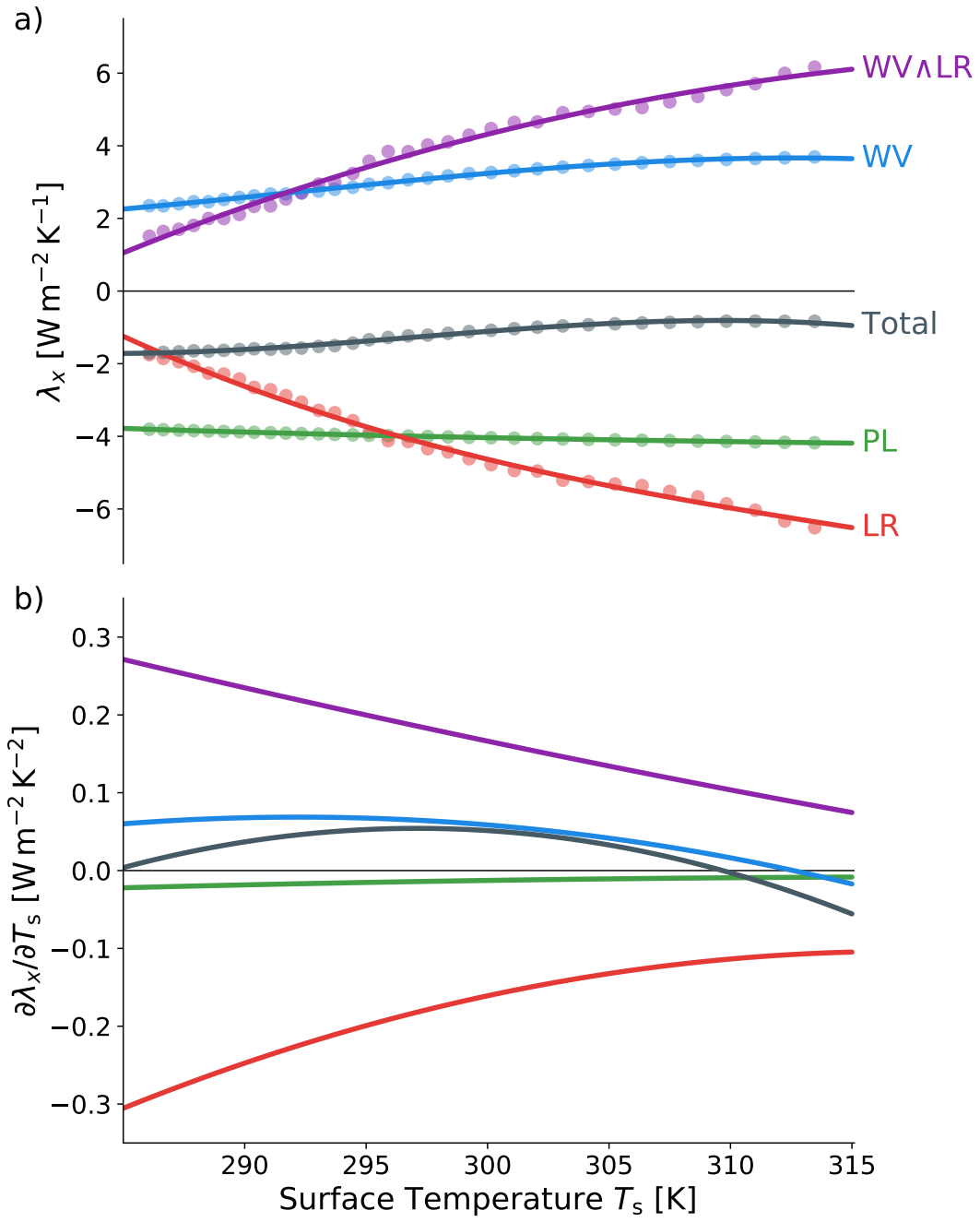

Figure B.2: **a)** Decomposed Planck (PL, green), water-vapor (WV, blue), lapse rate (LR, red), combined water-vapor—lapse-rate (WV∧LR, purple), and total feedback (gray) as function of surface temperature. Cubic fits for each data set are plotted as solid lines. **b)** The cubic fits are used to determine the surface-temperature derivative for each feedback individually. Positive values denote surface temperatures at which a radiative feedback increases.

change is about 1.5 times larger than for ARTS, which changes only 52 % from -1.72 to $-0.82\,\mathrm{Wm^{-2}K^{-1}}$ for the same temperature range. This is caused by an imbalance of the negative lapse-rate feedback and its upper-tropospheric counterpart (WV$\wedge$LR) when using RRTMG. In general, the magnitude of the lapse-rate feedback is only half as large as for the line-by-line calculations.

The simulated temperature profile is following the saturated isentropic lapse rate and exceeds the temperature validity range of RRTMG in the upper troposphere for surface temperatures above 308 K (Figure B.3b). As a result the pre-calculated lookup tables are out of bounds, which causes errors in the computed radiative fluxes. This threshold is consistent with the surface temperatures at which the radiative feedback decreases again. The modeling studies by Meraner et al. (2013) and Romps (2020) find a decrease in their feedback estimates at 310 K and 308 K respectively, which indicates that they are also exceeding the validity range of RRTMG.

It is worth noting, that RRTMG uses look up tables which are valid for surface temperatures as high as 320 K, but due to the construction of the look up tables at surface temperatures above 308 K the moist-adiabat implies mid- and upper-tropospheric temperatures which are out of bounds, leading to substantial errors. Therefore, when using RRTMG for surface temperatures above 308 K, one has to adapt the underlying lookup tables, as for example done by Popp et al. (2015), or use a different radiative transfer model.

B.5 Spectral radiative feedbacks

As discussed above, the near-constancy of the total climate feedback at high temperatures is in line with the qualitative model of Ingram (2010). The conceptual model predicts a zero radiative feedback in spectral regions that are both dominated by water vapor and fully opaque. These conditions are fulfilled for a large part of the spectrum at high surface temperatures. Koll and Cronin (2018) find a rapid closing of the atmospheric window at surface temperatures above 300 K, because the abundance of water vapor increases continuum absorption. We want to illuminate the validity of the theoretical model by calculating spectrally resolved radiative feedbacks.

The line-by-line radiative transfer model ARTS is used to simulate two outgoing longwave radiation (OLR) spectra, one after the stratospheric adjustment, and one in equilibrium, which are used to derive the spectral radiative feedback λ_ν:

$$\lambda_\nu = \frac{\Delta E_{\mathrm{OLR}}(\nu)}{\Delta T_\mathrm{s}} \tag{B.6}$$

with change in OLR $\Delta E_{\mathrm{OLR}}(\nu)$ and surface temperature change ΔT_s.

Figure B.4 shows the total spectral feedback as a function of wavenumber ν (see supporting information for decomposed spectral feedbacks). There is a strong temperature-dependence of the spectral feedback in the atmospheric window between

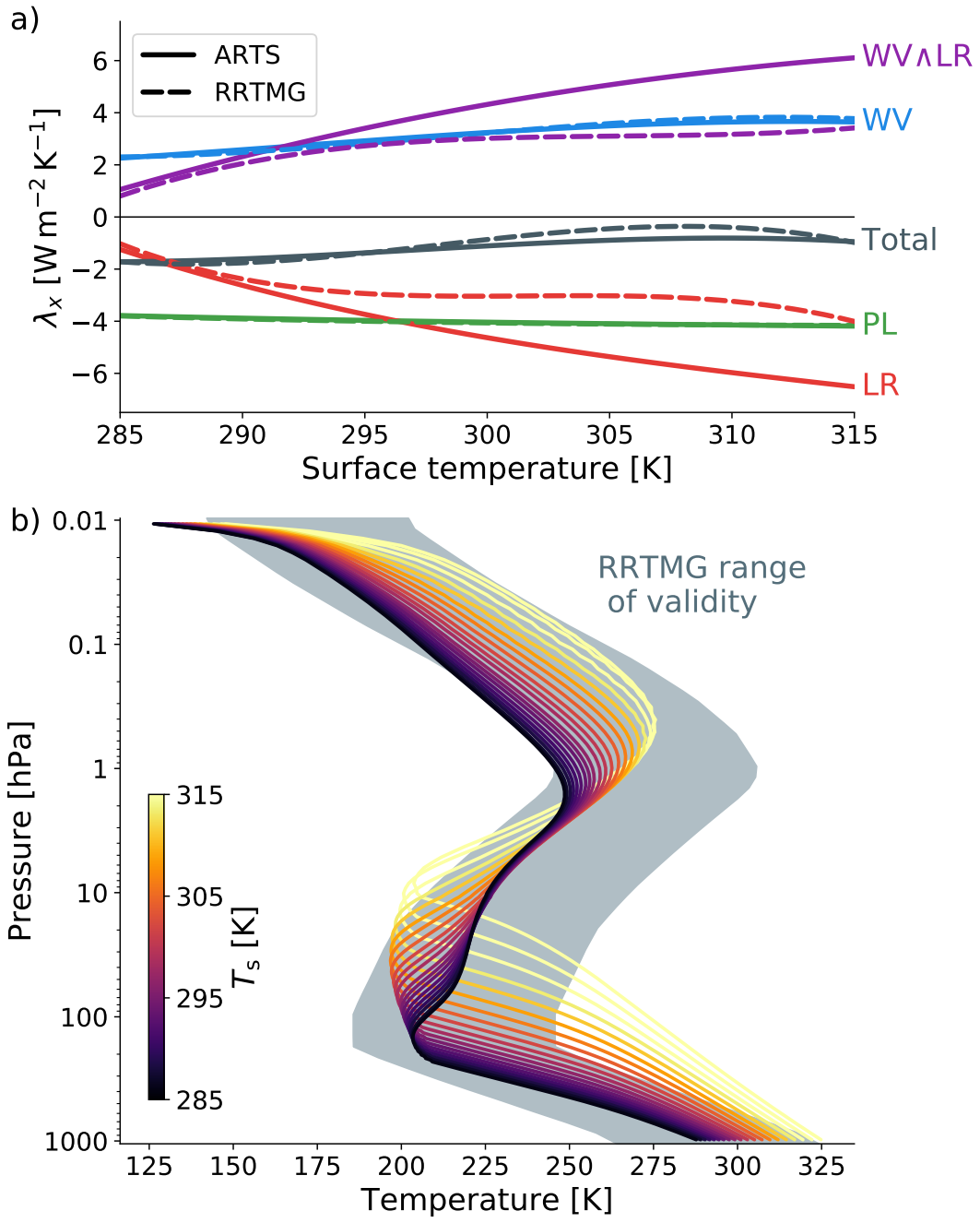

Figure B.3: **a)** Decomposed radiative feedbacks as a function of surface temperature. The feedbacks λ_x are shown for simulations using the radiation scheme RRTMG (dashed) as well as the line-by-line model ARTS (solid). **b)** Temperature profiles for different values of surface heat transport (in color) alongside the RRTMG temperature range.

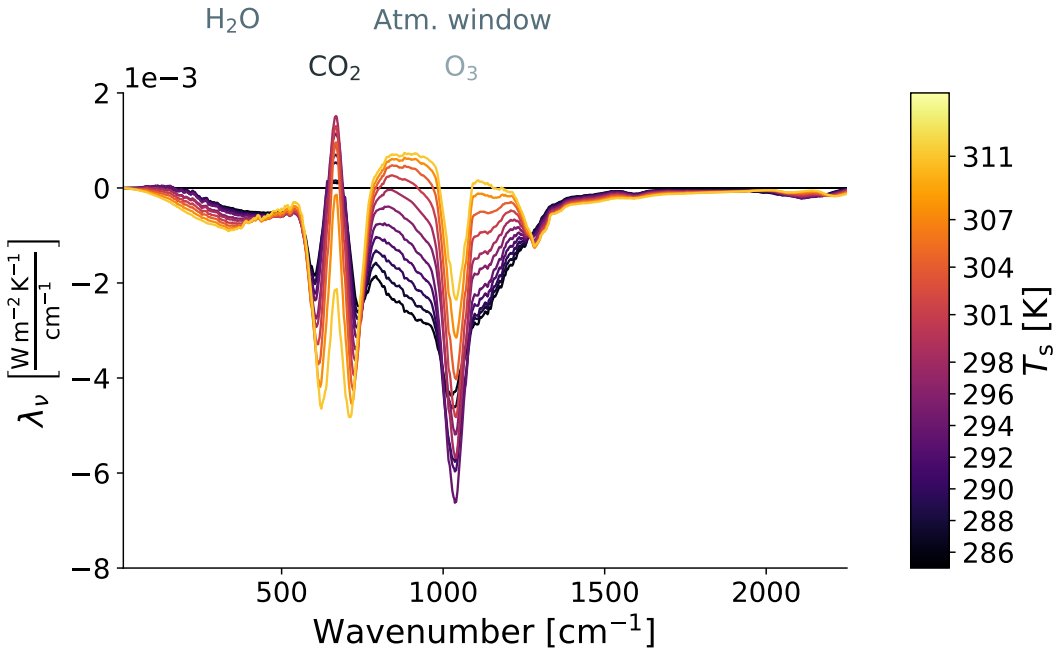

Figure B.4: Spectral radiative feedback as a function of wavenumber for different surface temperatures (in colors). The spectra are cut at 2,250 cm^{-1} to better resolve regions of interest. The actual line-by-line simulations cover a wavenumber range from 10–3,250 cm^{-1}.

800 and 1000 cm^{-1}, which is mainly driven by increased continuum absorption that shuts the atmospheric window (Koll and Cronin, 2018). As soon as the atmosphere is fully opaque in these spectral regions the radiative feedback is independent of the surface temperature, in agreement with Ingram (2010). The same behavior can be seen in the water-vapor dominated band below 500 cm^{-1}, which is opaque for all simulated surface temperatures.

We find that the total radiative feedback in spectral regions that are mainly dominated by water vapor absorption is indeed close to zero as soon as the atmosphere becomes fully opaque at high temperatures. Hence, our results link the findings of Koll and Cronin (2018) with the theory of Ingram (2010) to explain the temperature-dependence of the total radiative clear-sky feedback for a wide range of surface temperatures.

B.6 Conclusions

We tune our 1D-RCE model to different surface temperatures by introducing a surface enthalpy sink. We suggest that this is the best approach to analyze state-dependencies of radiative feedbacks in a single-column model.

The longwave radiation scheme used is the line-by-line model ARTS to ensure an accurate computation of radiative fluxes and heating rates over a wide temperature

range. By comparison to calculations with the RRTMG radiation scheme, we find that the use of that fast radiation scheme in extreme climates, outside its validity range, lead to false predictions on the state-dependence at high surface temperatures in at least two other modeling studies (Meraner et al., 2013; Romps, 2020).

The total radiative clear-sky feedback increases from -1.7 to $-0.8\,\mathrm{Wm^{-2}K^{-1}}$ for surface temperatures between 285 and 305 K, which can be attributed to a strengthening of the water-vapor feedback. This strengthening maximizes at surface temperatures of about 297 K at which the atmospheric window closes rapidly due to increased water-vapor continuum absorption.

After the closure of the atmospheric window, corresponding to surface temperatures above 305 K, the total radiative feedback is approximately independent of further surface temperature increases, in agreement with the conceptual model of Ingram (2010).

Acknowledgments. Contains modified Copernicus Climate Change Service Information (ERA5) [2018].
With this work we contribute to the Cluster of Excellence "CLICCS—Climate, Climatic Change, and Society" (EXC 2037, Project Number 390683824), and to the Center for Earth System Research and Sustainability (CEN) of Universität Hamburg.
The model source is developed under the MIT License and available on `github.com/atmtools/konrad`.

Bibliography

Becker, T. and B. Stevens (2014). "Climate and climate sensitivity to changing CO2 on an idealized land planet". In: *Journal of Advances in Modeling Earth Systems* 6.4, pp. 1205–1223. DOI: 10.1002/2014MS000369. eprint: https://agupubs.onlinelibrary.wiley.com/doi/pdf/10.1002/2014MS000369. URL: https://agupubs.onlinelibrary.wiley.com/doi/abs/10.1002/2014MS000369.

Budyko, M. I. (1969). "The effect of solar radiation variations on the climate of the Earth". In: *Tellus* 21.5, pp. 611–619. DOI: 10.3402/tellusa.v21i5.10109. URL: https://doi.org/10.3402/tellusa.v21i5.10109.

Buehler, S. A. et al. (2018). "ARTS, the atmospheric radiative transfer simulator — version 2.2, the planetary toolbox edition". In: *Geoscientific Model Development* 11.4, pp. 1537–1556. DOI: 10.5194/gmd-11-1537-2018.

Colman, R. and B. McAvaney (2009). "Climate feedbacks under a very broad range of forcing". In: *Geophysical Research Letters* 36.1. DOI: 10.1029/2008GL036268.

Cronin, T. W. (2014). "On the Choice of Average Solar Zenith Angle". In: *Journal of the Atmospheric Sciences* 71.8, pp. 2994–3003. DOI: 10.1175/JAS-D-13-0392.1.

Cronin, T. W. and K. A. Emanuel (2013). "The climate time scale in the approach to radiative-convective equilibrium". In: *Journal of Advances in Modeling Earth Systems* 5.4, pp. 843–849. DOI: 10.1002/jame.20049. URL: https://agupubs.onlinelibrary.wiley.com/doi/abs/10.1002/jame.20049.

Cronin, T. W. and A. A. Wing (2017). "Clouds, Circulation, and Climate Sensitivity in a Radiative-Convective Equilibrium Channel Model". In: *Journal of Advances in Modeling Earth Systems* 9.8, pp. 2883–2905. DOI: 10.1002/2017MS001111.

Dacie, S. et al. (2019). "A 1D RCE study of factors affecting the tropical tropopause layer and surface climate". In: *Journal of Climate* 32.20, pp. 6769–6782. DOI: 10.1175/JCLI-D-18-0778.1. URL: https://doi.org/10.1175/JCLI-D-18-0778.1.

Drotos, G. et al. (2020). "Global variability in radiative-convective equilibrium with a slab ocean under a wide range of CO2 concentrations". In: *Tellus A: Dynamic Meteorology and Oceanography* 72.1, pp. 1–19. DOI: 10.1080/16000870.2019.1699387. URL: https://doi.org/10.1080/16000870.2019.1699387.

Eriksson, P. et al. (2011). "ARTS, the atmospheric radiative transfer simulator, Version 2". In: *Journal of Quantitative Spectroscopy and Radiative Transfer* 112.10, pp. 1551–1558. DOI: 10.1016/j.jqsrt.2011.03.001.

Gordon, I. E. et al. (2017). "The HITRAN2016 molecular spectroscopic database". In: *Journal of Quantitative Spectroscopy and Radiative Transfer* 203, pp. 3–69. DOI: 10.1016/j.jqsrt.2017.06.038.

Gregory, J. M. et al. (2004). "A new method for diagnosing radiative forcing and climate sensitivity". In: *Geophysical Research Letters* 31.3, pp. 1–4. DOI: 10.1029/2003GL018747.

Hohenegger, C. and B. Stevens (2016). "Coupled radiative convective equilibrium simulations with explicit and parameterized convection". In: *Journal of Advances in Modeling Earth Systems* 8.3, pp. 1468–1482. DOI: 10.1002/2016MS000666. URL: https://agupubs.onlinelibrary.wiley.com/doi/abs/10.1002/2016MS000666.

Ingram, W. J. (2010). "A very simple model for the water vapour feedback on climate change". In: *Quarterly Journal of the Royal Meteorological Society* 136.646, pp. 30–40. DOI: 10.1002/qj.546.

Kluft, L. and S. Dacie (June 2020). *atmtools/konrad: Add line-by-line radiation and conceptual clouds*. Version v0.8.0. DOI: 10.5281/zenodo.3899702. URL: https://doi.org/10.5281/zenodo.3899702.

Kluft, L. et al. (2019). "Re-examining the first climate models: Climate sensitivity of a modern radiative-convective equilibrium model". In: *Journal of Climate* 32.23, pp. 8111–8125. DOI: 10.1175/JCLI-D-18-0774.1.

Koll, D. D. B. and T. W. Cronin (2018). "Earth's outgoing longwave radiation linear due to H2O greenhouse effect". In: *Proceedings of the National Academy of Sciences* 115.41, pp. 10293–10298. ISSN: 0027-8424. DOI: 10.1073/pnas.1809868115.

Manabe, S. and R. J. Stouffer (1980). "Sensitivity of a global climate model to an increase of CO2 concentration in the atmosphere". In: *Journal of Geophysical Research: Oceans* 85.C10, pp. 55290–5554. DOI: 10.1029/JC085iC10p05529.

Meraner, K. et al. (2013). "Robust increase in equilibrium climate sensitivity under global warming". In: *Geophysical Research Letters* 40.22, pp. 5944–5948. DOI: 10.1002/2013GL058118.

Minschwaner, K. and A. E. Dessler (2004). "Water Vapor Feedback in the Tropical Upper Troposphere: Model Results and Observations". In: *Journal of Climate* 17, pp. 1272–1282. DOI: 10.1175/1520-0442(2004)017<1272:WVFITT>2.0.CO;2.

Mlawer, E. J. et al. (1997). "Radiative transfer for inhomogeneous atmospheres: RRTM, a validated correlated-k model for the longwave". In: *Journal of Geophysical Research* 102, pp. 16663–16682.

Mlawer, E. J. et al. (2012). "Development and recent evaluation of the MT_CKD model of continuum absorption". In: *Philosophical Transactions of the Royal Society A* 370.1968, pp. 2520–2556. DOI: 10.1098/rsta.2011.0295.

Niiler, P. P. (1992). "The ocean circulation". In: *Climate system modeling*. Ed. by K. E. Trenberth. Cambridge University Press. Chap. 4.

Popke, D. et al. (2013). "Climate and climate change in a radiative-convective equilibrium version of ECHAM6". In: *Journal of Advances in Modeling Earth Systems* 5.1, pp. 1–14. DOI: 10.1029/2012MS000191.

Popp, M. et al. (Jan. 2015). "Initiation of a Runaway Greenhouse in a Cloudy Column". In: *Journal of the Atmospheric Sciences* 72.1, pp. 452–471. ISSN: 0022-4928. URL: https://doi.org/10.1175/JAS-D-13-047.1.

Romps, D. M. (2020). "Climate Sensitivity and the Direct Effect of Carbon Dioxide in a Limited-Area Cloud-Resolving Model". In: *Journal of Climate* 33.9, pp. 3413–3429. DOI: 10.1175/JCLI-D-19-0682.1. eprint: https://doi.org/10.1175/JCLI-D-19-0682.1. URL: https://doi.org/10.1175/JCLI-D-19-0682.1.

"Understanding the extreme spread in climate sensitivity within the Radiative-Convective Equilibrium Model Intercomparison Project" (n.d.). In: ().

Wing, A. A. et al. (2017). "Radiative-Convective Equilibrium Model Intercomparison Project". In: *Geoscientific Model Development Discussions* 2017, pp. 1–34. DOI: 10.5194/gmd-2017-213.

Appendix C

Cloud-altitude feedbacks in the 1D-RCE model konrad

Lukas Kluft, Manfred Brath, Stefan A. Buehler, and Bjorn Stevens

In preparation for submission

Contributions: L.K. and M.B. developed the algorithm to compute all-sky radiative fluxes; L.K. performed the research and analysed the data; L.K. wrote the draft manuscript; all authors contributed to the discussion of the results and the manuscript at all stages.

Abstract

We investigate the radiative effect and feedback of conceptual clouds in a 1D-RCE model. The clouds are chosen to resemble the trimodal characteristic of convection in the tropical atmosphere. The cloud physical properties are tuned in a way to match CERES satellite observations by using a large Monte Carlo Ensemble of about 100,000 members. A selected subset of ensemble members is forced with a doubling of the CO_2 concentration to investigate cloud feedbacks in a warming climate. High clouds that are fixed in pressure (FAP) cool the climate system by introducing a strong negative feedback of $-0.7\,\mathrm{Wm^{-2}K^{-1}}$, which is the same order of magnitude as the total clear-sky feedback. Keeping high clouds at the same temperature (FAT) results in a small but positive feedback of $0.1\,\mathrm{Wm^{-2}K^{-1}}$. If stability changes are taken into account (PHAT), the feedback slightly increases (more positive) to a value of $0.3\,\mathrm{Wm^{-2}K^{-1}}$. In contrast to existing literature, PHAT enhances the cloud feedback in our model because of a cooling of cloud top temperatures. This cooling is caused by the coupling of the vertical ozone distribution; a fixed ozone profile

results in the expected proportional heating of cloud top temperatures. We conclude that subtleties in the representation of the tropopause layer can be decisive for the sign of cloud feedbacks also in more complex models.

C.1 Introduction

We introduce idealized clouds into the radiative-convective equilibrium (RCE) model `konrad` (Kluft et al., 2019) to quantify their effect on radiative forcing and feedback. The idealized cloud scene consists of a trimodal cloud distribution with high, mid, and low clouds; in agreement with observations of the tropical atmosphere (Johnson et al., 1999; Mather et al., 2007). The cloud properties are chosen to match the cloud radiative effect retrieved from satellite observations.

In a first set of experiments, we verify that simulating realistic cloud-radiative effects (CRE) in our single-column model is feasible. Here, realistic is defined as in quantitative agreement with CERES EBAF satellite data (Doelling, 2019, Edition 4.1). CERES provides observational estimates for the longwave and shortwave CRE at the top-of-the atmosphere and the surface. We use these as constraints for the radiative effect of our clouds. Cloudy radiative transfer requires a variety of different parameters, e.g. the single scattering albedo, the cloud fraction, or the liquid water paths. The choice of these parameters is not trivial, because we want their radiative effect in a single-column to match the average cloud effect in the tropics. Therefore, we are running a large Monte Carlo ensemble with about 100,000 members to find sets of parameters that result in an equilibrium CRE in agreement with CERES.

In a next step, a selected sub-sample is forced with a doubling of the CO_2 concentrations to quantify the radiative forcing as well as the cloud longwave feedback. While doing so, the impact of three different assumptions on the evolution of high-cloud tops is investigated: In early studies, high clouds have been kept on fixed pressure levels (FAP) for computational simplicity (Manabe and Wetherald, 1967). The FAP mechanism introduces a strong negative feedback by increasing the outgoing longwave radiation (Ramanathan and Coakley, 1978; Ceppi et al., 2017). Later, Hartmann and Larson (2002) suggested that cloud anvils are more likely to keep a fixed temperature (FAT) under surface warming. This prevents the emission by high-clouds to increase, which causes a positive radiative feedback. More recently, Zelinka and Hartmann (2011) refined the FAT mechanism by taking changes in the static stability into account: The proportionally higher anvil temperature hypothesis (PHAT) is supposed to be less positive than FAT as it allows for a small warming of cloud top temperatures. Zelinka and Hartmann (2011) demonstrated that general circulation models show the PHAT behavior.

C.2 Explicit radiative fluxes in overlapping clouds

In radiative transfer simulations clouds are represented through a set of cloud optical parameters that describe their interaction with shortwave and longwave radiation. The cloud area fraction is defined as the area within an atmosphere column that is covered by cloud and, therefore, is descriptive of the chance that radiation interacts with a cloud.

The effect of a single cloud on radiation can be approximated by a weighted average between the overcast and the clear-sky radiative fluxes. This calculation becomes more difficult when clouds in different heights overlap horizontally. Then, the different overlapping combinations need to be taken into account. In an idealized example with only one high and one low cloud, an observer could see no cloud, both clouds, or only one of the two clouds. The chances for each of the constellations to be seen depends on the chances to see any of the single clouds, e.g. their cloud fraction. For simplicity, we assume that clouds in different heights overlap randomly, which is not necessarily true in the real atmosphere. However, for "block" clouds with height-constant properties, a random overlap is equivalent to the maximum-random overlap assumption used in most GCMs.

Global circulation models (GCM) try to reduce the computational expenses of radiative transfer in order to allow other components to be more elaborate. Therefore, most GCMs are using the so called Monte Carlo Independent Column Approximation (McICA) to approximate the variability of cloud overlapping in a single calculation (Barker et al., 2002; Pincus et al., 2003; Pincus et al., 2006). This method takes advantage of the internal structure of most radiation schemes, in which the electromagnetic spectrum is divided into spectral bands. In clear-sky simulations, these distinct bands are used to combine parts of the spectrum that are especially sensitive to certain gases in the atmosphere. In all-sky simulations, the different spectral bands are used to additionally create variability in the cloud state. Depending on the cloud fractions of each layer, every band will see one of the cloud overlapping constellations by chance. In a single simulation, this can cause large biases in the order of $50\,\mathrm{Wm}^{-2}$, because some cloud constellations can be statistically over- or underrepresented. However, when calculating radiative fluxes for a large amount of atmospheric columns and many time steps, the bias cancels out by random chance and by diffusion between the columns.

Unfortunately, in a single column RCE model McICA creates noise in the order of $50\,\mathrm{Wm}^{-2}$. A possible solution is to average multiple all-sky simulations for a single time step. However, the standard deviation decreases with $\sqrt{N}$, where N is the amount of independent simulations, and thus one needs about 2,000 simulations to reduce the noise to a magnitude of around $1\,\mathrm{Wm}^{-2}$.

For that reason, we introduce a new method to simulate overlapping cloud-layers in `konrad`. Instead of using the stochastical McICA approach, we calculate

every possible cloud combination separately and weigh the results according to their probability (Figure C.1). When assuming random cloud overlap, the computed radiative fluxes are equal to the convergence limit of McICA but without noise in any single time step.

For a cloudy atmosphere column with $J = 3$ individual cloud layers there are $2^J = 8$ different cloud constellations. A cloud constellation is characterized by the cloud area fraction p_j of each cloud layer, and a binary flag c_{ij}, which indicates whether cloud j is present in this constellation. The combined probability for a cloud constellation p_i is given by

$$p_i = \prod_{j=1}^{J} 1 - c_{ij} + (2c_{ij} - 1)p_j \quad . \tag{C.1}$$

where the multiplicant reduces to p_j if $c_{ij} = 1$ and $1 - p_j$ if $c_{ij} = 0$.

Figure C.1 shows the individual radiative fluxes for a trimodal cloud constellation. The low cloud is kept fixed on pressure levels between 850 and 950 hPa (no coupling). The mid-level cloud is centered around the freezing-level and the top of the high cloud is coupled to the level of maximum clear-sky subsidence divergence, which is consistent with the PHAT hypothesis (Zelinka and Hartmann, 2011) and the default choice for our RCE simulations. While mid and high-level clouds may change their altitude during a simulation, they keep a fixed depth of 100 hPa. The cloud area fractions for the high, mid-level, and low clouds are 30 %, 5 %, and 20 % respectively. These cloud fractions are chosen arbitrarily but are in a reasonable range for tropical clouds (Johnson et al., 1999). The colors indicate the combined probability for every single cloud constellation. One can see, that the single cloud events are most likely and their probability is close to the cloud fraction of each cloud. The chance to see all clouds together is the smallest, with less than a percent.

Figure C.1a shows the longwave upward flux. The strongest signal is seen at the high-cloud level, because cold emission temperatures at the cloud top reduce the emission compared to the clear-sky radiation. In the shortwave (C.1b), clouds contribute to the CRE mostly by reflecting radiation, thereby reducing the insolation. The atmospheric cloud radiative effect ACRE), which is the change of radiative heating due to the presence of clouds, shows a distinct cooling at the cloud-top and warming below the cloud base (Webster and Stephens, 1980; Ackerman et al., 1988).

C.3 Cloud-radiative effect

Our goal is to simulate a cloud ensemble that results in the same cloud radiative effect (CRE) as observed from space. The CRE is defined as the difference between all-sky and clear-sky radiative fluxes. For this purpose, we are using CERES EBAF satellite data (Doelling, 2019, Edition 4.1) to calculate a climatology of CRE over the tropical oceans (30S°–30N°). We define four individual targets, the longwave

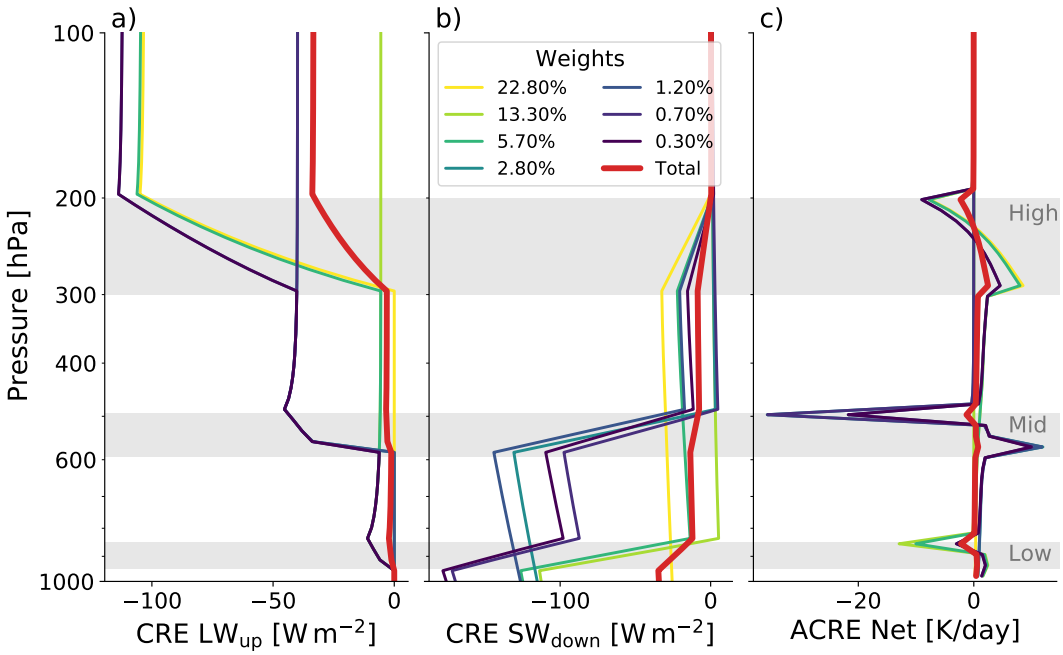

Figure C.1: Illustration of how to compute all-sky radiative fluxes as weighted average of different cloud overlap constellations of low, middle and high clouds. Shown are **a)** the upwelling longwave flux, **b)** the downwelling shortwave flux, and **c)** the radiative heating rates as a function of pressure. The total all-sky fluxes and heating rates are shown in red.

and shortwave CRE at the top of the atmosphere (TOA) and at the surface (SFC). Together, these values constrain the net cloud radiative effect for the climate system as a whole (TOA) as well as the atmospheric heating introduced by the presence of clouds (difference between TOA and SFC).

Figure C.2 shows the spatial distribution of longwave (LW) and shortwave (SW) CRE at the top of the atmosphere, as well as their net effect. Strong signals can be found along the ITCZ, where high cloud fractions increase the shortwave reflection (SW effect) and cool deep-convecting cloud-tops reduce the outgoing LW radiation (LW effect). In some areas, like the Indic warm pool, strong LW and SW signals almost completely cancel each other, while on the western coastlines of South America and Africa a negative net effect is found. This is caused by low-level clouds that are efficient in reflecting SW radiation, but only provide a weak contrast to the LW emission of the surrounding clear-sky atmosphere. In total, the net CRE amounts to $-17.7\,\mathrm{Wm}^{-2}$ in the tropics, which is almost five times larger than the $3.7\,\mathrm{Wm}^{-2}$ often cited for a doubling of CO_2.

Figure C.3 shows the zonal averages of our CRE targets. The zonal distribution is symmetric around the ITCZ, which is located at about 5°N. The absolute values of SW CRE at TOA and SFC show three distinct maxima, one in the ITCZ and two in the mid-latitudes, which are regions of high cloud cover.

Table C.1: Average of cloud radiative effects (CRE) over the tropical ocean between 30°S–30°N. The longwave (LW), shortwave (SW), and net (Net) cloud radiative effects are given at the top of the atmosphere (TOA) as well as the surface (SFC).

Wm^{-2}	SW	LW	Net
TOA	−43.6	25.9	−17.7
SFC	−45.7	17.0	−28.7

The LW TOA CRE has a pronounced peak in the ITCZ, where the deep convective clouds are found with cloud top heights reaching up to 12–16 km. The low temperatures at the cloud tops are causing a significant reduction in outgoing longwave radiation. In the mid-latitudes this effect is less pronounced, due to a smaller difference between surface temperature and cloud top temperature.

The LW CRE at the surface is the only CRE that is almost unrelated to cloud fraction. It is caused by a stronger emission at the cloud base compared to the clear-sky background. Therefore, it is highly influenced by the atmospheric state in which clouds exist. In the ITCZ, this atmospheric state is very warm and moist, which causes high back radiation already in clear-sky conditions; the additional back radiation by clouds is small. In higher latitudes, the temperatures and especially the humidity decrease. Both effects reduce the clear-sky LW radiation to the surface, which increases the difference to LW radiation originating from the cloud base. Therefore, the CRE at the surface is almost three times larger around 60°N/S compared to the ITCZ.

The tropical averages for latitudes between 30°S–30°N are given in Table C.1 and are chosen as a reference for a "realistic" cloud in the following RCE simulations.

C.4 Monte-Carlo ensemble to select cloud parameters

The radiative transfer of all-sky fluxes requires a set of cloud optical properties. In the real atmosphere, these properties depend on the phase of the cloud, and the amount of cloud particles at different sizes. Therefore, the properties depend on the atmospheric conditions the clouds are formed in. Here, we want to simulate this variety of different cloud optical parameters using a single representative cloud configuration. For that purpose, we tune a set of cloud physical parameters.

The effective radius is used to determine the single scattering albedo, the forward scattering fraction, as well as the asymmetry parameter from pre-calculated lookup tables. Here, we are using the same lookup-tables as ECHAM6 (Bjorn Stevens et al., 2013) We have chosen to set the effective radius of liquid cloud droplets to 10 μm and for ice crystals to 50 μm (Meyer et al., 2006).

In a next step, the cloud area fraction and the integrated water (or ice) path for each cloud layer needs to be chosen. The cloud area fraction is hard to constrain by

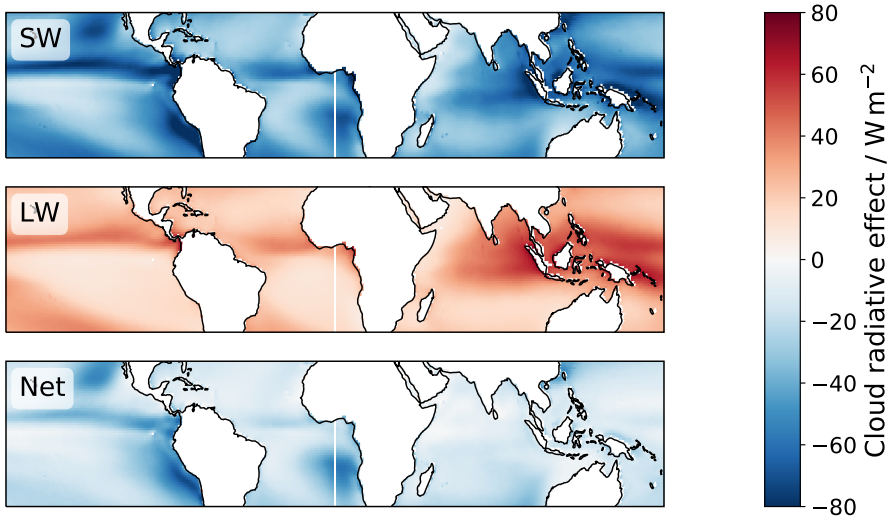

Figure C.2: Regional distribution of cloud-radiative effect (CRE) in the tropics based on CERES observations.

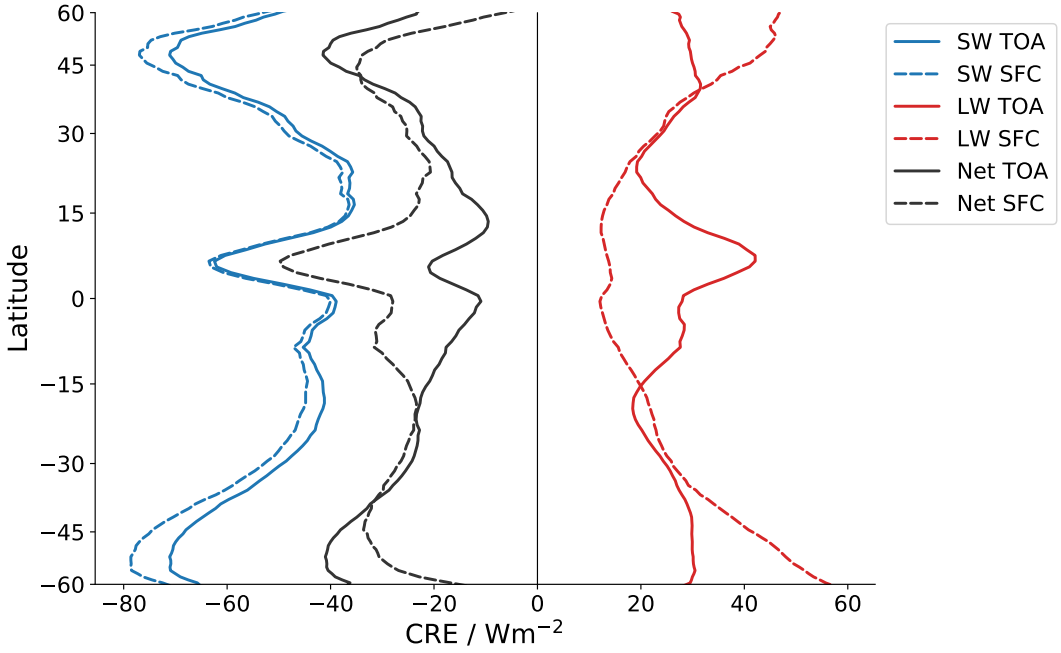

Figure C.3: Zonal averages of cloud-radiative effect (CRE) in the tropics based on CERES observations. In addition to the total CRE (black) the decomposed shortwave (blue) and longwave (red) components are shown. The CRE is given at the top-of-the-atmosphere (solid lines) and the surface (dashed lines).

Table C.2: Physical and optical cloud parameters.

Name	Value
Droplet size	$10\,\mu$m
Ice particle size	$50\,\mu$m
High cloud fraction	1%–35%
Mid cloud fraction	1%–35%
Low cloud fraction	1%–35%
IWP high cloud	2–70 $\mathrm{g\,m^{-2}}$
LWP mid-level cloud	20–200 $\mathrm{g\,m^{-2}}$
LWP low cloud	20–200 $\mathrm{g\,m^{-2}}$

observations, because it is highly dependent on the wavelength at which a cloud is observed, and on the way a cloud is defined. The integrated water path is observed more accurately (Meyer et al., 2006; Mather et al., 2007; Eliasson et al., 2011) but of limited use to constrain the radiative effect of clouds: The radiative fluxes of an average cloud profile will differ significantly from the average of the individual flux profiles, because of the non-linearity in radiative transfer. Therefore, we will tune the cloud area fraction and the water path of every cloud layer to find an "effective" combination that results in the CRE obtained from CERES EBAF.

A large Monte-Carlo ensemble with about 100,000 members was used to find a suitable set of cloud physical parameters. The chosen value range for every parameter is given in Table C.2. Each ensemble is initialized with a random combination of cloud parameters to test a multitude of parameter combinations. Because different cloud physical parameters will result in different climates, the CRE is a moving target, which requires iterative RCE simulations.

The simulations are run with a fixed relative humidity of 80% in the whole troposphere. Furthermore, the ozone profile is coupled to the atmospheric temperature in a way that it follows the development of the cold-point height. The coupling prevents unreasonably high ozone concentration in the upper troposphere when the tropopause expands in a warming climate. We are using simulations with a fixed surface temperature of 297 K to ensure the same initial climate state for each ensemble member. In addition, a fixed surface accelerates the convergence of a climate model (Romps, 2020). In combination with the fast simulation of all-sky radiative fluxes, this allows us to efficiently sample different cloud parameters.

For each ensemble member, we compute the root-mean-squared error (RMSE) with respect to the CERES EBAF observational targets (see Figure C.4). One can see that most of the ensemble members deviate $10\,\mathrm{Wm^{-2}}$ or even more from satellite observations. The long tail of outliers is mostly caused by an overestimation of the shortwave (SW) CRE. The SW CRE is controlled by the cloud area fraction which effectively ranges between 3–73 % due to a combination of the random overlap

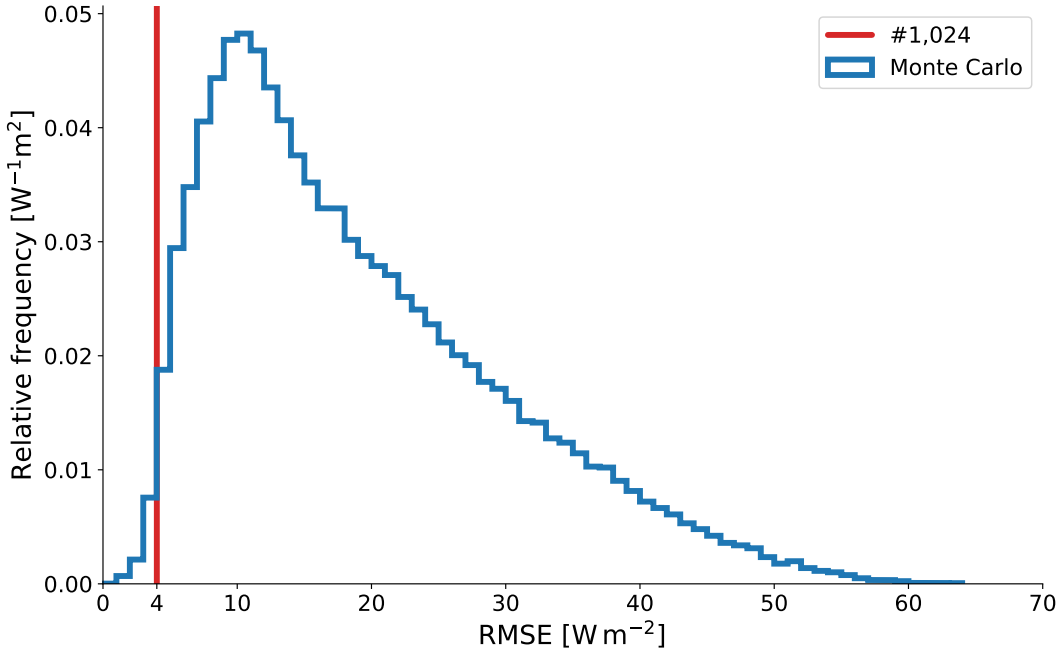

Figure C.4: Relative frequency of the root-mean-squared error (RMSE) of each Monte-Carlo ensemble member compared to the CERES EBAF observational target. In addition, the RMSE of the 1,024th best ensemble member is highlighted in red.

assumption and the chosen sampling range (see Table C.2). We select the 1,024 best ensemble members—which all have an RMSE of less than 4 Wm^{-2}—for further experiments.

C.5 Forced RCE simulations

C.5.1 Cloud feedback

The final goal of this study is to quantify the impact of clouds on RCE simulations that are forced with a doubling of CO_2. We are especially interested in the effective radiative forcing, the cloud radiative feedback, and their ratio the equilibrium climate sensitivity.

We are using cloud parameters from the selected subsample of a large Monte Carlo ensemble (see Section C.4). Each ensemble member has slightly different net CRE at the top-of-the-atmosphere, which would cause differences in the initial (surface temperature) states. To prevent this, each RCE model is run with an enthalpy sink in the surface layer that accounts for these differences(Drotos et al., 2020; Hohenegger and B. Stevens, 2016; Kluft et al., 2020, in review). This way, all models start in equilibrium with the same initial surface temperature of 297 K before they are forced with a doubling of the CO_2 concentration.

All RCE simulations are analyzed by plotting the radiative imbalance at the top-of-the-atmosphere as a function of surface temperature change as introduced by

(Gregory et al., 2004). Figure C.5 combines the individual Gregory plots as well as the linear regression, which visualizes the effective radiative forcing (y-intercept), the ECS (x-intercept) and the radiative feedback (slope). In addition, the clear-sky RCE at the same initial temperature is shown in black. A detailed description of the clear-sky configuration can be found in (Kluft et al., 2019; Kluft et al., 2020, in review). The effective radiative forcing is around $3.6\,\mathrm{Wm}^{-2}$ which is in good agreement with other modeling studies (Forster et al., 2016), even though it has not been tuned directly. The all-sky ECS is 3.5 K, well within the IPCC AR5 range of ECS from GCMs of 1.5–4.5 K. We define the cloud feedback λ_{cloud} as the difference between the radiative feedback of the clear-sky RCE (black) from the all-sky results

$$\lambda_{\mathrm{cloud}} = \lambda_{\mathrm{all}} - \lambda_{\mathrm{clear}} \tag{C.2}$$

Note, that this definition differs from the cloud feedback in other literature. Often the cloud feedback is computed by running offline radiative transfer simulations with perturbed cloud fields in an otherwise unperturbed control climate. When using this method, we calculate a higher cloud feedback of about $1\,\mathrm{Wm}^{-2}\mathrm{K}^{-1}$. We have chosen a different approach because `konrad`, in contrast to full GCMs, allows clear-sky and all-sky climate feedbacks to be directly compared.

When following the trajectory of single ensemble members, one can see distinct jumps in the radiative imbalance that are associated with an upward shift of the high-cloud tops. The ensemble is run with high-clouds that are coupled to the maximum clear-sky subsidence (PHAT). Later in this section, we compare the effects of fixing clouds at constant pressure (FAP) or temperature (FAT). The discrete jumps visualize two ways in which clouds interact with radiation: Firstly, high clouds increase the emissivity in the upper troposphere, which leads to a more negative climate feedback (steeper slope) and, on its own, would reduce surface warming. Secondly, the upward shift of the high-cloud top reduces the cloud-top temperature and increases the radiative imbalance (upward jumps) and hence the surface warming. In total, the rising of the cloud top is the stronger effect and causes a positive cloud feedback (a less steep slope in the Gregory plot). However, because of the reduced radiative forcing by masking of clouds, the ECS of the cloudy simulations is about the same value (3.5 K) as in the clear-sky simulation.

C.5.2 High-cloud coupling mechanisms

We quantify the effect of clouds by analyzing the spread in the magnitude of both, the radiative forcing and the cloud feedback. In addition, we introduce two more RCE ensembles, which use the same initial states but different assumptions about the high-cloud coupling. This allows us to quantitatively asses the differences of clouds that are fixed in pressure (FAP), fixed in temperature (FAT), or adjust to the level of maximum subsidence divergence (PHAT). PHAT is the most physical of

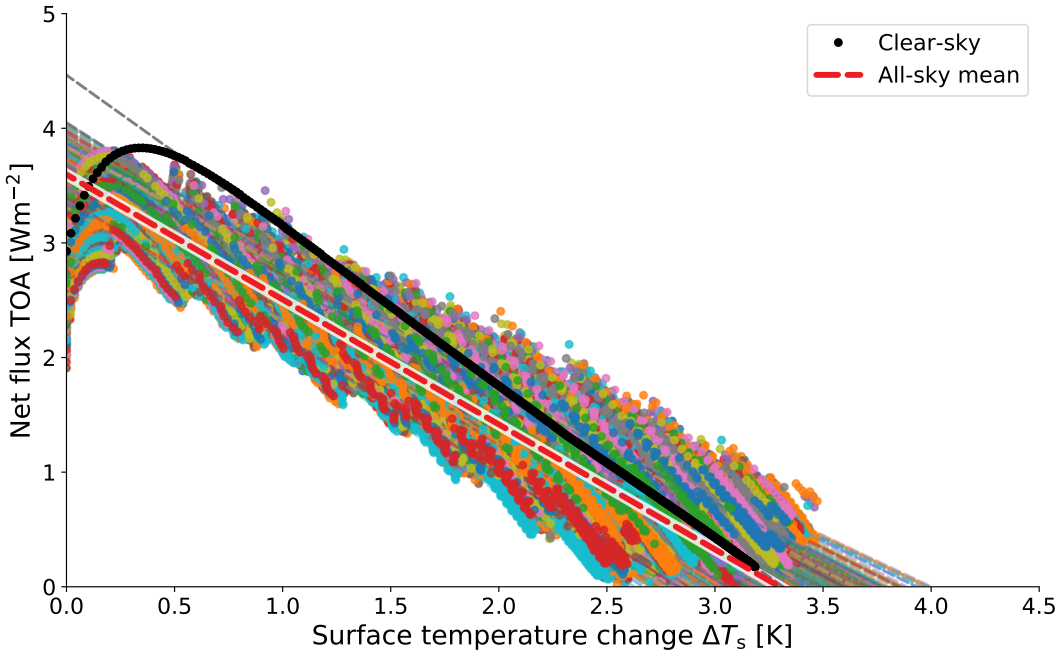

Figure C.5: Radiative imbalance as a function of surface warming of different all-sky RCE simulations (in colors). The Gregory plot visualizes the effective forcing (y-intercept), radiative feedback (slope of the regression), and the ECS (x-intercept).

these couplings according to our present-day understanding and is therefore chosen as the default configuration. FAT is a rough approximation, and FAP is unphysical but interesting in order to compare with historical studies. Every ensemble member uses the PHAT coupling to run into the present-day initial state, because it is the only mechanism that prescribes an actual cloud altitude and not only a change in a warming climate. Therefore, the initial states for all cloud simulations are comparable.

Figure C.6a shows the distribution of the effective radiative forcing. For the PHAT coupling, the effective forcing is around 3.6 Wm^{-2}, which is about 20 % smaller than the clear-sky value of 4.5 Wm^{-2}. Both, FAP and FAT, show a slightly smaller effective forcing of about 3.4 Wm^{-2}. In addition, the spread in the distribution is reduced.

Figure C.6b shows the equilibrium climate sensitivity (ECS), which is the eventual surface temperature change after a doubling of CO_2. The three ensembles cover an ECS range from 1.8–3.5 K. This is in good agreement with early RCE studies (Charney et al., 1979) as well as more recent emergent constraint approaches (Nijsse et al., 2020; Tokarska et al., 2020). We notice a clear separation of the mean ECS for the different coupling mechanisms. FAP results in the smallest ECS of about 1.8 K, which is only half of the clear-sky warming.

Figure C.6c and d show the total radiative feedback λ_{all} and the cloud feedback

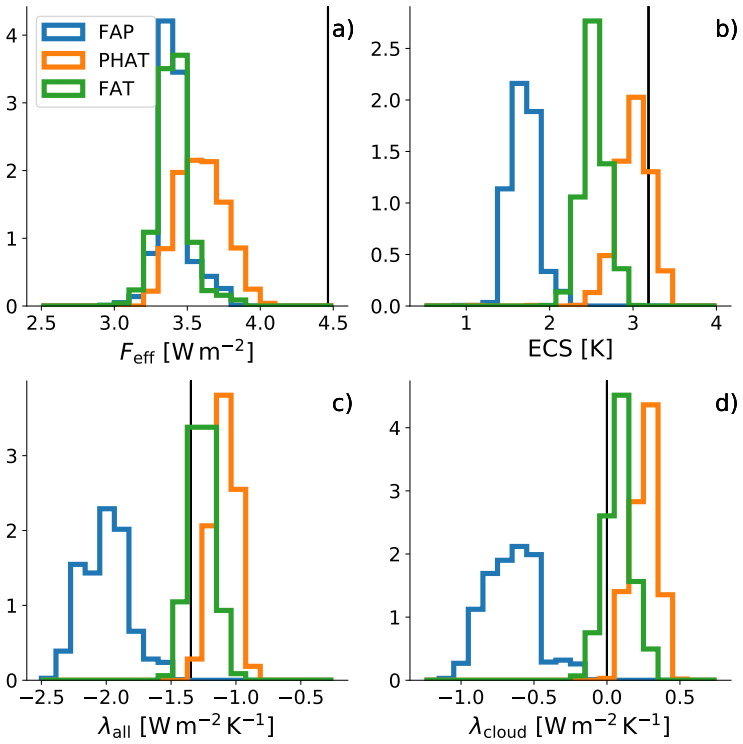

Figure C.6: Relative frequency of the **a)** effective forcing, **b)** equilibrium climate sensitivity, **c)** radiative feedback, and the **d)** cloud feedback. The clear-sky values are marked with black vertical lines as reference.

λ_{cloud}. Due to our model configuration, we neglect shortwave cloud feedbacks that are caused by changes in the cloud area fraction or the cloud optical properties (Ceppi et al., 2017). Therefore, clouds can only change their altitude and the corresponding cloud-top temperature, which controls the outgoing longwave emission. As a consequence, the way that high-cloud tops are evolving with respect to the atmospheric state is decisive for the strength of the cloud feedback.

Fixing high clouds at a constant pressure level introduces a strong negative feedback of $-0.7\,\mathrm{Wm^{-2}K^{-1}}$, which is about the same magnitude as the total clear-sky feedback. The negative FAP feedback is caused by increased longwave emission at the cloud top, which enhances temperature changes due to the lapse-rate feedback. High clouds that stay fixed at the same pressure level would reduce the ECS to half of its clear-sky value (Figure C.6b). Both the sign and the magnitude are in agreement with historical studies (Ramanathan and Coakley, 1978).

Fixing high clouds at a constant cloud top temperature (FAT) prevents an increase of the outgoing longwave radiation, which adds a positive feedback of about $0.1\,\mathrm{Wm^{-2}K^{-1}}$. Other studies have estimated FAT to causes a higher feedback of about $0.5\,\mathrm{Wm^{-2}K^{-1}}$. In our study, the clear-sky atmosphere is optically thick due to a large amount of water vapor absorption. (Ingram, 2010) predicted that, as soon as the atmosphere becomes optically thick, it will keep a constant emission temperature

in spectral regions dominated by water vapor absorption. This mechanism could explain, the small cloud feedback in our simulations: because both, the clear-sky and the all-sky atmosphere, tend to preserve a constant emission temperature, clouds do not contribute much to the all-sky climate feedback.

Fixing high clouds at the level of maximum subsidence divergence (PHAT) is expected to increase cloud top temperatures by about 0.5 K per 1 K surface warming (Zelinka and Hartmann, 2011). In an earlier study (Kluft et al., 2019) we have found the same temperature evolution for the convective-top temperature in clear-sky RCE simulations. Therefore, the PHAT mechanism is expected to lead to a more negative feedback than FAT, and this has been found for GCM simulations (Zelinka and Hartmann, 2011; Zelinka and Hartmann, 2010). In contrast, our simulations show a more positive feedback due to a decrease of cloud top temperatures (compare Figure C.5). This is caused by the coupling of the ozone profile with the tropopause height and the resulting upward shift in a warming climate. The reduced shortwave heating in the upper troposphere causes the tropopause layer, and the clouds located there, to cool (see Figure C.7). As a result, the PHAT mechanism increases the cloud feedback to about $0.3\,\mathrm{Wm^{-2}K^{-1}}$. If the ozone profile is fixed in height, cloud top temperatures do increase by about 0.5 K per K surface warming, which changes the sign of the cloud feedback (not shown). In other words, high clouds do not introduce a feedback on their own, but amplify the clear-sky signal introduced by the evolution of upper-tropospheric temperature.

However, both FAT and PHAT result in a cloud feedback whose magnitude is only about 10 % of the total clear-sky feedback. This is a significant decrease of the otherwise large FAP feedback.

We conclude that a trimodal cloud configuration is able to produce mean CRE in a single-column RCE model. When forced with a doubling of CO_2, clouds add a small but robust feedback of about 0.1–$0.3\,\mathrm{Wm^{-2}K^{-1}}$ (FAT/PHAT). However, the presence of clouds reduces the effective radiative forcing by 20 % to a value of $3.6\,\mathrm{Wm^{-2}}$. As a consequence, the resulting surface warming (ECS) is about the same as in the clear-sky—if at all it is slightly reduced.

C.6 Conclusions

We investigate the cloud radiative feedback in a single-column radiative-convective equilibrium (RCE) model by adding a trimodal cloud configuration. For this purpose, we introduce a method to calculate all-sky radiative fluxes for scenes with overlapping clouds. We explicitly simulate all possible cloud combinations and weigh them according to the probability of their occurrence. The resulting all-sky radiative fluxes are noise-free in every time step and equivalent to the convergence limit of stochastic methods like McICA.

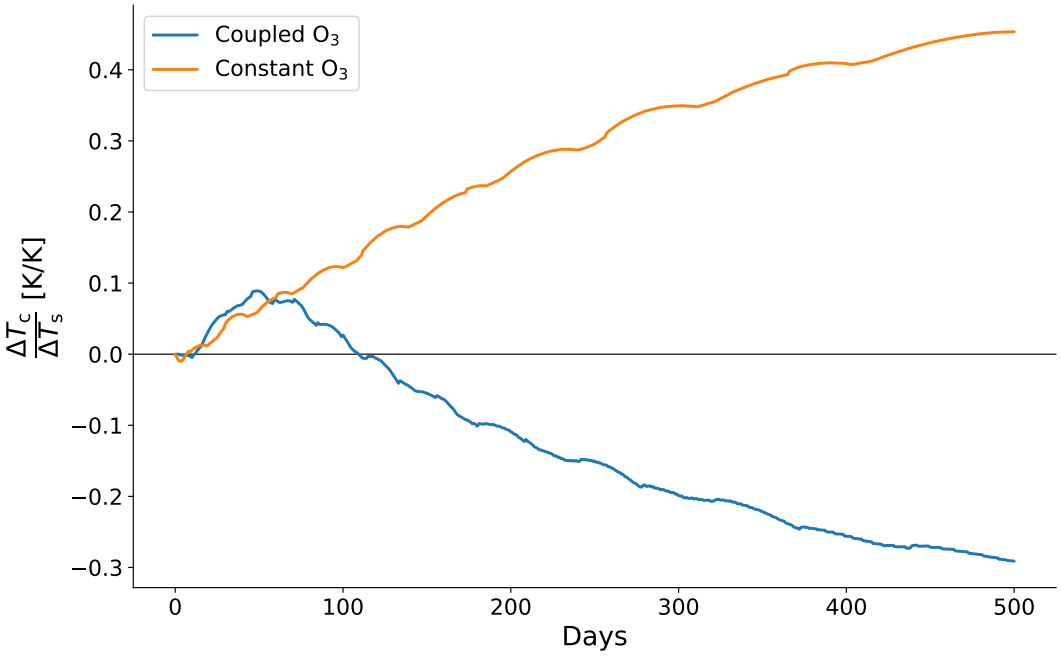

Figure C.7: Ratio of convective-top temperature change and surface warming as a function of simulated time. Results are shown for a fixed (orange) and coupled (blue) ozone profile.

The cloud physical parameters are tuned to match the tropical cloud-radiative effect as observed by CERES. The tuning is done using a large Monte-Carlo ensemble over cloud water content and cloud area fraction with about 100,000 members. A subset of 1,024 ensemble members closest to the CERES observations is forced with a doubling of the CO_2 concentration to quantify the radiative forcing, radiative feedback, and equilibrium climate sensitivity. The biggest limitation of our study probably is the neglect of shortwave effects due to changes in low-cloud fraction. However, there seems to be nothing in the 1D-RCE framework that would constrain this feedback in a physically meaningful way. This may be the reason why low-cloud feedbacks also differ greatly between GCMs. Instead, we focus on longwave cloud feedbacks, that are related to the altitude of high clouds.

We find, that the presence of clouds reduces the effective radiative forcing to a value of $3.6\,\mathrm{Wm}^{-2}$, which is about 20 % smaller than the clear-sky forcing of $4.5\,\mathrm{Wm}^{-2}$.

The cloud radiative feedback depends on the chosen coupling mechanism for high clouds. Clouds that are fixed at a given pressure level (FAP) introduce a negative feedback of about $-0.7\,\mathrm{Wm}^{-2}\mathrm{K}^{-1}$, which is the same magnitude as the total clear-sky feedback; thereby reducing ECS by a factor of two. Clouds that keep a constant cloud-top temperature (FAT) lead to a positive feedback of $0.1\,\mathrm{Wm}^{-2}\mathrm{K}^{-1}$, because they suppress an increase in outgoing-longwave radiation. The reductions in both, the effective forcing and the radiative feedback, almost cancel each other; the

remaining effect on the surface warming is smaller than 0.5 K.

High clouds that are coupled to the level of maximum clear-sky divergence (PHAT, the most realistic assumption) can contribute both, a positive or negative cloud feedback. The sign of the feedback depends on the development of the upper-tropospheric temperatures, which in our model, are tied to the evolution of the ozone profile. The decisive role of the upper-troposphere may have implications for full GCMs, because the treatment of atmospheric chemistry differs between models. Especially the differences between interactive and fixed ozone is often discussed in literature (Nowack et al., 2015; Marsh et al., 2016).

Our results suggest, that different treatment of ozone not only impacts the current atmospheric state, but also the evolution of upper-tropospheric temperatures under global warming. The latter affects the sign and strength of the cloud-altitude feedback and might explain a part of its spread.

Acknowledgments. These data were obtained from the NASA Langley Research Center Atmospheric Science Data Center.

Bibliography

Ackerman, Thomas P. et al. (May 1988). "Heating Rates in Tropical Anvils". In: *Journal of the Atmospheric Sciences* 45.10, pp. 1606–1623. ISSN: 0022-4928. DOI: 10.1175/1520-0469(1988)045<1606:HRITA>2.0.CO;2. URL: https://doi.org/10.1175/1520-0469(1988)045%3C1606:HRITA%3E2.0.CO;2.

Barker, H. W. et al. (2002). "The Monte Carlo independent column approximation: Application within large-scale models". In: *Proceedings of the GCSS/ARM workshop on the representation of cloud systems in large-scale models*.

Ceppi, Paulo et al. (2017). "Cloud feedback mechanisms and their representation in global climate models". In: *WIREs Climate Change* 8.4, e465. DOI: 10.1002/wcc.465. eprint: https://onlinelibrary.wiley.com/doi/pdf/10.1002/wcc.465. URL: https://onlinelibrary.wiley.com/doi/abs/10.1002/wcc.465.

Charney, J. G. et al. (1979). *Carbon dioxide and climate: a scientific assessment*. Tech. rep.

Doelling, David (2019). *CERES Energy Balanced and Filled (EBAF) TOA and Surface Monthly means data in netCDF Edition 4.1*. DOI: 10.5067/TERRA-AQUA/CERES/EBAF_L3B.004.1. URL: https://asdc.larc.nasa.gov/project/CERES/CERES_EBAF_Edition4.1.

Drotos, G. et al. (2020). "Global variability in radiative-convective equilibrium with a slab ocean under a wide range of CO2 concentrations". In: *Tellus A: Dynamic Meteorology and Oceanography* 72.1, pp. 1–19. DOI: 10.1080/16000870.2019.1699387. URL: https://doi.org/10.1080/16000870.2019.1699387.

Eliasson, S. et al. (2011). "Assessing observed and modelled spatial distributions of ice water path using satellite data". In: *Atmospheric Chemistry and Physics* 11, pp. 375–391. DOI: 10.5194/acp-11-375-2011.

Forster, Piers M. et al. (2016). "Recommendations for diagnosing effective radiative forcing from climate models for CMIP6". In: *Journal of Geophysical Research: Atmospheres* 121.20, pp. 12, 460–12, 475. DOI: 10.1002/2016JD025320. eprint: https://agupubs.onlinelibrary.wiley.com/doi/pdf/10.1002/2016JD025320. URL: https://agupubs.onlinelibrary.wiley.com/doi/abs/10.1002/2016JD025320.

Gregory, J. M. et al. (2004). "A new method for diagnosing radiative forcing and climate sensitivity". In: *Geophysical Research Letters* 31.3, pp. 1–4. DOI: 10.1029/2003GL018747.

Hartmann, D. L. and K. Larson (2002). "An important constraint on tropical cloud - climate feedback". In: *Geophysical Research Letters* 29.20, pp. 12-1–12-4. DOI: 10.1029/2002GL015835.

Hohenegger, C. and B. Stevens (2016). "Coupled radiative convective equilibrium simulations with explicit and parameterized convection". In: *Journal of Advances in Modeling Earth Systems* 8.3, pp. 1468–1482. DOI: 10.1002/2016MS000666. URL: https://agupubs.onlinelibrary.wiley.com/doi/abs/10.1002/2016MS000666.

Ingram, W. J. (2010). "A very simple model for the water vapour feedback on climate change". In: *Quarterly Journal of the Royal Meteorological Society* 136.646, pp. 30–40. DOI: 10.1002/qj.546.

Johnson, R. H. et al. (1999). "Trimodal characteristics of tropical convection". In: *Journal of Climate* 12.8, pp. 2397–2418.

Kluft, L. et al. (2020, in review). "Temperature-dependent clear-sky feedbacks in radiative-convective equilibrium". In: *Geophysical Research Letters*.

Kluft, L. et al. (2019). "Re-examining the first climate models: Climate sensitivity of a modern radiative-convective equilibrium model". In: *Journal of Climate* 32.23, pp. 8111–8125. DOI: 10.1175/JCLI-D-18-0774.1.

Manabe, S. and R. T. Wetherald (1967). "Thermal equilibrium of the atmosphere with a given distribution of relative humidity". In: *Journal of the Atmospheric Sciences* 24.3, pp. 241–259. DOI: 10.1175/1520-0469(1967)024<0241:TEOTAW>2.0.CO;2.

Marsh, Daniel R. et al. (2016). "Stratospheric ozone chemistry feedbacks are not critical for the determination of climate sensitivity in CESM1(WACCM)". In: *Geophysical Research Letters* 43.8, pp. 3928–3934. DOI: 10.1002/2016GL068344. eprint: https://agupubs.onlinelibrary.wiley.com/doi/pdf/10.1002/2016GL068344. URL: https://agupubs.onlinelibrary.wiley.com/doi/abs/10.1002/2016GL068344.

Mather, J. H. et al. (2007). "Cloud properties and associated radiative heating rates in the tropical western Pacific". In: *Journal of Climate* 112.D5. DOI: 10.1029/2006JD007555.

Meyer, K. et al. (2006). "Tropical ice cloud optical depth, ice water path, and frequency fields inferred from the MODIS level-3 data". In: *Atmospheric Research* 85, pp. 171–182. DOI: 10.1016/j.atmosres.2006.09.009.

Nijsse, F. J. M. M. et al. (2020). "Emergent constraints on transient climate response (TCR) and equilibrium climate sensitivity (ECS) from historical warming in CMIP5 and CMIP6 models". In: *Earth System Dynamics* 11.3, pp. 737–750. DOI:

10.5194/esd-11-737-2020. URL: https://esd.copernicus.org/articles/11/737/2020/.

Nowack, Peer J et al. (2015). "A large ozone-circulation feedback and its implications for global warming assessments". In: *Nature Climate Change* 5.1, pp. 41–45.

Pincus, Robert et al. (2003). "A fast, flexible, approximate technique for computing radiative transfer in inhomogeneous cloud fields". In: *Journal of Geophysical Research: Atmospheres* 108.D13. DOI: 10.1029/2002JD003322. eprint: https://agupubs.onlinelibrary.wiley.com/doi/pdf/10.1029/2002JD003322. URL: https://agupubs.onlinelibrary.wiley.com/doi/abs/10.1029/2002JD003322.

Pincus, Robert et al. (Dec. 2006). "Using Stochastically Generated Subcolumns to Represent Cloud Structure in a Large-Scale Model". In: *Monthly Weather Review* 134.12, pp. 3644–3656. ISSN: 0027-0644. DOI: 10.1175/MWR3257.1. eprint: https://journals.ametsoc.org/mwr/article-pdf/134/12/3644/4217796/mwr3257_1.pdf. URL: https://doi.org/10.1175/MWR3257.1.

Ramanathan, V. and J. A. Coakley (1978). "Climate modeling through radiative-convective models". In: *Reviews of Geophysics and Space Physics* 16.4, pp. 465–489.

Romps, D. M. (2020). "Climate Sensitivity and the Direct Effect of Carbon Dioxide in a Limited-Area Cloud-Resolving Model". In: *Journal of Climate* 33.9, pp. 3413–3429. DOI: 10.1175/JCLI-D-19-0682.1. eprint: https://doi.org/10.1175/JCLI-D-19-0682.1. URL: https://doi.org/10.1175/JCLI-D-19-0682.1.

Stevens, Bjorn et al. (2013). "Atmospheric component of the MPI-M Earth System Model: ECHAM6". In: *Journal of Advances in Modeling Earth Systems* 5.2, pp. 146–172. DOI: 10.1002/jame.20015. eprint: https://agupubs.onlinelibrary.wiley.com/doi/pdf/10.1002/jame.20015. URL: https://agupubs.onlinelibrary.wiley.com/doi/abs/10.1002/jame.20015.

Tokarska, Katarzyna B. et al. (2020). "Past warming trend constrains future warming in CMIP6 models". In: *Scientific American* 6.12. DOI: 10.1126/sciadv.aaz9549. eprint: https://advances.sciencemag.org/content/6/12/eaaz9549.full.pdf. URL: https://advances.sciencemag.org/content/6/12/eaaz9549.

Webster, Peter J. and Graeme L. Stephens (July 1980). "Tropical Upper-Tropospheric Extended Clouds: Inferences from Winter MONEX". In: *Journal of the Atmospheric Sciences* 37.7, pp. 1521–1541. ISSN: 0022-4928. DOI: 10.1175/1520-0469(1980)037<1521:TUTECI>2.0.CO;2. URL: https://doi.org/10.1175/1520-0469(1980)037%3C1521:TUTECI%3E2.0.CO;2.

Zelinka, M. D. and D. L. Hartmann (2010). "Why is longwave cloud feedback positive?" In: *Journal of Geophysical Research: Atmospheres* 115.D16, p. D16117. DOI: 10.1029/2010JD013817,.

— (2011). “The observed sensitivity of high clouds to mean surface temperature anomalies in the tropics”. In: *Journal of Geophysical Research* 116.D23, p. D23103. DOI: 10.1029/2011JD016459,.

Versicherung an Eides statt

Hiermit versichere ich an Eides statt, dass ich die vorliegende Dissertation mit dem Titel: “Benchmark Calculations of the Climate Sensitivity of Radiative-Convective Equilibrium” selbstständig verfasst und keine anderen als die angegebenen Hilfsmittel — insbesondere keine im Quellenverzeichnis nicht benannten Internet-Quellen — benutzt habe. Alle Stellen, die wörtlich oder sinngemäß aus Veröffentlichungen entnommen wurden, sind als solche kenntlich gemacht. Ich versichere weiterhin, dass ich die Dissertation oder Teile davon vorher weder im In- noch im Ausland in einem anderen Prüfungsverfahren eingereicht habe und die eingereichte schriftliche Fassung der auf dem elektronischen Speichermedium entspricht.

Hamburg, den 5. Oktober 2020 Lukas Kluft

Hinweis / Reference

Die gesamten Veröffentlichungen in der Publikationsreihe des MPI-M
„Berichte zur Erdsystemforschung / Reports on Earth System Science“,
ISSN 1614-1199

sind über die Internetseiten des Max-Planck-Instituts für Meteorologie erhältlich:
http://www.mpimet.mpg.de/wissenschaft/publikationen.html

All the publications in the series of the MPI -M
„Berichte zur Erdsystemforschung / Reports on Earth System Science“,
ISSN 1614-1199

are available on the website of the Max Planck Institute for Meteorology:
http://www.mpimet.mpg.de/wissenschaft/publikationen.html